2014

Investigation of factors controlling the dynamics of beach surface moisture content

Phillip P. Schmutz
Louisiana State University and Agricultural and Mechanical College

INVESTIGATION OF FACTORS CONTROLLING THE DYNAMICS OF BEACH SURFACE MOISTURE CONTENT

A Dissertation

Submitted to the Graduate Faculty of the
Louisiana State University and
Agricultural Mechanical College
in partial fulfillment of the
requirements for the degree of
Doctor of Philosophy

in

Department of Geography and Anthropology

by
Phillip P. Schmutz
B.A., Baylor University, 2004
M.S., Louisiana State University, 2007
August 2014

To Van H. Schmutz (Andaddy)

Thank you for awaking my curiosity into the world of science and nature.
Without you I would not be where I am today!

Acknowledgements

First and foremost, I would like to thank my family for all their love and support as I have ventured through my academic career. They have continually inspired me to do my best as I strived to pursue my dreams.

Next I would like to thank my advisor, Dr. Steven Namikas, for his patience and willingness to go out of his way to provide the best possible guidance over these past nine years. You have led me through a multitude of the hurdles and difficulties I have confronted throughout my academic career. I also am thankful to Dr. David P. Brown and Dr. Robert Rohli for serving on my committee and for all your wisdom and knowledge during this endeavor. Special thanks to my fellow colleagues, Dr. Brandon Edwards, Ms. Katherine Renken, and Mr. Jeremy LeMieux for all of your assistance during those long, grueling hours in the field. I would also like to thank Mr. Wade Stablein and the staff at Padre Island National Seashore for all your help during my field endeavors.

Finally, my wife Amy! You are my rock and partner on this life-long geographical journey. I am so thankful for all the love and support you have given me during the crazy and stressful journey through my dissertation. I love you!

Table of Contents

Abstract

This dissertation investigates the factors that control beach surface moisture dynamics. The study consists of a suite of laboratory and field experiments to document, analyze, and model the role of the key input parameters (groundwater table fluctuations, capillary actions (i.e., moisture retention, hysteresis, and hydraulic conductivity), evaporation-condensation, and sediment size) on the spatio-temporal variability of beach surface moisture content.

Results from the laboratory experiments demonstrated that the capillary processes of hysteresis and hydraulic conductivity heavily influence the spatial and temporal dynamics of beach moisture. Additionally, different sediment grain sizes produced marked differences in capillary processes within the sediment column, under the same hydrological conditions.

Analysis of evaporation dynamics reveals that evaporation from the beach surface differs dramatically from that of a free water surface. Initially, evaporation of moisture occurs almost entirely at the surface layer and at a rate that approximates the potential evaporation rate. However, after this time period the rate of evaporation at the upper surface layer stabilizes and remains approximately constant and the sub-surface layer becomes the dominant source of moisture for evaporation.

Field measurements of surface moisture content demonstrated that spatially the beach surface can be characterized by three moisture-content zones: a consistently dry back beach zone, a variable content zone, and finally a persistently wet fore beach zone. Temporally, moisture contents varied over both short-term (daily) and long-term (multi-day) sequences. Over the short-term, diurnal fluctuations in the groundwater table played a significant role in influencing surface moisture across the wet and variable-content zones, whereas evaporation

and condensation processes were the dominant factors in the dry zone. Over the longer term, variations in the lunar spring/neap tidal range produced distinct changes in the range of moisture contents, as it regulated the amplitude of the beach groundwater table over multi-day time scales.

Modeling of surface moisture content demonstrated that a hysteresis based modeling approach provides a quite accurate and thorough representation of field-measured beach surface moisture dynamics. Simulations revealed that the inclusion of evaporation only influences predicted surface moisture contents across the dry back beach, whereas simulations across the wet fore beach and moisture variable middle beach are virtually unchanged by the inclusion of evaporation.

Chapter 1 -- Introduction

1.1 Project Context

The surface moisture content of soils is widely recognized as a critical parameter influencing a broad range of physical environmental phenomena occurring at or near the land surface. It is considered to be an important factor influencing earth-atmospheric energy fluxes (Bosilovich and Sun, 1998; Eltahir, 1998; Wythers *et al.*, 1999; Chen and Hu, 2004), and it is a fundamental component regulating the terrestrial hydrological cycle (Gardner and McLaren, 1999; Olyphant, 2003). Additionally, it is an important element influencing the soil temperature regime (Abu-Hamdeh, 2003), which profoundly affects seed germination and plant growth (Hesp, 1991; Barrilleaux and Grace, 2000). Of particular concern in the context of the present study, surface moisture is an important, but poorly understood, factor that affects the operation of aeolian sediment transport systems by limiting the frequency and magnitude of sediment transport events from beach to dune (Sherman *et al*., 1998; Wiggs *et al.*, 2004a,b; Davidson-Arnott *et al*., 2005; Ravi *et al.*, 2006).

The movement of sand by wind is the primary mechanism responsible for delivering sediment from beach to dune (Bauer *et al*., 1990; Sherman and Bauer, 1993; Arens, 1996; Bauer and Davidson-Arnott, 2002; Davidson-Arnott *et al.*, 2008; Hugenholtz *et al.*, 2009). Beach surface moisture represents a critical control on the interconnection between these sub-environments, and on coastal dune development over time (Short and Hesp, 1982, Psuty, 1988, Sherman and Bauer, 1993; Sherman and Lyons, 1994; Davidson-Arnott and Dawson, 2001; Bauer and Davidson-Arnott, 2002; Aagaard *et al*., 2004; Houser, 2009). A key uncertainty in modeling beach-dune interaction lies in the representation of spatial and temporal variations in

beach surface moisture content (Jackson and Nordstrom, 1997; Wiggs *et al*., 2004b; Yang and Davidson-Arnott, 2005; McKenna Neuman and Langston, 2006; Zhu, 2007; Namikas *et al*., 2010). This is in large part due to the fact that these variations are controlled by complex interactions between a suite of hydrological, meteorological, and sedimentary parameters that include precipitation, groundwater flow, capillary transport, evaporation, condensation, soil grain size, and tidal oscillations (Figure 1.1). This study will address this gap in knowledge through a set of field and laboratory experiments designed to identify and quantify the role of these variables in influencing the surface moisture content of beach environments.

A small number of recent studies have mapped spatial and temporal variations in beach surface moisture content in varying degrees of detail (Atherton *et al*., 2001; Wiggs *et al.*, 2004b; Yang and Davidson-Arnott, 2005; Zhu, 2007; Bauer *et al*., 2009; Namikas *et al.*, 2010). The basic spatial pattern that emerges from these reports is a cross-shore gradient with surface moisture levels typically at or near saturation adjacent to the swash zone and decreasing in the landward direction to become nearly or fully dry approaching the base of the foredune (Figure 1.2). Zhu (2007) and Namikas *et al.* (2010) documented the temporal evolution of surface moisture distributions over periods of a few days. It was found that surface moisture could be characterized in terms of three distinct zones. The first zone is a wet fore beach zone adjacent to the swash zone where moisture levels remain consistently at saturated/near-saturated levels where water table depths are very shallow (the relationship is comparable to that of diagram C in Figure 1.3). Second is a dry zone found on the backbeach next to the foredune. Here moisture levels are consistently low due to relatively deep water table depths (> than 1 m) and small fluctuations in the water table (comparable to diagram A in Figure 1.3). The third zone is a

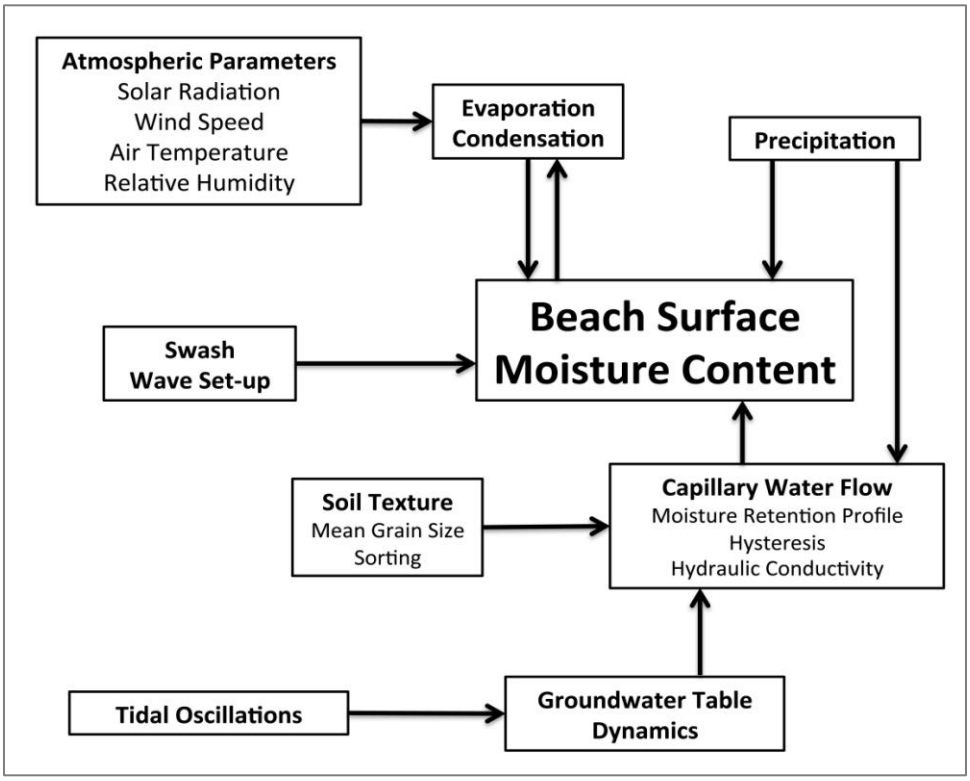

Figure 1.1: Key processes and parameters that control beach surface moisture dynamics.

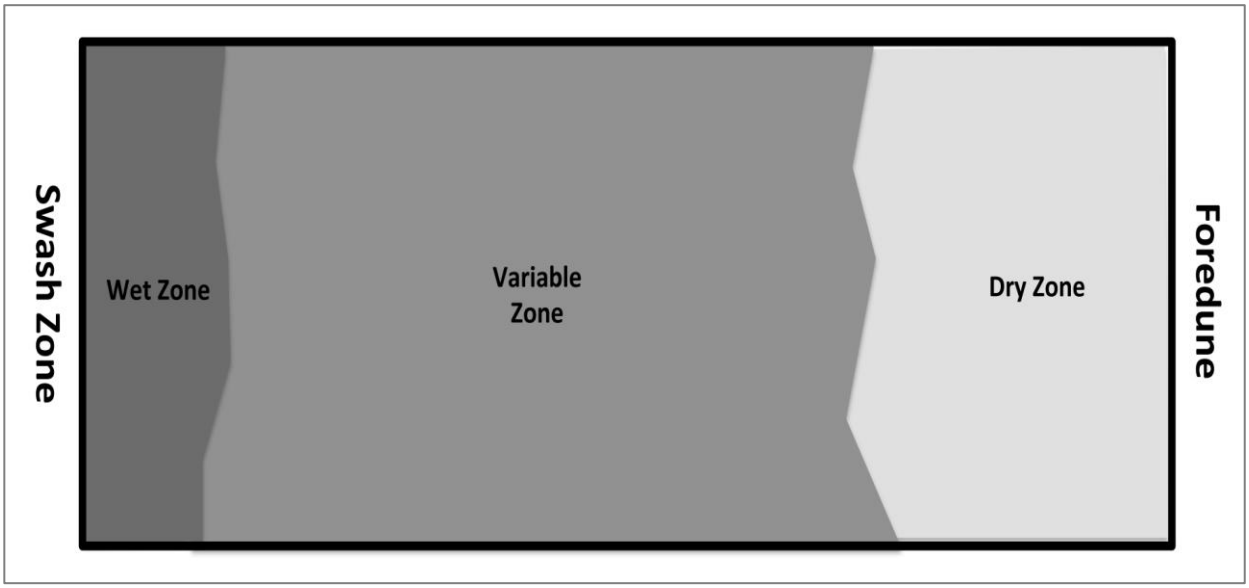

Figure 1.2: Schematic representation of the changes in the spatial coverage of the cross-shore moisture zones.

highly variable zone that lies within the middle beach between the wet and dry zones. Here moisture levels fluctuate widely in accordance with variations in water table depth and oscillation (comparable with diagram B in Figure 1.3). Aeolian transport is primarily restricted to the dry zone and portions of the variable zone that periodically experience low moisture levels. An understanding of the dynamics of these zones is vital to determining the available source area and fetch width for sediment transport, and for modeling transport at intermediate or larger spatial scales (Bauer and Davidson-Arnott, 2002; Bauer *et al*., 2009).

Accurate modeling of surface moisture content requires an understanding of more precise relationships describing the interactions between the controlling processes and parameters and their influence on beach surface moisture dynamics than are currently available. In response, this dissertation aims to improve our understanding of the spatio-temporal variability in surficial moisture generated by these processes.

1.2 Research Objectives

This study involves a suite of field and laboratory experiments designed to accomplish the following specific research objectives:

1) Document and model the influence of capillary flows driven by an oscillating water table on surface moisture dynamics
2) Identify the role of evaporation and condensation on surface moisture dynamics
3) Analyze the influence that different sediment grain sizes have on capillary processes

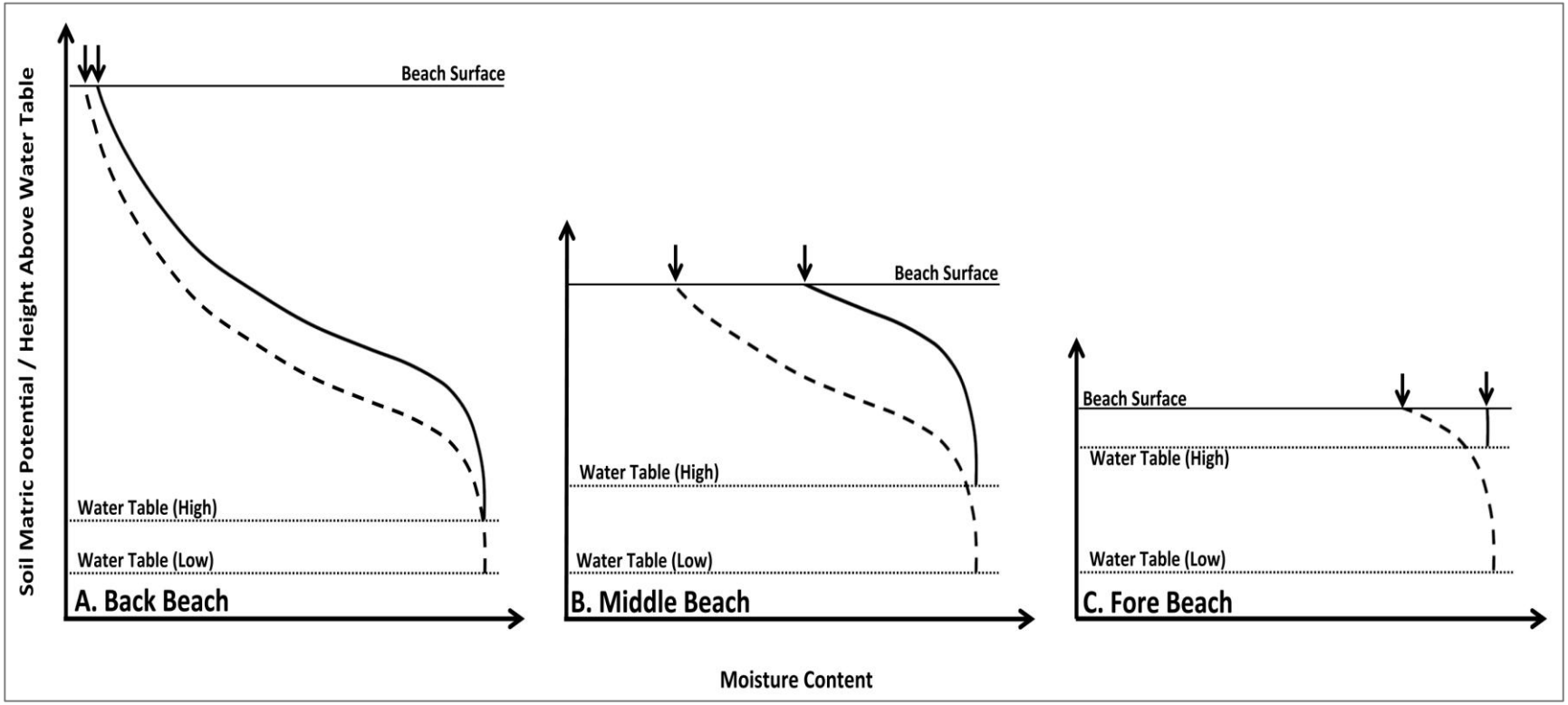

Figure 1.3: Schematic illustrations of the relationship between surface moisture dynamics, soil matric potential (pressure head) and the soil moisture retention curve during high and low water table conditions in the beach environment: (a) the back beach; (b) the middle beach; (c) the fore beach. Solid line illustrates the moisture retention curve at high water whereas the dashed line represents the moisture retention curve at low water.

1.3 Research Needs

1.3.1 Capillary Water Flow

The beach groundwater system is strongly influenced by tidal cycles, which generate cyclic fluctuations in the elevation of the beach water table. This causes corresponding shifts in the capillary zone above the water table and in the vertical profile of sediment moisture content above the water table (Raubenheimer *et al.*, 1999; Stauffer and Kinzelbach, 2001; Zhu 2007). As beach environments often have very shallow water table depths (centimeters to a few meters), the zone above the groundwater table influenced by capillary transport often reaches portions of the beach surface (Atherton *et al.*, 2001; Yang and Davidson-Arnott, 2005; McKenna Neuman and Langston, 2006; Zhu, 2007; Namikas *et al.*, 2010). Therefore, the dynamics of the beach groundwater system may play a key role in regulating the status of beach surface moisture (Atherton *et al.*, 2001; Zhu, 2007; Namikas *et al.*, 2010).

In theory, the response of beach surface moisture content to beach groundwater dynamics can be established based on knowledge of i) the moisture retention profile of the sediment column, ii) depth of the water table, and iii) the magnitude and rate of water table fluctuations (Raubenheimer *et al.*, 1999; Ruz and Meur-Ferec, 2004; Chuang and Yeh, 2006; Zhu, 2007). In reality, however, the hydrological dynamics of a beach system are rarely simple. Capillary water flow within the sediment column tends to exhibit a non-linear, hysteretic behavior as well as experience transient water flow time lags.

Hysteresis dictates that at any given pressure head, the equilibrium moisture content level obtained by a drying soil is greater than that obtained by a wetting soil at the same pressure head (Figure 1.4) (Raats and Gardner, 1974; Parlange, 1976). While hysteresis can

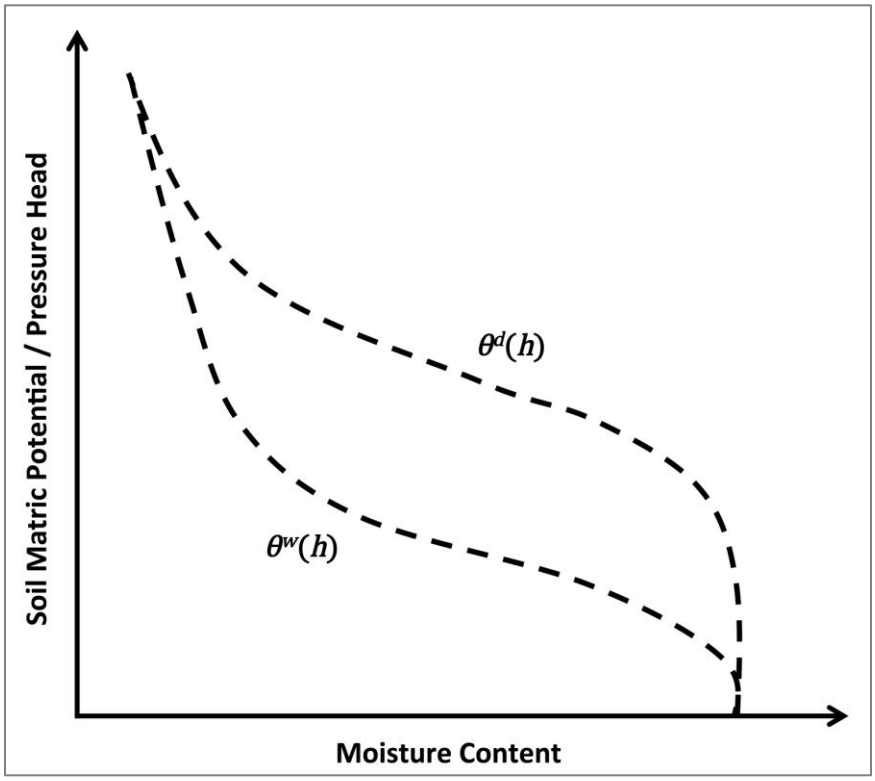

Figure 1.4: Representation of hysteresis in capillary water flow illustrating the boundary wetting ($\theta^w(h)$) and drying ($\theta^d(h)$) moisture retention curves.

occur due to several causes (i.e., air entrapment from restricted pore connectivity, pore contact angle variations, etc.), Miller and Miller (1956) postulated that hysteresis effects arise due to the greater capillary potential required to allow water entry into the soil pores during the wetting process compared to the lower capillary potential required to empty the soil pores during soil drying. Therefore, higher moisture content values are maintained at any given pressure head value, during soil drying relative to soil wetting. Although this hysteresis effect has long been recognized (Haines, 1930), there is debate in the literature regarding the need for inclusion of hysteresis in modeling periodic unsaturated groundwater movement. Early studies tended to disregard hysteresis effects for simple, homogeneous sediment systems such as beach sand (e.g., Childs and Poulovassilis, 1962; Childs, 1969; Raats and Gardner, 1974;

Kessler and Rubin, 1987). However, several recent studies have demonstrated that when hysteresis is accounted for it is possible to obtain significantly improved simulations of observed capillary water flow above a fluctuating water table (i.e., Hinz, 1998; Raubenheimer *et al.*, 1999; Nielsen and Perrochet, 2000; Werner and Lockington, 2003; Cartwright *et al.*, 2005; Cartwright *et al.*, 2009). Thus, our understanding of the influence of hysteresis on beach surface moisture dynamics remains incomplete.

Time-dependent signals in surface moisture content associated with the transient nature of capillary water flow are poorly understood and have largely been ignored within the literature. Conventionally, the rate of change within the moisture profile of the sediment column is determined under steady-state conditions independent of the velocity at which the water table fluctuates (Childs and Poulovassilis, 1962). This implies that moisture contents correspond exactly and synchronously with the cyclic movement of the water table. In reality, however, capillary water flows at a faster rate at higher water contents than it does at lower water contents due to the increase in hydraulic conductivity (Childs, 1969; Raats and Gardner, 1974; Kool and Parker, 1987). Therefore, the moisture content at the surface may lag significantly behind water table oscillations, and do so to a degree that increases both proportionally and non-linearly with depth of the water table (Hinz, 1998). This phenomenon is likely to have a very substantial impact on the temporal dynamics of beach surface moisture content, and this impact should increase moving landward from the shoreline. As one moves landward across the beach the water table becomes deeper and the surface moisture contents decrease, producing slower capillary flows across larger distances and thus increasing the time lag between water table position and surface moisture content.

In summary, our understanding of beach surface moisture dynamics above an oscillating water table includes at least two key sources of uncertainty: i) the magnitude of hysteresis effects during periods of water table rise and fall, and ii) the time lags associated with transient water flow. To date only a few studies have attempted to link oscillating groundwater dynamics to variability in beach surface moisture content (i.e., Atherton *et al.*, 2001; Zhu, 2007; Namikas *et al.*, 2010); and none of these studies incorporated hysteresis effects and transient water flow dynamics in their analyses.

1.3.2 Evaporation and Condensation

The rate of evaporation from soil surfaces has traditionally been considered to approximate the rate of evaporation from an open water surface, that is, potential evaporation (Penman, 1948; Beese *et al.*, 1977; Mahfouf and Noilhan, 1991; van de Griend and Owe, 1994). However, this approach becomes increasingly inaccurate as the soil surface dries. Evaporation of moisture from the soil decreases the moisture content, which in turn reduces the rate of actual evaporation from the soil surface, as water availability is increasingly restricted (Morton, 1985; Granger, 1989; Entekhabi *et al.*, 1996; Wilson *et al.*, 1997). This concept illustrates that surface moisture and evaporation mutually influence one another. As a result, traditional methods for calculating evaporation based on saturated soil conditions provide overestimates of evaporation for soil surfaces, which are generally in a state of unsaturated moisture conditions.

The actual rate soil evaporation is recognized to respond to surface moisture conditions in three distinct stages: constant-rate stage; falling-rate stage; and low-rate stage (Figure 1.5)

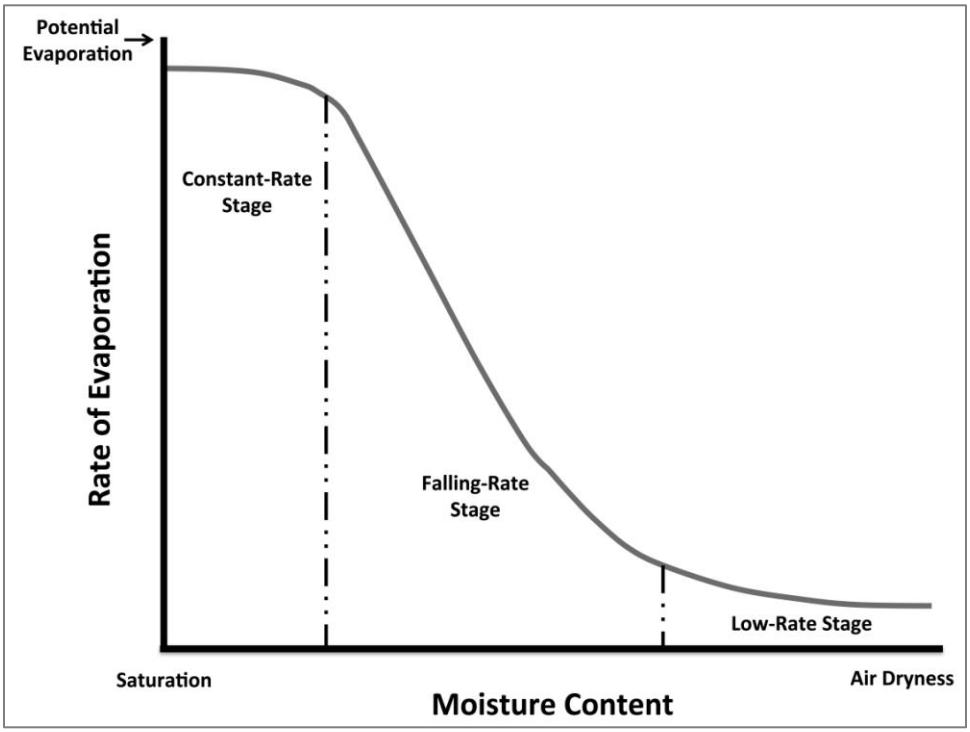

Figure 1.5: The relation between the rate of evaporation from a soil surface and moisture content.

(Holmes, 1961; Ritchie, 1972; Idso *et al*., 1974; Monteith, 1981; Parlange and Katul, 1992; Wilson *et al*., 1997; Aydin *et al.*, 2005). Actual evaporation from a wet soil initially proceeds at a constant-rate approximating the potential evaporation rate, until a surface moisture content threshold is reached (typically field capacity). When this threshold is crossed, the actual rate of evaporation starts to decrease, falling progressively further below the potential rate as the soil surface becomes progressively drier. With time, the soil surface approaches an equilibrium with the overlying atmosphere and the evaporation rate slows to a low-rate stage.

Moisture transfer in the soil occurs primarily in two phases, liquid and vapor (Philip and de Vries, 1957). Therefore, soil can be classified into three distinct moisture layers; liquid, liquid and vapor, and vapor, according to the phases in which moisture moves through them. The soil layer in which moisture transfer occurs only in the liquid phase is associated with the "wet soil

layer” (WSL), and that only in the vapor phase the "dry soil layer” (DSL). The soil layer in which moisture moves in both phases, liquid and vapor, is associated with the "evaporative transformation layer” (ETL) due to the phase transformation of liquid into vapor as a result of evaporation mechanics. A conceptual model that combines the three stages of actual evaporation rates with the development of the WSL, DSL, and ETL can illustrate the dynamics of soil evaporation with time and depth, as follows (Figure 1.6).

1) Stage 1:

The process of soil surface evaporation in the first stage may be treated in the same way as water surface evaporation. The sediment surface is completely saturated as the WSL extends all the way to the sediment surface and therefore the ETL has a thickness that is near zero and vaporization of moisture occurs entirely at the soil surface. Thus, actual evaporation proceeds at a high, constant rate approximating the potential evaporation rate, which is controlled by external atmospheric conditions (radiation, wind speed, air temperature, humidity, etc.).

2) Stage 2:

The second stage of evaporation is associated with a continual decline in the rate of evaporation as the evaporative system transitions from being controlled by the atmosphere to being limited by the soil moisture conditions of the sediment. The WSL has fallen below the soil surface so that vaporization of moisture occurs not only at the surface but also within the soil. Over time moisture availability within the ETL becomes increasing limited due to evaporative drying, and thus the rate of vaporization will continue to decrease with time, which is the key feature of falling-rate evaporation dynamics.

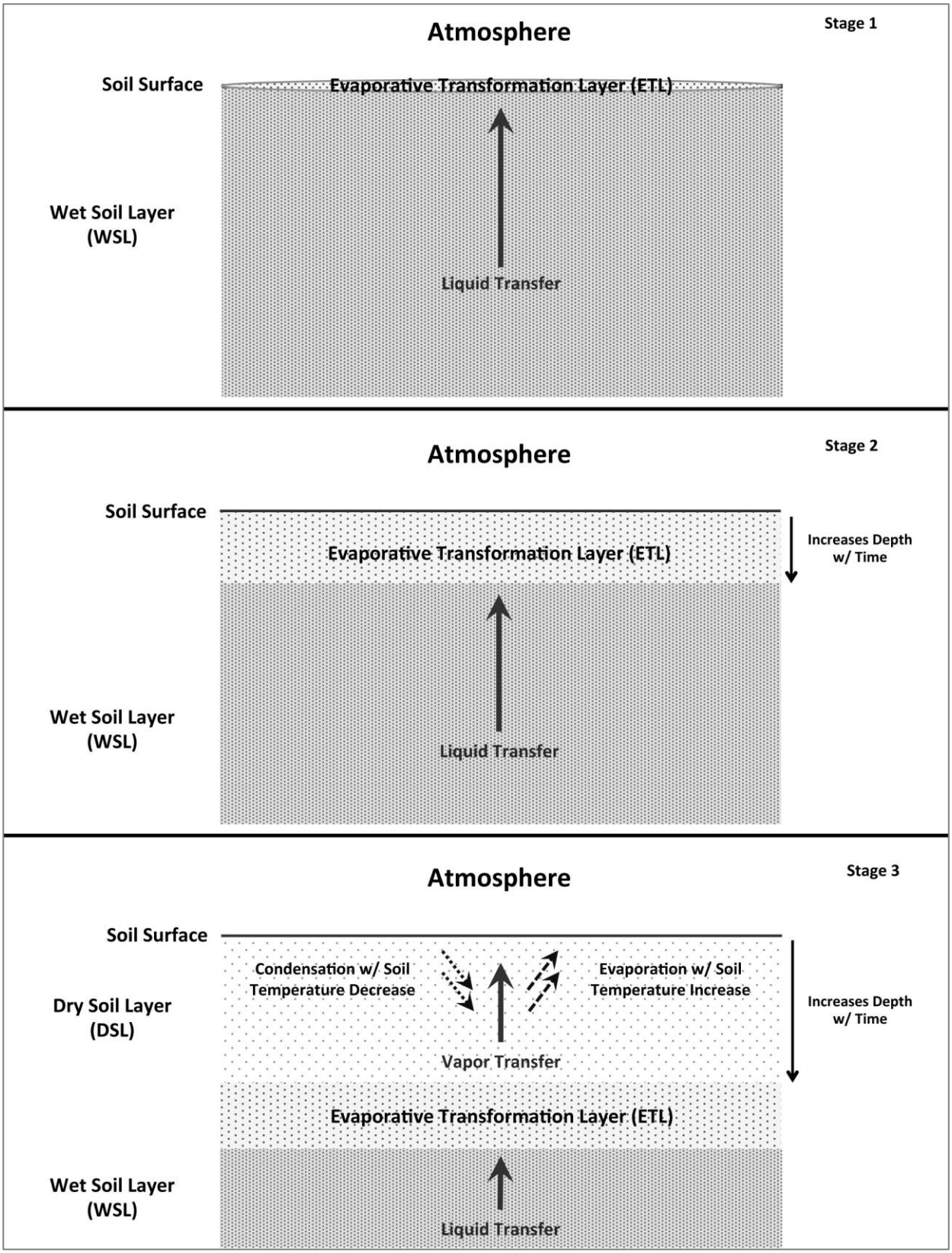

Figure 1.6: Schematic illustration of the conceptual evaporative model

3) Stage 3:

When moisture transfer through the soil consists entirely of vapor flux, the system switches from the falling evaporation rate stage to a near-constant low rate, as a result of vapor movement becoming the dominant mechanism of moisture transport through the DSL to the sediment surface. According to Hillel (1971) and Campbell (1985), the evaporation rate within the dry soil layer is reduced due the differences in the magnitudes of liquid water conductivity and vapor conductivity at the bottom boundary of the DSL. Additionally, recent studies have illustrated that ephemeral vaporization and condensation of atmospheric moisture occurs within the DSL (Yamanaka *et al.*, 1997; Yamanaka *et al.*, 1998; Yamanaka and Yonetani, 1999); outlining that the DSL acts as an evaporation zone during the day and a condensation zone in early evening and overnight.

Based on the above model it is evident that the soil surface will experience different evaporative mechanisms over time. For a deeper understanding of evaporation dynamics during beach sediment drying, more detailed studies of the process of evaporation are necessary and a better understanding of the development of the ETL, DSL, and WSL under field conditions are needed.

1.3.3. Sediment Grain Size

The grain size characteristics of native beach sediment represent one of the most important factors controlling the moisture retention properties, hysteresis, and hydraulic conductivity of the sediment column (Terzaghi, 1943; Childs, 1969; Hillel 1971; Hillel 1980; Hanks 1992; Fredlund and Rahardjo, 1993). These properties in turn influence the capillary

dynamics of the beach hydrological system and thereby play a major role in influencing the spatial and temporal dynamics of surface moisture.

The moisture retention properties of the sediment profile are a function of the soil suction relative to a pressure head above the water table and the physical water content of an unsaturated soil at that same pressure head (Childs and Collis-George, 1950; Brooks and Corey, 1964; van Genuchten, 1980). Soil suction arises due to the formation of curved water menisci at the air–water interfaces within the soil pores. At a basic level the pores of a porous medium can be idealized to function as capillary tubes and based on the capillary relation the relationship between soil suction/pressure head (*h*) and soil moisture content can be established depending upon the pore characteristics of the soil medium. A number of researchers have demonstrated that these pore characteristics scale in direct proportion to the representative grain size (e.g., Gupta and Larson, 1979; Arya and Paris, 1981; Haverkamp and Parlange, 1986; Fredlund *et al.*, 1994; Aubertin *et al.*, 2003). Therefore, sediment systems with contrasting grain sizes will equilibrate at different moisture contents at any given height above the water table. The relationship that develops dictates that the smaller the grain size of the soil material, the greater the moisture retention of that soil will be at any particular suction magnitude. Thus larger grained sediments will exhibit a lower moisture content value in comparison to finer grain sediments at the same pressure head above the water table (Figure 1.7).

The moisture retention properties of the soil column are generally calculated under steady-state linear one-dimensional capillary conditions (Childs and Poulovassilis, 1962). However, capillary water flow of natural environments such as beaches tend to exhibit a non-linear behavior due to hysteresis effects and variations in the hydraulic conductivity of

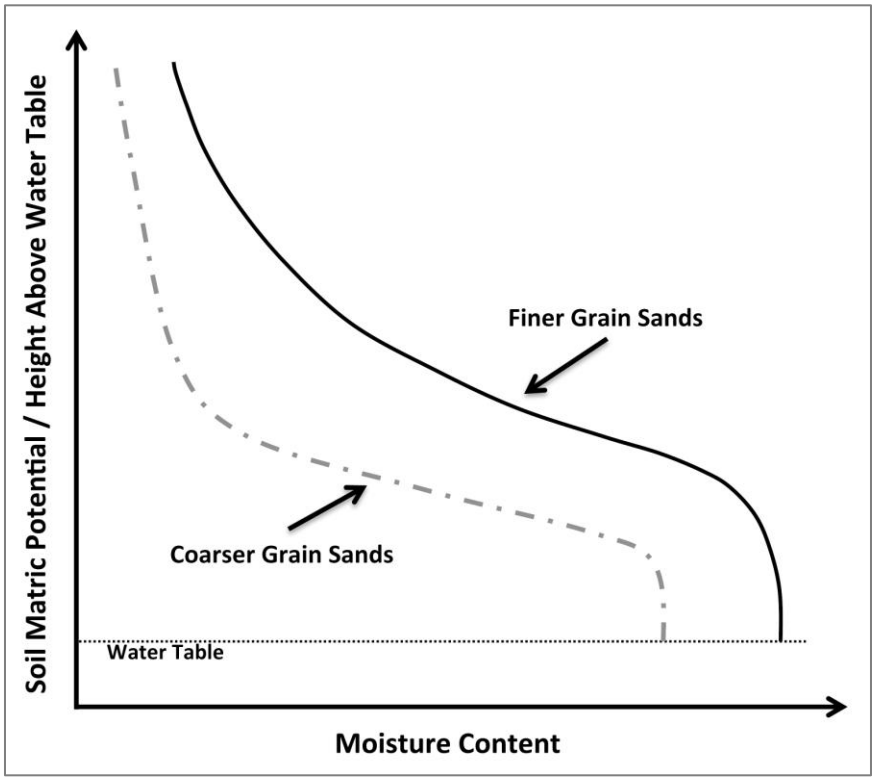

Figure 1.7: Representation of the capillary moisture retention properties of the soil column for different grain-sizes.

unsaturated soils. Since the classic work of Haines (1930), hysteresis in the moisture retention relation during wetting-drying cycles has become accepted as a fundamental aspect of capillary water flow behavior. Although hysteresis can occur due to several causes (i.e., air entrapment from restricted pore connectivity, pore contact angle variations, etc.), Miller and Miller (1956) postulated that hysteresis effects primarily arise because of the existence of different pore structures within a soil medium. In general, a soil medium can be simply characterized by two basic pore structures, the pore body and pore throat. Pore bodies are angular voids that are interconnected through narrow pore throats (Nimmo, 2004). During a drying cycle higher moisture contents are maintained at any given suction/pressure head relative to a wetting cycle, because soil drainage is controlled by the narrow pore throats, which require lower

suction/pressure head potential to empty. Conversely, rewetting of the soil requires increasing the suction/pressure head potential high enough to allow water entry into the larger pore bodies (Figure 1.8).

Since the hysteretic nature of capillary water during the wetting-drying cycles is a function of the pore structure within the soil medium and the pore structure characteristics scale in proportion to the representative grain size of the soil medium, it is possible to elucidate the general control that grain size will have on hysteresis dynamics (Barbour, 1998). A number of studies have illustrated that hysteresis effects decrease with increasing grain-size (e.g., Tokunaga *et al.*, 2004; Yang *et al.*, 2004; Gallage and Uchimura, 2010). Gallage and Uchimura (2010) suggested that the reasons for this behavior are the higher pore-volume and lower suction potential of coarser-grained soils. In other words, soils with large pore sizes require a smaller/larger suction (pressure head) value in order to commence desaturation/saturation of the soil pores. There is then a faster rate of water exchange from the soil pores and thus a decrease in the hysteretic effect.

In addition to hysteresis effects, variations in hydraulic conductivity have a profound effect on the capillary water flow behavior of the sediment profile. Hydraulic conductivity is the measure of a soil medium's ability to transmit water through the interconnected voids of the porous material (Hillel, 1971; Hanks, 1992). The flow of water through an unsaturated soil is driven by a hydraulic gradient that occurs in the direction of increasing hydraulic potential, and its rate is inversely proportional to the magnitude of the potential gradient (Campbell, 1974). For unsaturated soils, water is subjected to a negative hydraulic pressure potential corresponding to a suction gradient magnitude, which constitutes the primary force moving

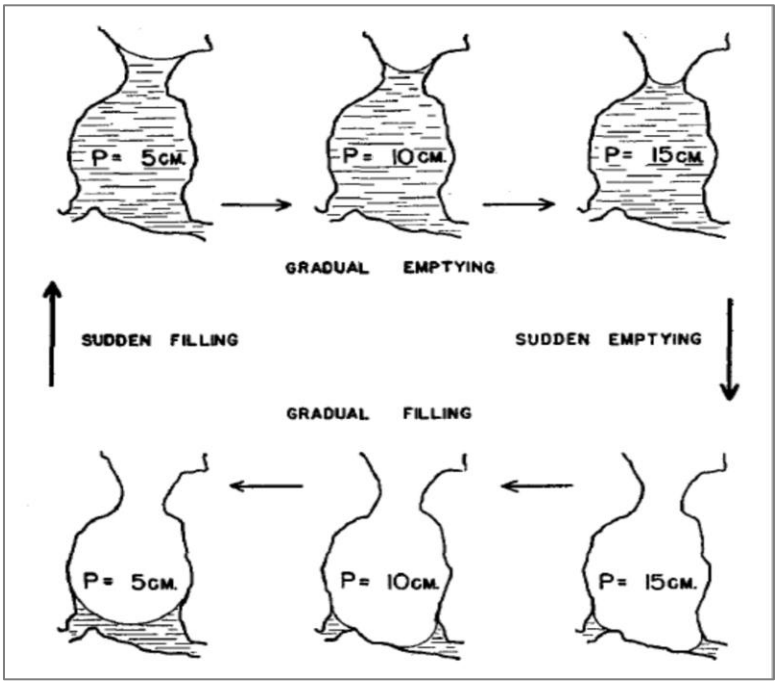

Figure 1.8: Schematic representation illustrating the control of pore structure characteristics on hysteresis. After: Miller and Miller, 1956

water through the soil from lower to higher suction/pressure head values. With increasing suction/pressure head, the first pores to empty are the largest ones, which are the most conductive, thus relegating flow to the smaller pores, and therefore, the conductive potential of the soil decreases.

A number of investigators have related the hydraulic conductivity of a soil to a representative grain size (e.g., Mualem, 1976; van Genuchten and Nielsen, 1985; Raats, 1992; Durner, 1994; Kosugi, 1999; Assouline 2005, Tokunaga, 2009). Results from these studies show that at low suction/pressure heads, which equates to saturated/near-saturated soil moisture conditions, the hydraulic conductivity for coarser grained soils is typically greater than that of finer grained soils. However, with increasing suction/pressure head the conductivity of the coarser soils will decrease more steeply as the larger pores drain; and thus the coarser soil will

have lower unsaturated hydraulic conductivities than finer soils at the same larger suction/pressure head values. Figure 1.9 shows a generalized relationship between conductivity and suction/pressure head in soils of different grain size.

The variation in hydraulic conductivity between grain sizes has important implications for soil capillary dynamics. It suggests that processes taking place in saturated/near-saturated soil conditions are inherently faster than those occurring in drier soil conditions. Therefore, at high suctions/pressure heads equating to lower moisture contents, the conductivity may become so low that very steep suction gradients are required for any appreciable flow to occur, resulting in very long times for capillary water flow, especially with coarser grain-sizes (Hillel, 1971).

These phenomena clearly demonstrate that varying sediment grain size characteristics will have a very substantial impact on the capillary dynamics of the beach hydrological system and thus will strongly influence the moisture dynamics of the beach surface. Although our theoretical understanding of the influence of sediment grain size on the capillary dynamics is sound, very few studies have attempted to document and quantify the subsequent influence that grain size has on controlling beach surface moisture dynamics (Malaya and Sreedeep, 2012).

1.4 Chapter Outlines

Chapters 2-4 are laboratory experiments that were designed to improve understanding of capillary water flow in relation to beach surface moisture. Chapters 2 and 3 focus on

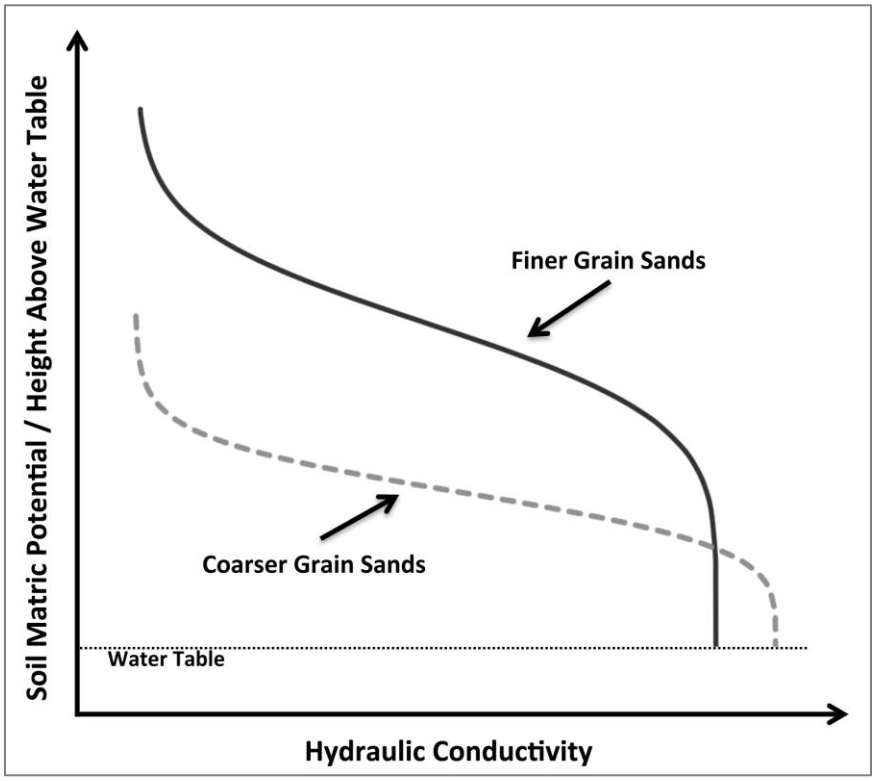

Figure 1.9: Representation of hydraulic conductivity properties of the soil column for different grain sizes.

identifying the hysteretic nature and transient time lags of capillary water flow in a beach sand column beach sand column, and evaluate the utility of established capillary models to simulate surface moisture content. Chapter 4 documents the effect of sediment grain size on hysteresis and transient time lag effects, and on how these factors influence beach surface moisture content. Chapter 5 examines the role of evaporation and condensation on beach surface moisture content, primarily focusing on improving our understanding of evaporation over time and at depth. Chapters 6 and 7 document, analyze, and model the spatial and temporal surface moisture patterns of a natural beach environment. Chapter 6 presents results from a series of field experiments designed to measure the interrelationships between evaporation, groundwater fluctuations, and soil moisture content, and evaluates the relative strength of

these factors in controlling surface moisture variability. Chapter 7 assesses the viability and accuracy of capillary flow models for simulating and predicting spatial and temporal variations of surface moisture content.

Chapter 2 -- Measurement and Modeling of Moisture Content Above an Oscillating Water Table: Implications for Beach Surface Moisture Dynamics

2.1 Introduction

Beach environments often have very shallow water table depths (centimeters to a few meters), resulting in the capillary zone above the groundwater table reaching the beach surface (Atherton *et al.*, 2001; Yang and Davidson-Arnott, 2005; McKenna Neuman and Langston, 2006; Zhu, 2007; Namikas *et al.*, 2010). Therefore, the dynamics of the beach groundwater system will thus play a key role in regulating the status of beach surface moisture (Atherton *et al.*, 2001; Zhu, 2007; Namikas *et al.*, 2010).

In theory, the response of beach surface moisture content to beach groundwater dynamics can be established relatively easily and accurately based on knowledge of i) the vertical profile of moisture in the sediment column, ii) the elevation of the sand surface above the water table, and iii) the magnitude and rate of water table fluctuation (Raubenheimer *et al.*, 1999; Ruz and Meur-Ferec, 2004; Chuang and Yeh, 2006; Zhu, 2007). In reality, however, the hydrological dynamics of a beach system are rarely simple. Capillary water flow within the sediment column tends to exhibit a non-linear, hysteretic behavior as well as experience transient water flow time lags. Although this hysteresis effect has long been recognized (Haines, 1930), there is some debate in the literature regarding the need for inclusion of hysteresis in modeling of periodic unsaturated groundwater movement (i.e., Childs and Poulovassilis, 1962; Childs, 1969; Raats and Gardner, 1974; Kessler and Rubin, 1987; Hinz, 1998; Raubenheimer *et al.*, 1999; Nielsen and Perrochet, 2000; Werner and Lockington, 2003; Cartwright *et al.*, 2005; Cartwright *et al.*, 2009). Furthermore, time-dependent signals in surface moisture content associated with the transient nature of capillary water flow are poorly understood and have largely been

ignored within the literature. Therefore, our understanding of beach surface moisture dynamics above an oscillating water table includes at least two key sources of uncertainty: i) the magnitude of hysteresis effects during periods of water table rise and fall, and ii) the time lags associated with transient water flow.

To date only a few studies have attempted to link oscillating groundwater dynamics to variability in beach surface moisture content (i.e., Raubenheimer *et al.*, 1999; Atherton *et al.*, 2001; Zhu, 2007; Namikas *et al.*, 2010); and none of these studies incorporated hysteresis effects and transient water flow dynamics in their analyses. The primary objective of the present study is to document the response of surface moisture contents to tidally induced groundwater dynamics and identify the influence of hysteresis and transient flow effects.

2.2 Methods

2.2.1 Laboratory Experimental Design

The experimental apparatus employed in the study consists of a square PVC tube 122 cm in height with a cross-sectional area of 144 cm^2 (12 cm x 12 cm), partially immersed in a reservoir of water (Figure 2.1). The tube was filled with a very well sorted fine to very-fine quartz sand obtained from a beach at Padre Island National Seashore on the Texas Coast of the Gulf of Mexico with a mean grain size of 0.13 mm (2.94 phi, Figure 2.2). The tube was perforated below the low waterline to allow free exchange of water with the tank, and the perforated section was screened with fine mesh to retain sediment in the column. A diaphragm-metering pump was used to raise and lower the water level in the reservoir, to simulate tidally induced groundwater fluctuations. A pressure transducer installed at the base of the water reservoir

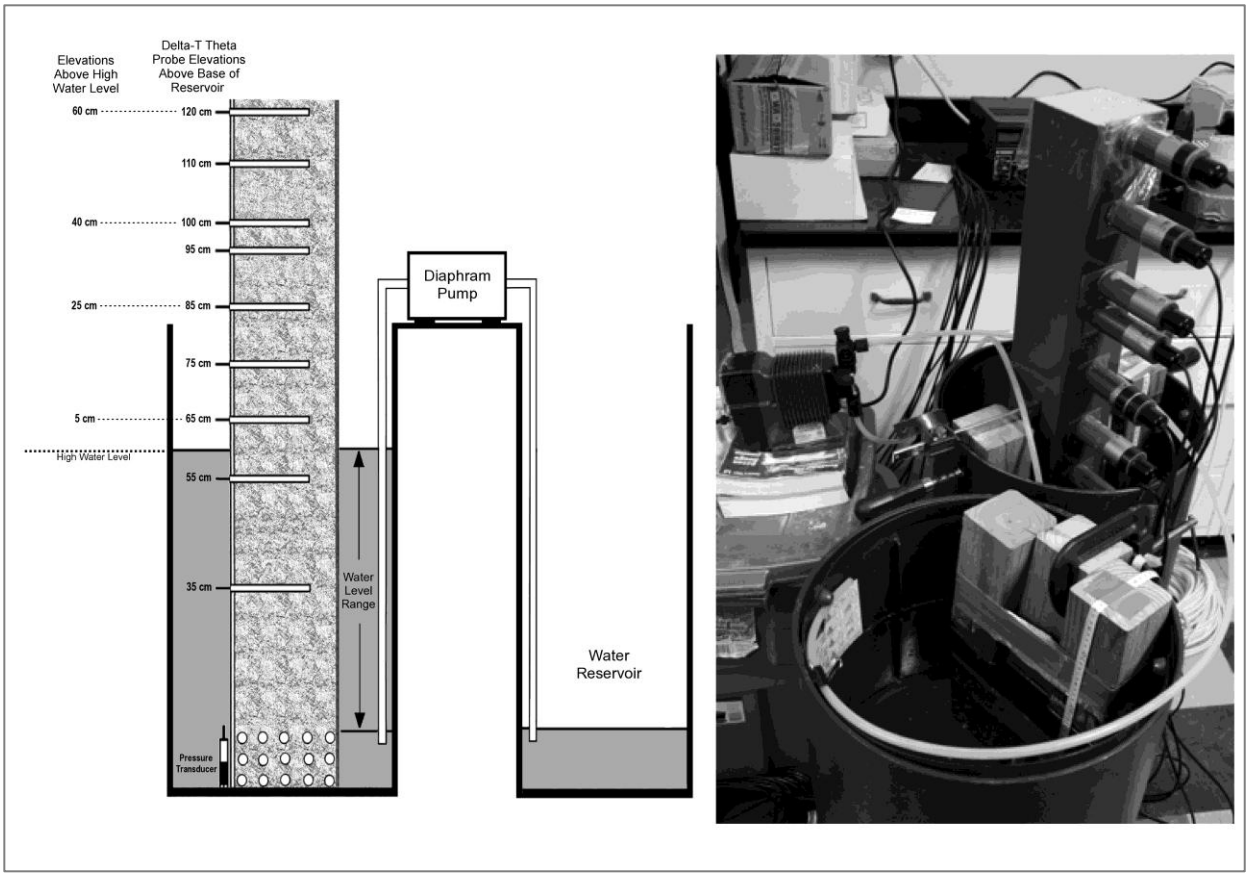

Figure 2.1: Schematic (left) and photograph (right) of the laboratory experimental apparatus

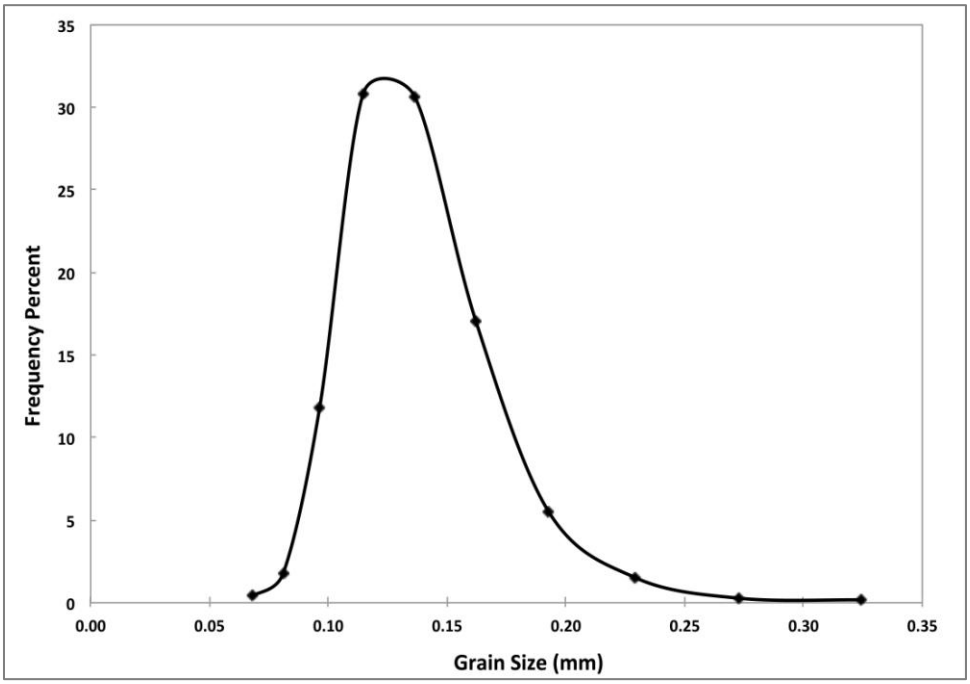

Figure 2.2: Grain size analysis

was used to monitor water table elevation throughout each of the experimental runs. Changes in the vertical profile of moisture content within the sediment column were monitored at five-minute intervals using an array of Delta-T Theta probes inserted in the sediment column at elevations of 35, 55, 65, 75, 85, 95, 100, 110, and 120 cm above the base of the reservoir (Figure 2.1). To isolate the influence of groundwater oscillation and capillary transport, the top of the PVC tube was sealed with plastic wrap to prevent evaporative losses or condensation inputs at the upper surface of the sediment column. All sensors were cabled to a Campbell Scientific data logger for recording.

Three individual experimental runs were conducted with vertical water table fluctuations of 25, 40, and 55 cm, respectively. The high water elevation was fixed at 60 cm above the base of the reservoir in all three experiments and the elevation of low water was varied, so that the moisture probe positions could be held constant relative to high water. The water table ranges employed here were chosen to be representative of fluctuations reported for various positions (fore beach, middle beach, and back beach) on northern Gulf of Mexico beaches (Zhu, 2007; Namikas *et al.*, 2010).

Before each experimental run the sediment column was completely saturated and the water level within the reservoir was set at the high water table elevation of 60 cm from the base of the reservoir. The system was left undisturbed for 10 days to allow gravitational drainage and moisture retention in the sediment column to reach equilibrium. After this equilibration period the water level in the reservoir was cyclically lowered and then raised at each desired water table fluctuation increment over an osculation period (fall and rise) of 24 hours, via the diaphragm-metering pump. This cycle was repeated 5.5 times for a sequence of

132 hours. To eliminate the transitional period that occurred as the system shifted from a static equilibrium with a stationary water table to a dynamic equilibrium with a fluctuating water table, the analysis presented herein includes only the data collected between hours 36 to 132 (96 total hrs) for each experimental run.

2.2.2 Surface Moisture Content Data Analysis

To analyze the influence of water table fluctuations on moisture dynamics at various surface elevations above the water table, the measured moisture contents at four Delta-T Theta probe elevations within the sediment column were used as proxies to represent 'true' surface elevations above a fluctuating water table. In the following analyses, the Delta-T Theta probes located at elevations of 65, 85, 100, and 120 cm above the base of the reservoir were employed as representative 'true' surface elevations of 5, 25, 40, and 60 cm above the high water table, respectively (Figure 2.1). Additionally, the moisture dynamics at these individual 'true' surface elevations were analyzed under specific water table fluctuation conditions. The 5 cm elevation was analyzed using the 55 cm water table oscillation, whereas the moisture dynamics at the 25 cm and 40 cm elevations were examined utilizing the 40 cm water table oscillation range, and lastly the moisture dynamics at the 60 cm elevation was investigated under the smallest water table oscillation range of 25 cm. These surface elevation/water table fluctuation relations were selected based on documented water table oscillation ranges and water table depths from fieldwork conducted across the central Texas coast for various fore beach, middle beach, and back beach locations on northern Gulf of Mexico beaches (i.e., Zhu, 2007; Namikas *et al.*, 2010).

These analyses represent only a subset of the entire collected data. Although the moisture conditions across a full soil profile were recorded for the various water table oscillation ranges, the analyses presented in this chapter focus only on the moisture/pressure head/water table dynamics associated with various positions across a beach surface. It is not the intent of this chapter to focus on the hydrological dynamics below the surface layer.

2.2.3 Surface Moisture Content Models

Surface moisture contents were modeled using hysteretic and non-hysteretic capillary water flow simulations via the HYDRUS-1D computer software program developed by Šimůnek *et al.* (1998). HYDRUS calculates hysteretic water flow in the sediment profile by numerically solving the empirically-derived hysteretic function developed by Scott *et al.* (1984), which was further modified by Vogel *et al.* (1996) in order to incorporate hysteresis in the hydraulic conductivity function. Non-hysteretic water flow in the sediment profile is calculated within HYDRUS by numerically solving the Richards (1931) one-dimensional water flow equation.

2.2.3.1 Hysteretic Model

Modeling hysteretic capillary water flow modeling requires that both the main drying and wetting boundary moisture retention, $\theta^d(h)$ and $\theta^w(h)$ and unsaturated hydraulic conductivity, $K^d(h)$ and $K^w(h)$ curves are known. Once the soil hydraulic functions have been ascertained, the model implements a scaling procedure designed to simplify the variability in the unsaturated soil hydraulic properties in the direction of flow. The model dictates that the variability in the hydraulic properties of a given soil profile can be calculated through a set of

scaling transformations, which relate the soil hydraulic characteristics, $\theta(h)$ and $K(h)$, to reference characteristics, $\theta^*(h)$ and $K^*(h)$. The drying and wetting moisture retention, $\theta^d(h)$ and $\theta^w(h)$ and unsaturated hydraulic conductivity, $K^d(h)$ and $K^w(h)$ curves are thus described as follows:

$$\begin{aligned} \theta^d\ h\ &= \theta_s + \alpha_\theta\ \theta^{d*}\ h\ + \theta_r \\ \theta^w\ h\ &= \theta_r + \alpha_\theta\ \theta^{w*}\ h\ + \theta_s \end{aligned} \qquad [1]$$

and

$$\begin{aligned} K^d\ h\ &= \alpha_K K^{d*}(h) \\ K^w\ h\ &= K_r + \alpha_K K^{w*}(h) \end{aligned} \qquad [2]$$

in which, α_θ and α_K are mutually independent scaling factors for the water content and the hydraulic conductivity, respectively. The technique is based on the 'similar media concept' introduced by Miller and Miller (1956) for porous media, which differ only in the scale of their internal geometry.

2.2.3.2 Non-Hysteretic Model

Modeling one-dimensional uniform, isothermal, vertical water flow in a partially saturated porous medium is described by the Richards (1931) equation under the assumptions that the air phase plays an insignificant role in the liquid flow process and that water flow due to thermal gradients can be neglected:

$$\frac{\partial \theta}{\partial t} = \frac{\partial}{\partial z}\ K\ h\ \ \frac{\partial h}{\partial z} + 1\ \ - S \qquad [3]$$

in which θ is the volumetric water content, t is time, z is the vertical coordinate (upward from

water table), $K(h)$ is the unsaturated hydraulic conductivity function [see equation 4], h is the pressure head elevation above the water table, S is water sources and sinks.

2.2.4 Moisture Retention Curves and Hydraulic Conductivity

Although a number of models have been developed, the analytical form of the soil hydraulic functions proposed by van Genuchten (1980) has been shown to match experimental data more satisfactorily than others (Stankovich and Lockington, 1995; Cornelis *et al.*, 2001). The expressions of van Genuchten (1980) are given by:

$$\theta\ h\ = \theta_r + \frac{\theta_s - \theta_r}{1+\ \alpha h^{\ n\ m}}$$
$$K\ h\ = \mathrm{K_s}\Theta^{\lambda}\ 1 -\ \ 1 - \Theta^{1/\ m\ \ \ m\ 2} \qquad [4]$$

in which, θ_r and θ_s denote the residual and saturated water contents, respectively, α is an empirical parameter denoting the inverse of the air-entry value, n is an empirical parameter representing the pore-size distribution index of the soil profile, m = 1-(1/n), K_s is the saturated hydraulic conductivity, Θ is the effective degree of saturation [= (θ - θ_r)/(θ_r - θ_s)], and λ is a pore connectivity parameter derived by Mualem (1976) to equal 0.5. To designate the main drying and wetting main boundary moisture retention and unsaturated hydraulic conductivity curves the function parameters θ_r, θ_s, α, n, m, and K_s are denoted with superscripts d and w to indicate either a drying or wetting curve, respectively. Additionally, the following restrictions are expected to hold in most practical soil profile applications: $\theta_r^{\ d} = \theta_r^{\ w}$, $\alpha^d \leq \alpha^w$, $n^d = n^w$, and $K_s^{\ d} = K_s^{\ w}$.

Based on moisture content measurements collected at each of the moisture probe elevations, the main drying, wetting, and non-hysterestic moisture retention and unsaturated

hydraulic conductivity curves were constructed. Figure 2.3 shows the calculated drying and wetting moisture retention, calculated drying and wetting hydraulic conductivity curves as well as the non-hysteresis moisture retention and hydraulic conductivity curves, in which θ_r = 0.09 cm^3/cm^3, θ_s = 0.4448 cm^3/cm^3, n = 4.931, m = 0.797, and K_s = 30.68 cm/hr for the drying, wetting and non-hysteresis moisture retention and unsaturated hydraulic conductivity curves; whereas α^d = 0.019, α^w = 0.034 for the drying and wetting curves, respectively, and α = 0.025 for the non-hysteresis moisture retention curve.

2.3 Results

2.3.1 Surface Moisture Response

The response of surface moisture content to water table fluctuations is illustrated in Figure 2.4. Several trends in moisture content are clearly apparent among the various sediment surface elevations. First, there is a noticeable decrease in both absolute moisture content and the range in moisture content with increasing elevation at high water level. At an elevation of 5 cm, moisture content varied from a low of 22% to a high of 44% (by volume). As the surface elevation increases to 60 cm above high water, the range in surface moisture content is reduced to 11-14%.

A second trend apparent in Figure 2.4 is a decrease in the symmetry of the moisture content traces with decreasing surface elevation. With a near-surface water table, the surface moisture content remains steady for a substantial period of time following the transitions between both a rising and falling water table. This is strongly evident at the 5 cm elevation, and although present at the 25 cm elevation the occurrence is clearly muted. These observations

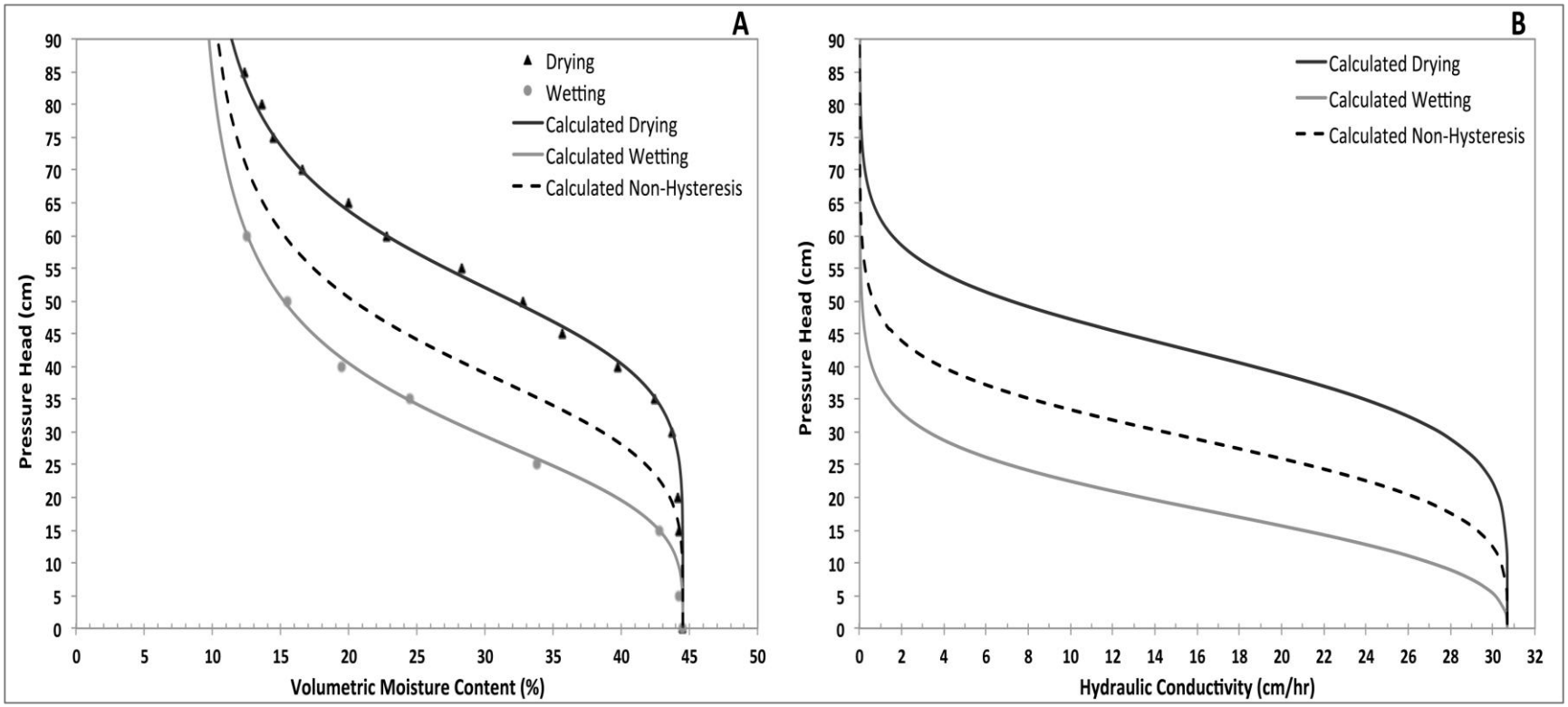

Figure 2.3: Measured volumetric moisture content measurements collected at the high water table and low water table pressure head conditions, and the calculated van Genuchten (1980) boundary wetting, drying and non-hysteresis moisture retention curves (A). The calculated van Genuchten (1980) boundary wetting, drying, and non-hysteresis unsaturated hydraulic conductivity curves (B). The pressure head is equivalent to the height of the surface above the water table.

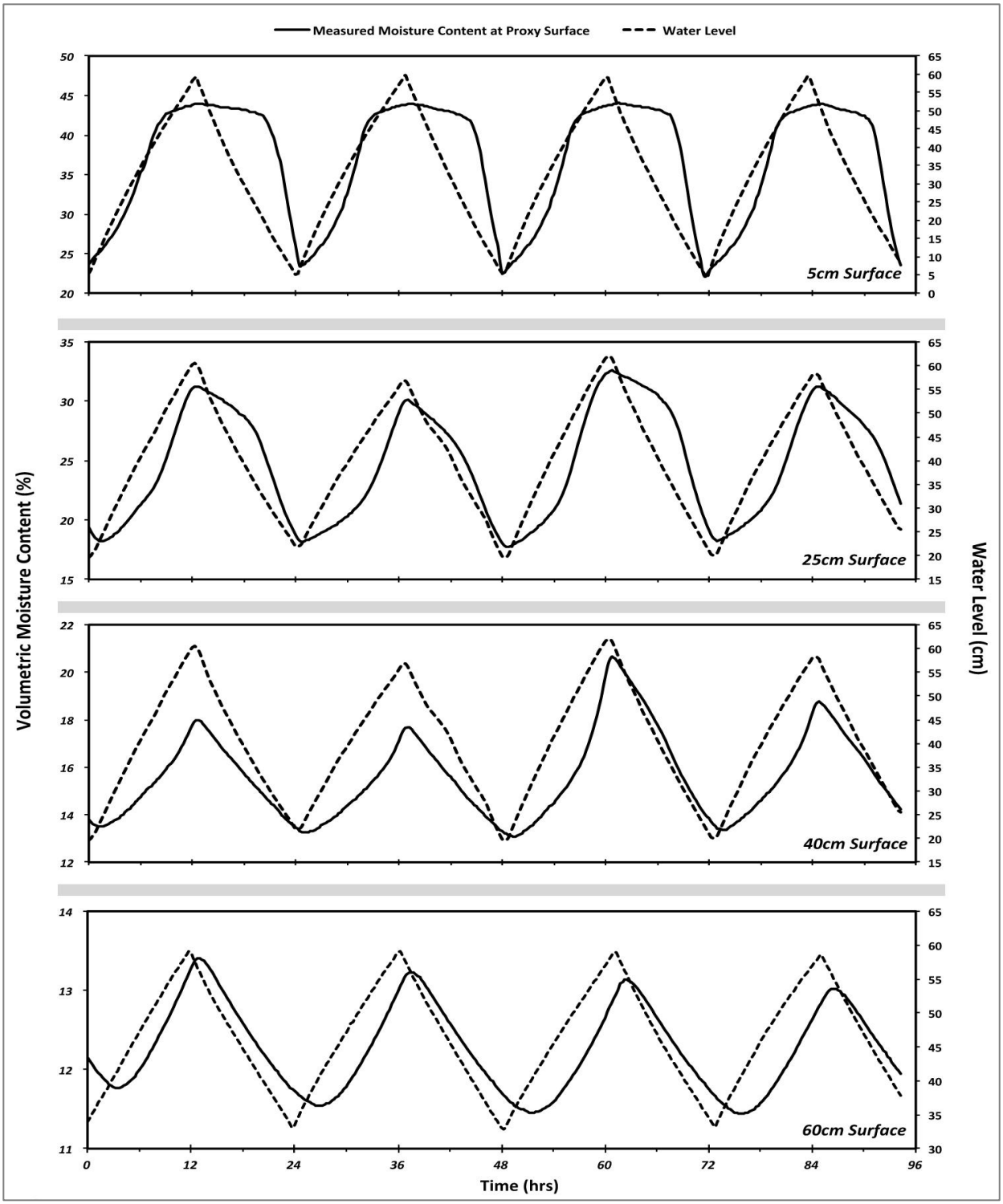

Figure 2.4: Variations in volumetric moisture contents and water level period at each of the four 'proxy' surface elevations. The 60 cm surface elevation was associated with a water level fluctuation of 25 cm, where as the 40 and 25 cm elevations were subjected to a water level fluctuation of 40 cm, and the 5 cm surface elevation experienced a 55 cm water level fluctuation.

correspond well with the findings of Zhu (2007) for the fore beach zone and are associated with an aspect of hysteresis known as Haines Jump (after Haines 1930), or the inkbottle effect. Haines Jump hysteresis is a water flow process dependent upon the nature of the pressure head at which individual pores drain and fill (Miller and Miller, 1956; Childs, 1969). As the pressure head within the soil column increases in association with a drying sequence, the moisture content within the soil column stays at a wetted level until the soil matric suction at a particular pressure head becomes too large. At that point the sediment column will abruptly drain. Conversely, as the pressure head within the soil column begins to decrease associated with a wetting sequence, the soil moisture content will remain at a relatively constant moisture content until the soil matric suction decreases to a point where the soil column will abruptly fill. At the 5 cm elevation, moisture contents corresponding with a rising water table reached a maximum saturated level on average a few hours prior to actual high water level occurring (Figure 2.5). This observation should be expected based on the moisture retention curve of the sediment column, which illustrates a near-saturated capillary fringe extending approximately 15 cm above the water table during a wetting sequence. As the water table rises within the sediment column, the advancement of the capillary fringe saturates the surface layer prior to the maximum water level occurring.

Finally, at each surface elevation the measured moisture contents lag significantly behind water table oscillations. Table 2.1 illustrates the average time lags between the measured minimum and maximum moisture contents and the associated low and high water table levels. There are two apparent patterns in regard to the time lag behavior. First, the

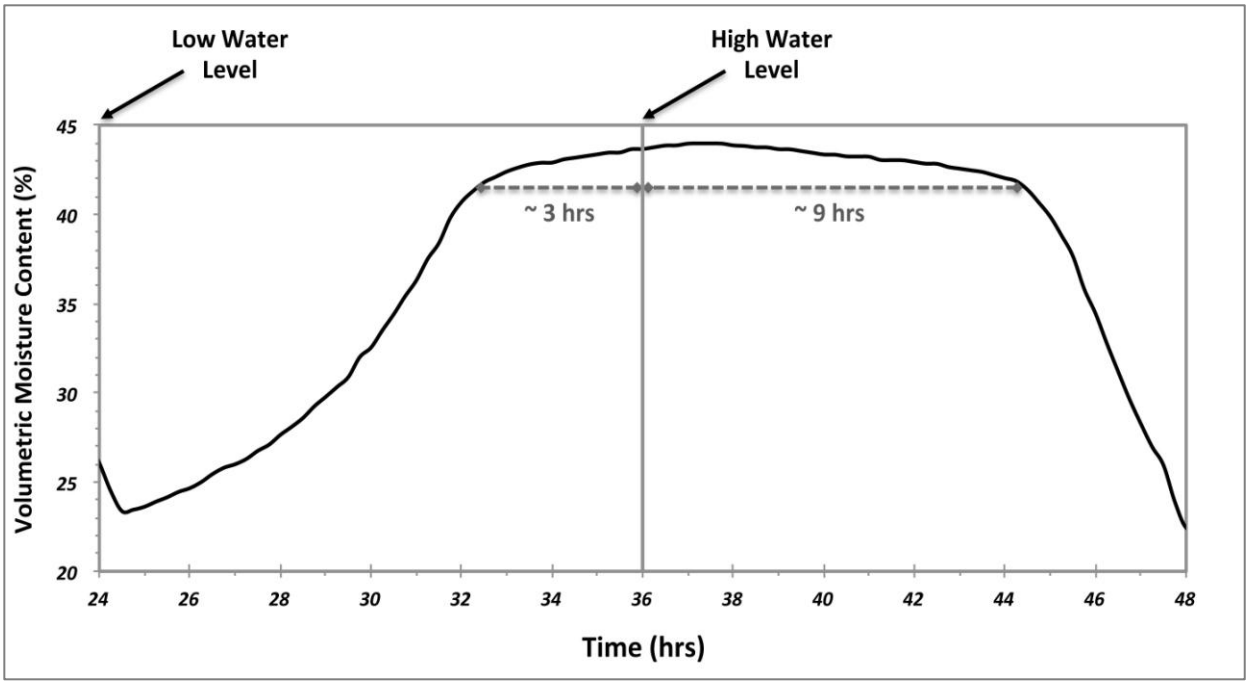

Figure 2.5: A 24-hour time sequence (24–48 hours) of measured volumetric moisture contents at the 5 cm surface elevation. Moisture content reaches saturated level prior to actual high water level and persists for an extended period of time afterwards.

Table 2.1: Average time lags (minutes) between min/max moisture contents and low/high water table levels.

Surface Elevation	Low Water Table	High Water Table
5 cm	38	N/A***
25 cm	58	42
40 cm	105	61
60 cm	185	89

*** In every case the surface content reached saturation ~ 3hrs before high water and remained saturated for some time afterwards.

duration of the lag increased with increasing surface elevation; and second, is the time lags at low water table are larger than high water table.

These results correspond well with the existing literature (Childs, 1969; Kool and Parker, 1987; Hinz, 1998) and can be attributed to the lower hydraulic conductivity values at greater surface elevations above the water table. Figure 2.3B illustrates a decrease in hydraulic

conductivity with increasing pressure head as well as shows that lower conductivity values during the wetting compared to the drying stage at the same pressure head. Accordingly, slower capillary transport will occur after the transitions from a low water table (i.e., wetting conditions) and at greater water table depths, resulting in the larger temporal lag values at the higher surface elevations during low water.

2.3.2 Water Flow Scanning Curves

An efficient way to assess the hysteretic nature of the surface moisture is through evaluation of a sequence of water flow scanning loops. When a wetted soil begins to drain, or when a dry soil column is rewetted, the relation between the pressure head and the soil moisture content follows some intermediate moisture retention curve as it moves from the main wetting or drying branch to the other. Such intermediate retention curves are called scanning curves. A wetting and drying scanning curve sequence forms a scanning loop that falls between the main wetting and drying moisture retention curves (Childs and Poulovassilis 1962; Poulovassilis, 1962). Figure 2.6 shows a single scanning loop (24 hrs) for each of the four surface elevations considered in this analysis. In all four cases the scanning loops illustrate that at a given pressure head higher moisture contents occur during the drying cycle than during the wetting cycle. This finding agrees with the results of Werner and Lockington (2003) and demonstrates that tidally induced groundwater dynamics can have a very strong hysteretic influence on surface moisture contents. At the 5 cm and 25 cm elevations the Haines Jump phenomenon is apparent in the near-horizontal segments of the scanning curve loops. At higher surface elevations (40 and 60 cm) this phenomena is absent. This observation

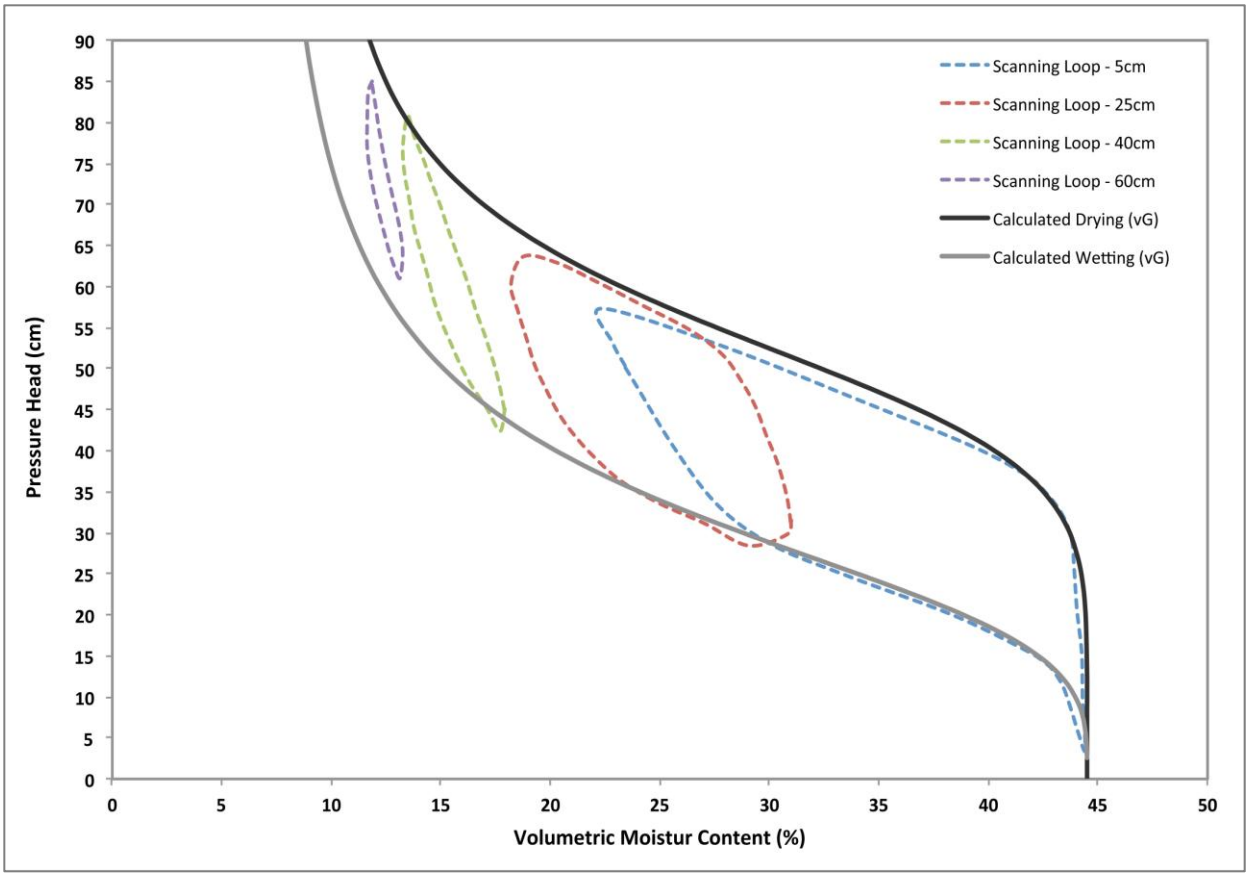

Figure 2.6: Illustration depicting a single water flow scanning loop (24 hours) for each of the four 'proxy' surface elevations. Also shown are the calculated van Genuchten (1980) drying and wetting boundary curves.

corresponds well with those illustrated in the literature, which indicate that Haines Jump effects are more pronounced in the lower pressure head range where individual pores empty at larger pressure heads than those at which they fill (Hillel, 1971; Hillel, 1980; Hanks, 1992).

2.3.3 Hysteresis and Non-Hysteresis Simulations

A comparison between the simulations from the two approaches relative to measured surface moisture content is depicted in Figure 2.7. At the 5 cm surface elevation the hysteresis model produces values that are quite close in predicting the range of surface moisture contents. However, the non-hysteresis model over-predicts the moisture fluctuation range as

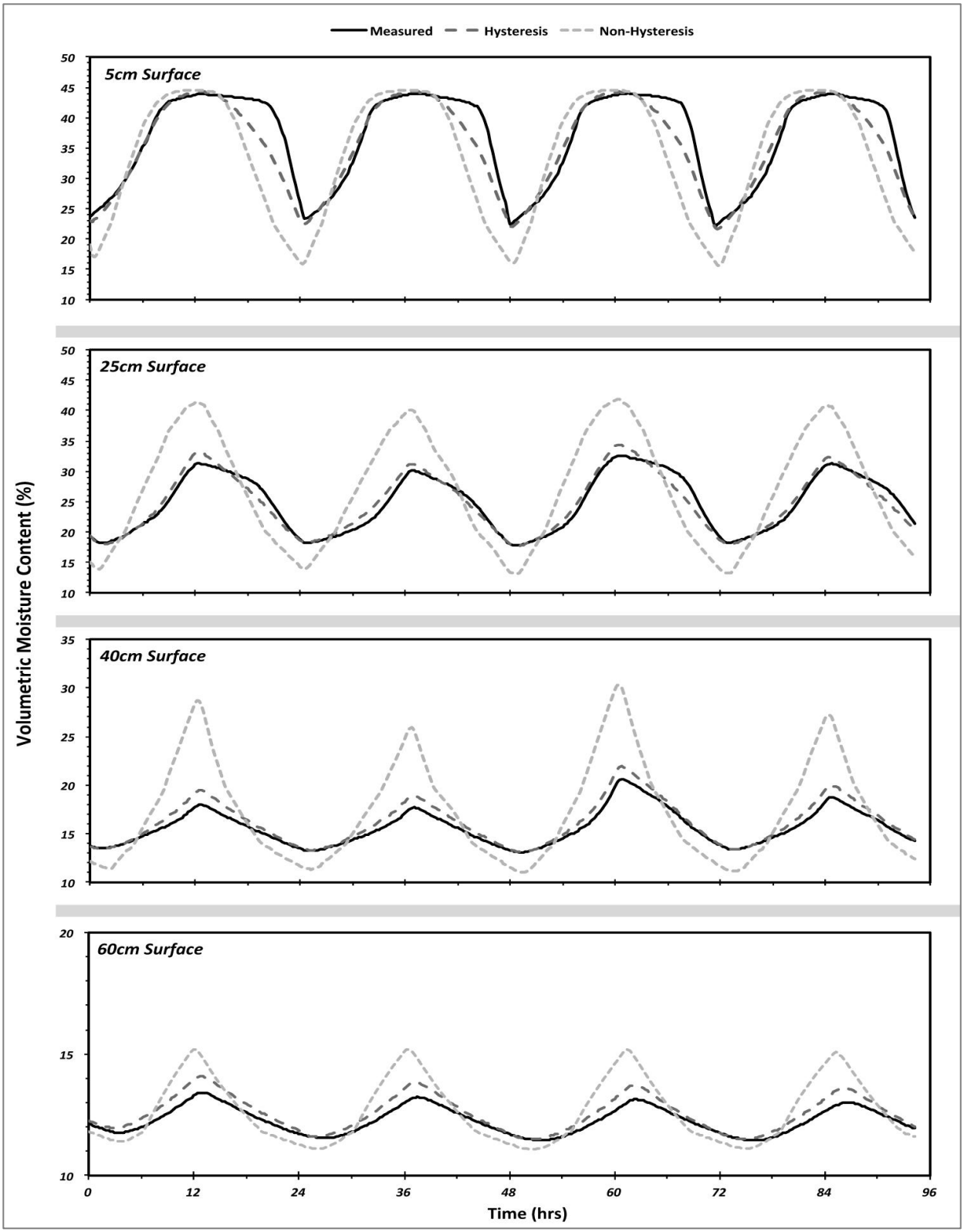

Figure 2.7: Hysteretic and non-hysteretic model simulations relative to measured volumetric moisture contents for each of the four 'proxy' surface elevations conducted throughout this study.

the model vastly under-estimates moisture content values at the low water table levels. Additionally, both approaches fail to adequately capture the Haines Jump effect. This latter aspect of the system dynamics clearly requires additional attention. Furthermore, with increasing surface elevation above the water table, the non-hysteretic model consistently over-predicted and under-predicted moisture contents values at the high and low water table levels, respectively, where as the hysteresis model only over-predicted moisture contents at the high water table levels, as the model produced relatively accurate simulated moisture content values at the low water table levels. These findings clearly demonstrate that the utilization of hysteretic water flow calculations provides a better representation of the observed moisture contents compared to non-hysteretic simulations. These findings correspond well with those previously presented in the literature (Stauffer, 1996; Lehmann *et al.*, 1998; Stauffer and Kinzelback, 2001; Werner and Lockington, 2003).

A quantitative assessment of the simulations was conducted by calculating the standard error (SE) in predicted volumetric moisture contents for each surface elevation (Table 2.2). It is apparent that the inclusion of hysteresis improves results significantly, as in each case the error magnitude from the non-hysteresis simulations is more than double the error from the hysteresis approach and at the 25 cm and 40 cm surface elevations the errors from the non-hysteresis simulations are nearly four times that of the hysteresis simulations, As illustrated above, this results from the fact that the non-hysteresis simulations both over-predicted moisture content values at the high water table levels and under-predicted moisture contents at the low water table levels. Although at the 60 cm elevation the non-hysteresis simulations both over-predicted and under-predicted moisture contents at the high and low water table

Table 2.2: Standard error (% volumetric moisture content) for hysteresis and non-hysteresis model simulations against measured moisture contents

Surface Elevation	Hysteresis	Non-hysteresis	% Difference
5 cm	2.80	7.22	258%
25 cm	1.65	6.13	372%
40 cm	1.06	3.98	375%
60 cm	0.41	0.93	227%

levels, respectively, the total moisture content range was ~4% moisture so the overall standard error level was very low. Furthermore, at the 5 cm surface elevation the non-hysteresis simulations only under-predicted moisture contents at the low water table levels. Nevertheless, there is a clear benefit from the inclusion of hysteresis in attempts to model surface moisture dynamics.

A remaining question is how well the hysteretic model is able to predict the transient time lags in surface moisture contents. Table 2.3 provides a comparison of the average time lags between the measured moisture contents and the predicted moisture content values for the hysteretic model simulation. At the shallowest surface elevations of 5, 25, and 40 cm, the hysteresis approach very closely reproduced the measured lag values after low water table levels. However, at the 60 cm surface elevation the hysteresis approach significantly underestimated the time lag of capillary water flow, predicting minimum moisture contents on average more than 50 minutes before the measured lag values. Additionally, after the occurrence of high water table levels, the hysteresis simulation predicted moisture values that underestimated the measured transient nature of the sediment column at the 25, 40, and 60 cm by about 10 to 20 minutes. Notably, at the 5 cm elevation the hysteresis approach calculated a time lag of 26 minutes after high water whereas the measured values show

Table 2.3: Comparison of the average time lags (minutes) between max/min moisture contents and high/low water table levels for the measured and hysteresis simulation approach.

Surface Elevaton	Low Water Table			High Water Table		
	Measured	Hysteresis	Difference	Measured	Hysteresis	Difference
5 cm	38	27	9	N/A***	26	N/A
25 cm	58	50	8	42	34	11
40 cm	105	98	8	61	46	15
60 cm	187	135	52	89	68	21

*** In every case the surface content reached saturation ~ 3hrs before high water and remained saturated for some time afterwards.

maximum content occurring hours prior to high water. This is an aspect of the system dynamics that merits additional attention, as there is no obvious explanation why the Scott *et al.* (1984) hysteresis model would not capture the saturation of the sediment column associated with the advancement of the capillary fringe. Nevertheless, the hysteresis model produced values that are quite close in capturing the time lag signals in the measured surface moisture contents, and therefore indicates that the hysteresis model is largely able to replicate the transient nature of beach surface moisture dynamics.

2.4 Summary and Conclusion

The primary goal of this study was to document the response of surface moisture contents to an oscillating water table, specifically the influence of hysteresis and transient flow effects on surface moisture dynamics. Several useful findings emerge. First, Haines Jump hysteresis exerts a significant influence on surface moisture dynamics when the water table is near the surface, and surface moisture contents remain steady for a substantial period of time following the transition between a rising and falling water table. Second, a substantial time lag exists between tidally induced water table oscillations and surface moisture content response,

and this time lag increases with increasing surface elevation (relative to the water table). These results indicate that for drier areas of the middle and back beach, capillary water flow in the sediment column could produce surface moisture contents corresponding to water table positions that occurred hours previously.

Simulations of moisture contents from hysteretic and non-hysteretic models illustrated that the utilization of a hysteretic model provides substantially improved accuracy. This finding suggests that studies that employed a non-hysteretic water flow approach to link oscillating groundwater dynamics to variability in beach surface moisture content (i.e., Raubenheimer *et al.*, 1999; Atherton *et al.*, 2001; Zhu, 2007; Namikas *et al.*, 2010) may have drastically overestimated surface moisture contents, particularly across areas of the middle beach and back beach zones.

Chapter 3 -- Justification of the Utilization of 'Proxy' Surfaces to Represent the Moisture Content Dynamics for Comparable 'True' Surface Elevations

3.1 Introduction

During the peer-review process for the publication of Chapter 2 in the journal *Earth Surface Processes and Landforms* (Schmutz and Namikas, 2013), the use of measured moisture content within the sediment profile as a 'proxy' to represent 'true' surface moisture content at the same distance above the water table was questioned by the reviewers. One reviewer completely disagreed with the assumption that moisture content measured at depths below the sediment surface can be used as a 'proxy' for surface moisture content, whereas the other review requested that data should be presented illustrating the variance in moisture data collected at the 'proxy' layer and a 'true' surface layer. This chapter to addresses those concerns and validates the utilization of these 'proxy' surfaces as representations of 'true' surface moisture dynamics. To accomplish this, a theoretical explanation based on capillary theory will be developed and additional laboratory experiments will be conducted to merit this approach.

3.2 Theoretical Justification

The use of below-surface proxies to represent surface moisture content at comparable distances above the water table is reasonable because the presence (or absence) of overburden above a given point in the sediment column should not substantively influence capillary transport below that elevation. Rather, the moisture dynamics at a specified elevation above the water table is a function of the soil matric suction relative to the pressure head (h) above the water table at that elevation (Childs and Collis-George, 1950; Brooks and Corey, 1964; van

Genuchten, 1980). This phenomenon is in effect a function of the theory of capillarity, which simply dictates that water will rise to a specific elevation (*h*) above the water table in a tube of specific radius (Croney and Coleman, 1954; Aitchison, 1960). This process results from the formation of a suction gradient which develops in the tube, as the pressure in the tube is less than that at the water table; in effect the smaller the radius of the tube the larger the suction gradient/pressure head and thus the higher the water will rise.

At a basic level, the soil pores of a porous medium can be idealized to function as a set of capillary tubes and thus based on the theory of capillary a relationship for the moisture content at a specific elevation (*h*) above the water table can be determined based on the suction gradient/pressure head at that elevation. In essence, an increase in the suction gradient/pressure head associated with increasing elevation above the water table results in the emptying of the larger soil pore cavities until, at very high suction values; only the very narrow pore cavities are able to retain water. Therefore an increase in suction/pressure head is associated with a decrease in the moisture content of the sediment (Childs, 1969). Since the prevailing suction/pressure head at any specified elevation above the water table is related to the moisture content of the soil at that elevation, a relationship between soil moisture content and soil matric suction/pressure head can be determined. Thus, the moisture content of the sediment at a specified height above the water table is ultimately a function of the matric suction/pressure head at that elevation above the water table; and the presence or absence of overburden sediment above that elevation will not affect this relationship. This relationship between soil matric suction/pressure head and soil moisture content is represented for the

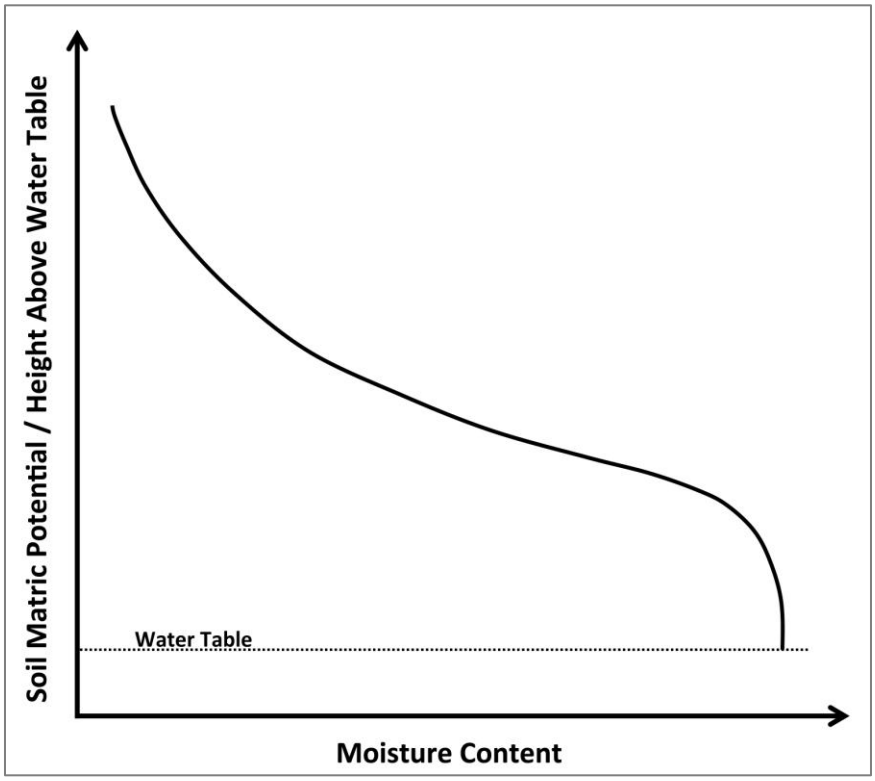

Figure 3.1: Representation of the relationship between soil matric potential (pressure head) and the soil moisture retention curve

entire soil column by a soil moisture retention curve (Figure 3.1) (Childs and Poulovassilis, 1962; Brooks and Corey, 1964; Childs, 1969; Van Genuchten, 1980).

Once the moisture retention curve has been established for a given soil, the soil column can be truncated at any pressure head (i.e., height above the water table), and the moisture content values at that elevation should be indicated by the curve (Childs, 1969). Figure 3.2 illustrates this concept applied to a beach environment, depicting the association between the moisture retention curve and moisture content at the sediment surface for various locations across the beach with different water table depths. (i.e., the back beach, middle beach and fore beach regions). Surface moisture content at various locations across the beach can be determined based on the intersection of the moisture retention profile curve with the sediment

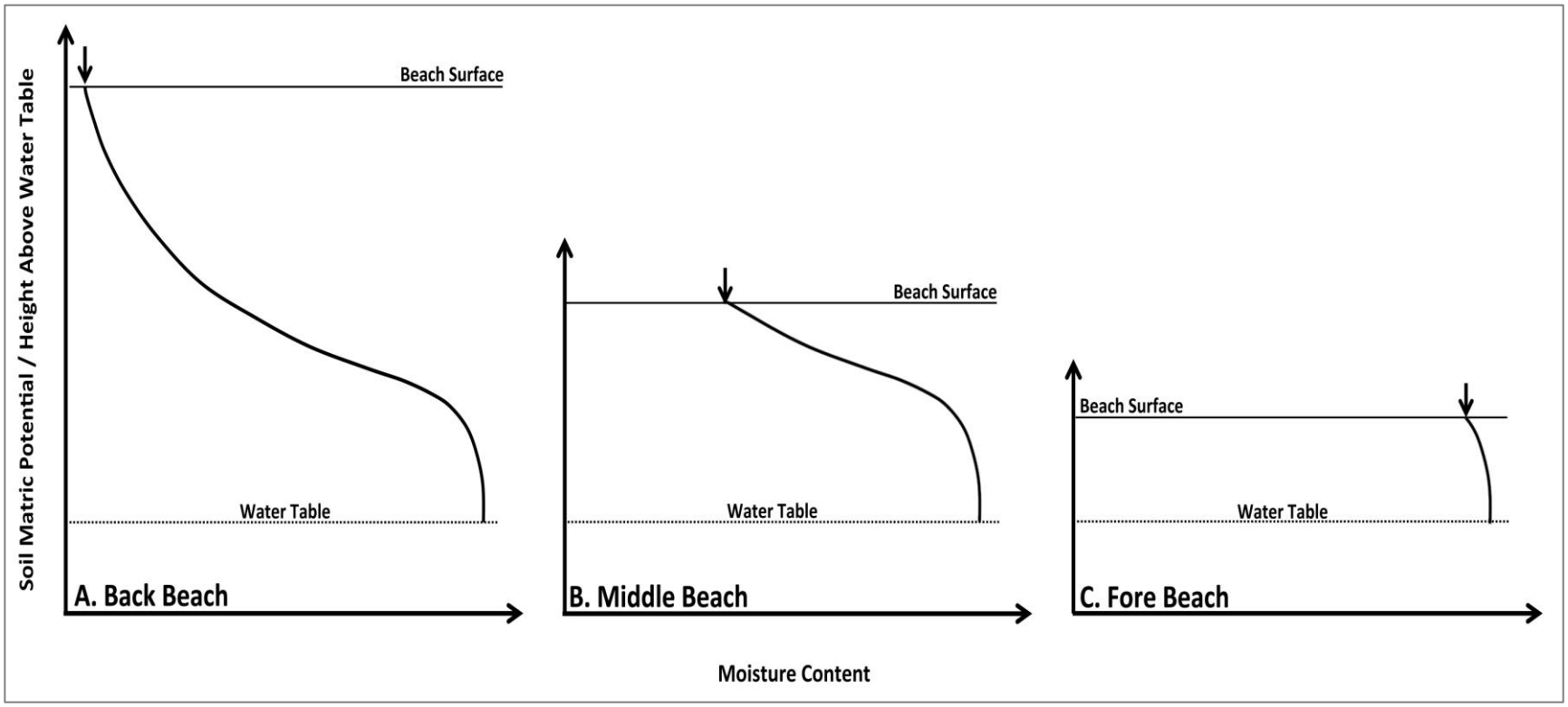

Figure 3.2: Schematic illustrations of the relationship between beach surface moisture dynamics, soil matric potential (pressure head) and the soil moisture retention curve in the beach environment: (a) the back beach; (b) the middle beach; (c) the fore beach.

surface. The point of intersection shifts along the moisture retention curve at the different locations across the beach as the height of the surface above the water table changes. In essence the moisture retention curve is being truncated at the pressure head elevation of the sediment surface layer. Therefore, the moisture contents at that surface elevation are determined by the pore characteristics of the sediment, and the ability of the sediment to draw moisture upward from below and retain it against the pull of gravity. The presence of more overburden at the back beach does not change the slope of the moisture retention curve close to the water table, in comparison, to the curve slope close to the water table for the middle beach and fore beach locations. Hence, from a theoretical standpoint the utilization of 'proxy' surfaces to represent moisture content dynamics for comparable 'true' surface elevations is reasonable and justified.

3.3 Laboratory Experimental Support

The laboratory experiment utilized a shortened sediment column to compare the moisture dynamics for an actual surface height of 25 cm above high water level with those measured at the 25 cm 'proxy' surface height as represented in Chapter 2. This verified that the presence of overburden has no effect, as expected from theory.

3.3.1 Methods

The experiment employed the same basic apparatus set-up as that of Chapter 2. A square PVC tube (85 cm in height), filled with the same very well sorted fine to very-fine quartz sand, was partially immersed in a reservoir of water (Figure 3.3). Before the experimental run,

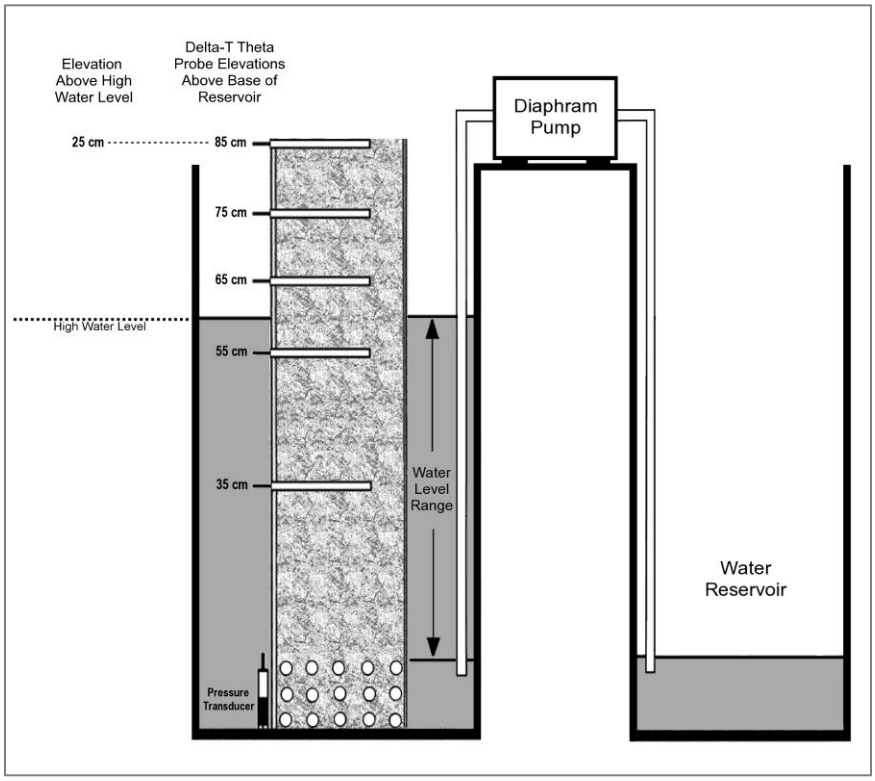

Figure 3.3: Schematic illustration of the laboratory experimental apparatus.

the sediment column was completely saturated and the water level within the reservoir was set at a high water table elevation of 60 cm from the base of the reservoir (25 cm below the actual surface of the sediment column). The system was left undisturbed for 10 days to allow gravitational drainage and moisture retention in the sediment column to reach equilibrium. After this equilibration period the water level in the reservoir was cyclically lowered then raised across a 40 cm vertical range over a period (fall and rise) of 24 hours, via a diaphragm-metering pump. This cycle was repeated 5.5 times for a sequence of 132 hours. Water table elevation was monitored using a pressure transducer (PT) installed at the base of the water reservoir. Changes in the vertical profile of moisture content within the sediment column were monitored using an array of Delta-T Theta probes inserted in the sediment column at elevations of 35, 55, 65, 75, and 85 cm above base of the reservoir (Figure 3.3). Due to a transitional period as the

system shifted from a static equilibrium with a stationary water table to a dynamic equilibrium with a fluctuating water table; the analyses presented herein include only data collected between hours 36 to 132 (96 total hours).

3.3.2 Surface Moisture Response Results

Figures 3.4 and 3.5 compare the measured moisture contents of the 25 cm 'true' surface at the 85 cm column and the 25 cm 'proxy' surface obtained with the 122 cm column (see Chapter 2). Both figures reveal a high degree of similarity between the two sets of measurements, in terms of both the moisture content range and symmetry of the moisture content traces. Moisture content fluctuates for both experiments between ~32% moisture by volume at high water level (low pressure head) to ~18% moisture at low water level (high pressure head). Symmetrically both sets of experiments follow the same pattern, the moisture contents remain relatively steady for a substantial period of time following the transitions between both a rising and falling water table, which is associated with an aspect of hysteresis known as Haines Jump (discussed in detail in Chapter 2). However, the moisture contents at the 'true' surface (85 cm column) depict a stronger Haines Jump signal compared to the 'proxy' surface measured within the 122 cm column, particularly after the transition from a rising into a falling water table.

Nevertheless, this finding is actually strong evidence that the moisture content present in the overburden sediment of the soil column does not alter the moisture content values at the 'proxy' surface layers. One of the reviewers suggested that the maintained high moisture content values, which we associated with the Haines Jump hysteresis phenomenon, is actually a

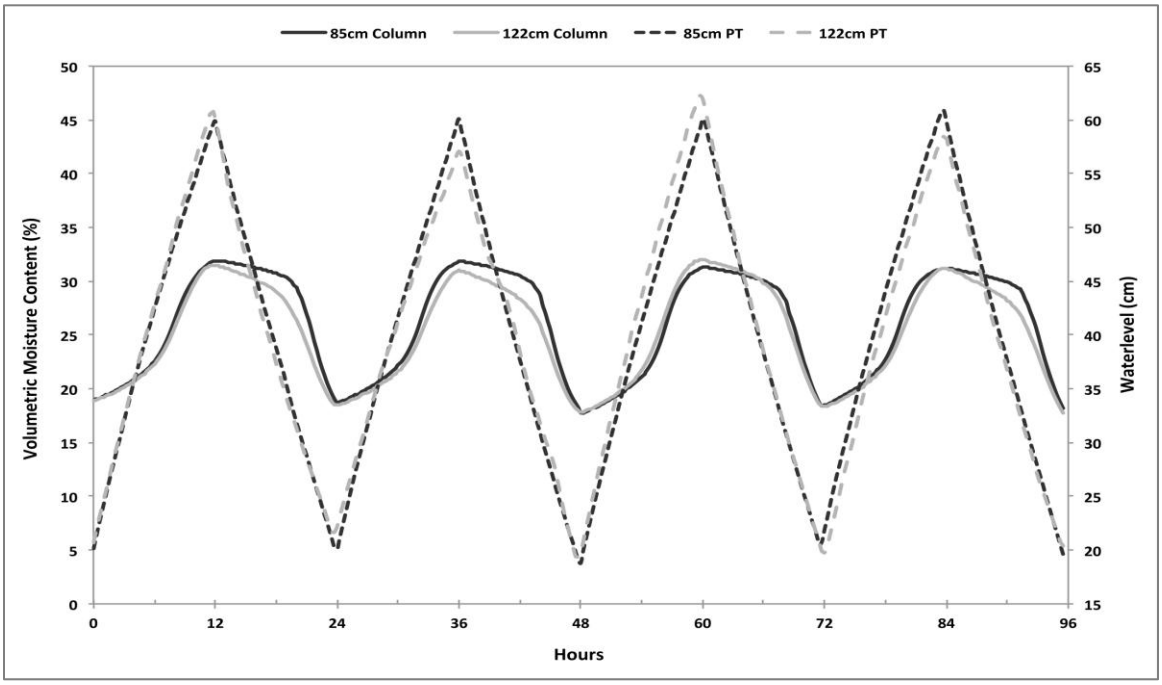

Figure 3.4: Variations in volumetric moisture contents and water level period both the 85cm column and 122 cm column experiments throughout the entire 96-hour pumping analysis sequence.

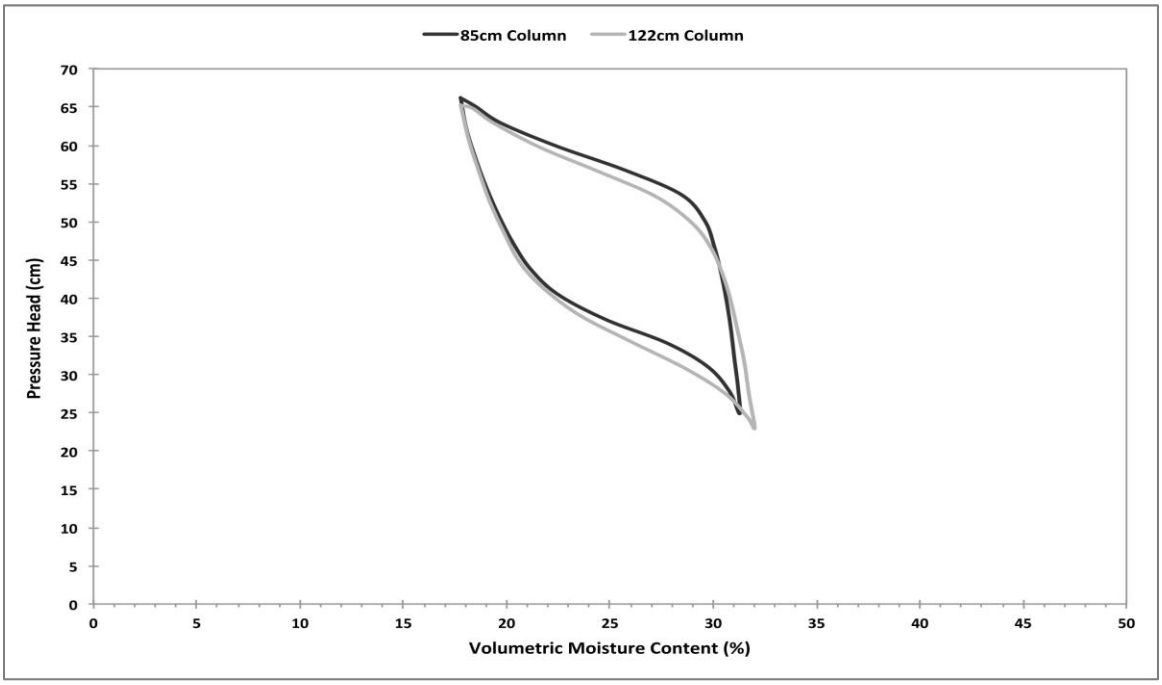

Figure 3.5: Illustration depicting a single 24-hour water flow scanning loop (48-72 hours) between the measured moisture contents for the 85 cm column and the 122 cm column experiments.

product of moisture drainage from above during a falling water table. Based on this assumption the above result could not occur, as there is no drainage from above at the surface of the 85 cm column. If drainage from the above overburden sediment was influencing the moisture content signal at the 'proxy' surface the reverse would actually occur, demonstrating that higher moisture content values occur after the transitions from a rising into a falling water table for the full 122 cm column. Consequently, this finding illustrates the presence of overburden sediment should not substantively influence the moisture content values at the 'proxy' surface layers.

In this instance a possible explanation causing the stronger Haines Jump signal at the 85 cm column could be that sand in the 85 cm column is more tightly packed, creating a smaller pore volume compared to the 122 cm column. Gallage and Uchimura (2010), established that soils with smaller pore sizes require a larger suction (pressure head) value in order to commence desaturation of the soil pores. In other words, there will be a slower rate of water drainage from the soil pores and thus an increase in the hysteretic effect.

A quantitative assessment of the simulations was conducted by calculating the standard error (SE) in measured volumetric moisture contents at the 85 cm column compared to the full 122 cm column (Table 1). The standard error between the two sets of moisture content measurements was ±1.6% by volume, which falls just outside of the measurement error of the Delta-T Theta probes at ±1.5%. These outcomes clearly signify that the results from the experimental analysis of Chapter 2 utilizing the 'proxy' surfaces correspond well with the analysis of the shortened 85 cm column length representing 'true' surface moisture measurements.

3.4 Conclusion

The goal of this chapter was to address methodological concerns and validate the utilization of moisture contents from below-surface elevations as 'proxy' surfaces to represent 'true' surface level moisture dynamics. Based on the findings in the report it is evident from both a theoretical and empirical standpoint the use of these below ground 'proxy' surfaces provide highly accurate representations of 'true' surface moisture dynamics. Therefore, the use of the moisture content dynamics at these 'proxy' surfaces to represent 'true' surface moisture content dynamics at comparable elevations above the water table is reasonable and appropriate.

Chapter 4 -- Influence of Sediment Texture on Capillary Dynamics of the Sediment Column: Implications on the Spatial and Temporal Dynamics of Beach Surface Moisture

4.1 Introduction

Sediment grain-size characteristics represent one of the most important factors controlling the moisture retention properties, hysteretic nature, and hydraulic conductivity of the sediment profile (Terzaghi, 1943; Childs, 1969; Hillel 1971; Hillel 1980; Hanks 1992; Fredlund and Rahardjo, 1993). A number of researchers have demonstrated that these capillary water characteristics scale in proportion to a soil medium's representative grain size (e.g., Gupta and Larson, 1979; Haverkamp and Parlange, 1986; Raats, 1992; Aubertin *et al.*, 2003; Durner, 1994; Kosugi, K., 1999; Tokunaga *et al.*, 2004; Tokunaga, 2009; Gallage and Uchimura, 2010). Coarser-grained soils exhibit a lower moisture content value in comparison to finer-grained soils at the same pressure head above the water table (Gupta and Larson, 1979; Arya and Paris, 1981; Haverkamp and Parlange, 1986; Fredlund *et al.*, 1994; Aubertin *et al.*, 2003); hysteresis effects decrease with increasing grain-size (Tokunaga *et al.*, 2004; Yang *et al.*, 2004; Gallage and Uchimura, 2010); and coarser-grained soils have lower unsaturated hydraulic conductivities than finer-grained soils at the same pressure head above the water table (Mualem, 1976; van Genuchten and Nielsen 1985; Raats, 1992; Durner, 1994; Kosugi, K., 1999; Assouline 2005, Tokunaga, 2009). Accordingly, our theoretical understanding of the influence of sediment grain size on capillary dynamics is sound.

Given that surface moisture dynamics are heavily controlled by the capillary properties of the sediment column (see analysis from Chapter 2) and the fact that deviations in sediment grain size heavily alter the dynamics of these properties, it should be expected that variations in

grain size will have dramatic effects on the spatial and temporal dynamics of surface moisture content. To date very few studies have attempted to analyze the influence of grain size on surface moisture dynamics (Malaya and Sreedeep, 2012). This study will address this issue by 1) investigating and analyzing the influence of sediment grain size on the capillary properties of the sediment and 2) discussing the effect that these properties in turn have on regulating beach surface moisture content. To document these processes a set of laboratory experiments were conducted utilizing beach sands with two different mean grain sizes.

4.2 Methods

4.2.1 Laboratory Experimental Design

The laboratory experiments employ the same basic apparatus and experimental design as that of Chapter 2. A square PVC tube 122 cm in height, filled with sediment, was partially immersed in a reservoir of water (Figure 4.1). The first set of experiments utilized a very well sorted fine to very-fine quartz sand obtained from a beach at Padre Island National Seashore on the Texas Coast of the Gulf of Mexico with a mean grain size of 0.13 mm (2.94 phi), whereas the second set of experiments employed a moderately sorted medium quartz sand exhibiting a coarse skew, commercially available as “play sand”, with a mean grain size of 0.36 mm (1.47 phi) (Figure 4.2). A diaphragm-metering pump was used to raise and lower the water level in the reservoir, to simulate tidally induced groundwater fluctuations. Three individual experimental runs were conducted for each set of sediment grain-size experiments with vertical water table fluctuations of 25, 40, and 55 cm. The high water elevation was fixed at 60 cm above the base of the reservoir and the elevation of the water table down to low water was

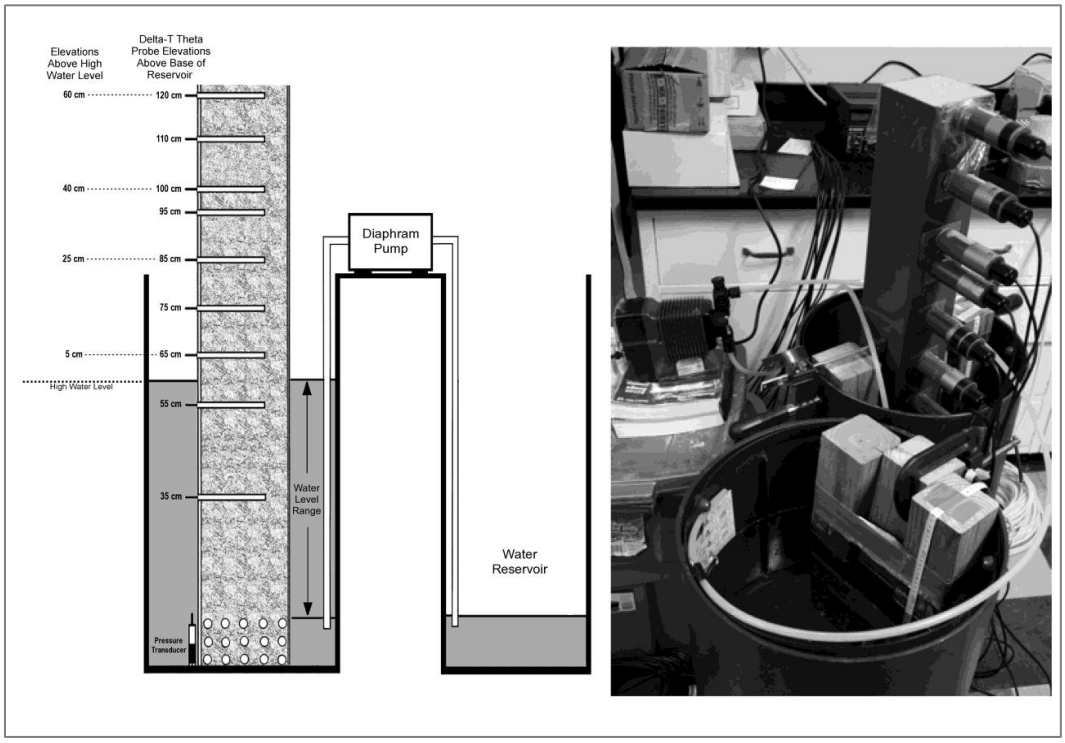

Figure 4.1: Schematic (left) and photograph (right) of the laboratory experimental apparatus.

so that the moisture probe positions could be held constant relative to high water. Changes in the vertical profile of moisture content within the sediment column were monitored at using an array of Delta-T Theta probes inserted in the sediment column at elevations of 35, 55, 65, 75, 85, 95, 100, 110, and 120 cm above base of the reservoir (Figure 4.1).

Before each experimental run, the sediment column was completely saturated and the water level within the reservoir was set at the high water table elevation of 60 cm from the base of the reservoir. The system was left undisturbed for 10 days to allow gravitational drainage and moisture retention in the sediment column to reach equilibrium. After this equilibration period, the water level in the reservoir was cyclically lowered then raised to each desired water table fluctuation increment over an oscillation period (fall and rise) of 24 hours,

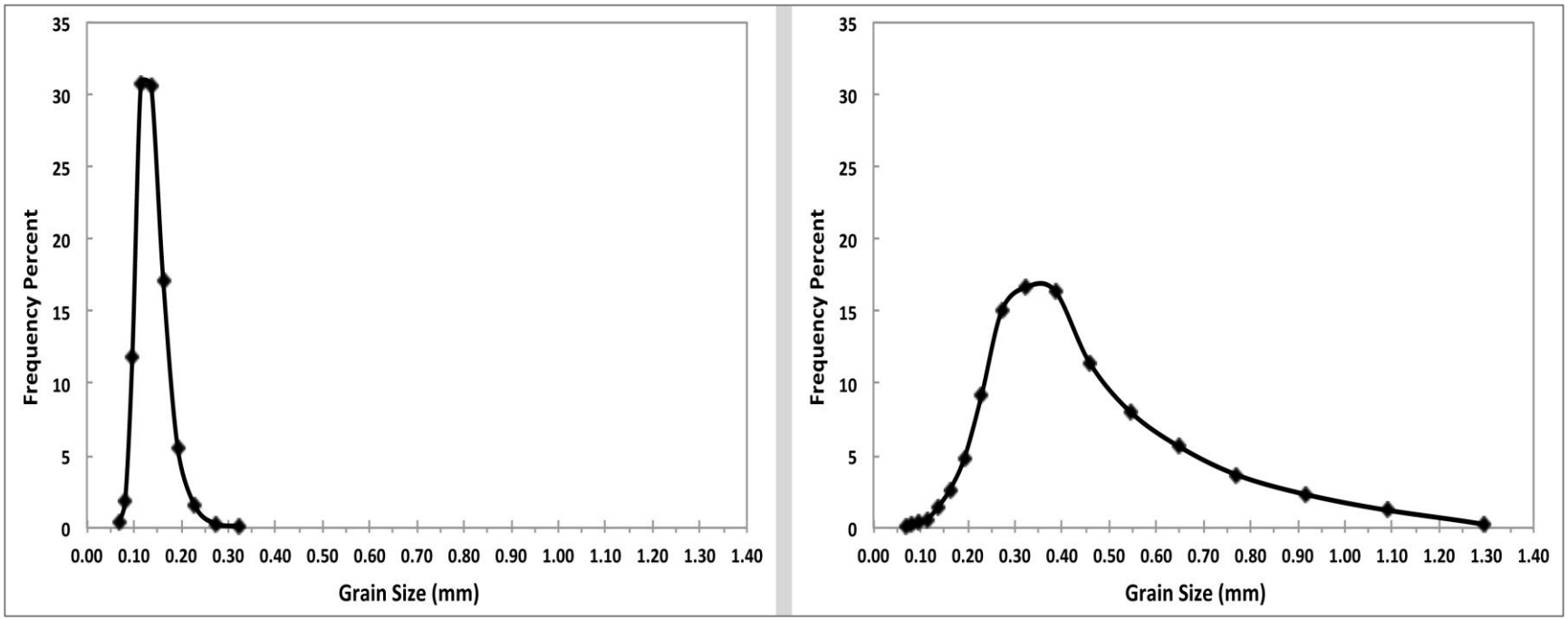

Figure 4.2: Grain size analysis. Fine grained sand on left and medium grained sand on right.

via the diaphragm-metering pump. This cycle was repeated 5.5 times for a sequence of 132hours. To eliminate the transitional period that occurred as the system shifted from a static equilibrium with a stationary water table to a dynamic equilibrium with a fluctuating water table, the analyses presented herein include only the data collected between hours 36 to 132 (96 total hours) in each experiment.

4.2.2 Surface Moisture Content Data Analysis

To analyze the influence of water table fluctuations on moisture dynamics at various surface elevations above the water table, the measured moisture contents at four Delta-T Theta probe elevations within the sediment column were used as proxies to represent 'true' surface elevations above a fluctuating water table. In the following analyses, the Delta-T Theta probes located at elevations of 65, 85, 100, and 120 cm above the base of the reservoir were employed as representative 'true' surface elevations of 5, 25, 40, and 60 cm above the high water table, respectively (Figure 4.1). Additionally, the moisture dynamics at these individual 'true' surface elevations were analyzed under specific water table fluctuation conditions. The 5 cm elevation was analyzed using the 55 cm water table oscillation, the moisture dynamics at the 25 cm and 40 cm elevations were examined utilizing the 40 cm water table oscillation range, and the moisture dynamics at the 60 cm elevation was investigated under the smallest water table oscillation range of 25 cm. These surface elevation/water table fluctuation relations were selected based on documented water table oscillation ranges and water table depths from fieldwork conducted across the central Texas coast for various fore beach, middle beach,

and back beach locations on northern Gulf of Mexico beaches (i.e., Zhu, 2007; Namikas *et al.*, 2010).

These analyses represent only a subset of the entire collected data. Although the moisture conditions across a full soil profile were recorded for the various water table oscillation ranges, the analyses presented in this chapter highlight specifically the moisture/pressure head/water table dynamics associated with various positions across a beach surface. It is not the intent of this chapter to focus on the hydrological dynamics below the surface layer.

4.2.3 Moisture Retention Curves and Hydraulic Conductivity

The moisture retention and unsaturated hydraulic conductivity curves are given by the analytical form of the soil hydraulic functions proposed by van Genuchten (1980):

$$\theta\ h\ = \theta_r + \frac{\theta_s - \theta_r}{1+\ \alpha h^{\ n\ m}}$$

$$K\ h\ = \mathrm{K_s}\Theta^{\lambda}\ 1 -\ \ 1 - \Theta^{1/\ m\ \ \ m\ 2} \qquad [1]$$

in which, θ_r and θ_s denote the residual and saturated water contents, respectively, α and n are empirical parameters, m = 1-(1/n), K_s is the saturated hydraulic conductivity, Θ is the effective degree of saturation, and λ is a pore connectivity parameter derived by Mualem (1976) to equal 0.5. To designate the main drying and wetting main boundary moisture retention and unsaturated hydraulic conductivity curves, the function parameters θ_r, θ_s, α, n, m, and K_s are denoted with superscripts *d* and *w* to indicate either a drying or wetting curve, respectively.

Based on moisture content measurements collected at each of the moisture probe elevations, the main drying and wetting moisture retention and unsaturated hydraulic

conductivity curves were constructed for both the fine-grained and medium-grained sands (Figure 4.3).

4.3 Results

The response of surface moisture contents to water table fluctuations for the fine and medium sands is illustrated in Figures 4.4. Several trends in moisture content response are clearly apparent between the two grain sizes. First, there is a lower surface moisture content for the medium sand in all cases. At the 5 cm surface elevation, moisture content varied from a 22% to 44% (by volume) for the fine sediment and 7% to 31% for the medium sand. As the surface elevation increases to 60 cm, moisture content decreased to 11 to 14% moisture for the fine-grain sand and a moisture content of about 4% for the medium sand with a negligible fluctuation moisture range of less than 1%. These findings agree with the literature, which suggests that the larger pores of the medium sediment will exhibit less moisture retention in comparison to the smaller pore spaces of the finer grained sediment at any particular pressure head/surface elevation (Arya and Paris, 1981; Fredlund *et al.*, 1994; Aubertin *et al.*, 2003).

A second trend evident in Figure 4.4 is the dissimilarity in the symmetry of the moisture content response between the test sands, relative to the groundwater level fluctuations. At the near surface elevations of 5 cm and 25 cm there is a distinct Haines Jump hysteresis signature (Haines, 1930) for both grain sizes following the transitions in direction of water table fluctuations; however, the hysteresis dynamics exhibit very different behaviors. For both surface elevations the Haines Jump hysteresis effects following the transition from a rising into falling water level are much smaller for the medium sand compared to the fine sand, yet

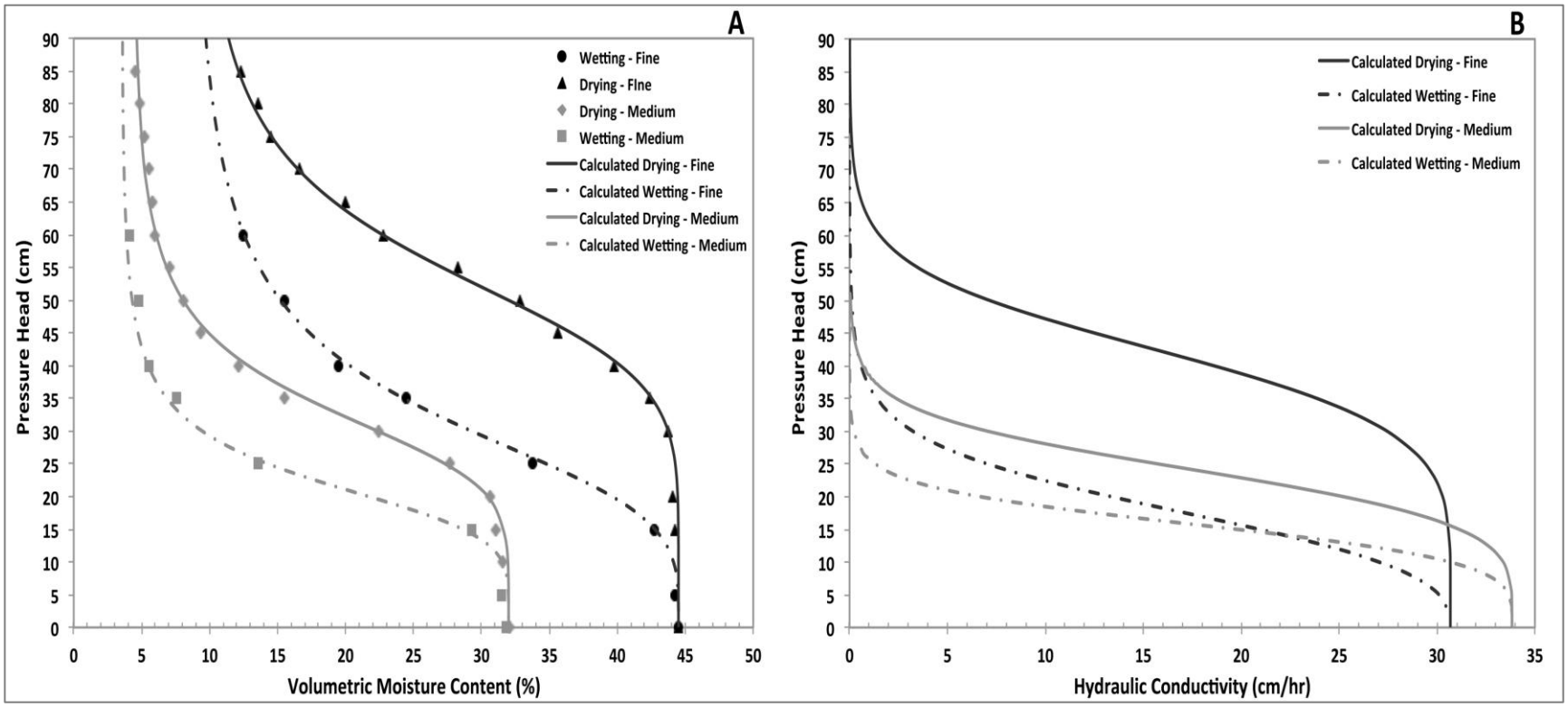

Figure 4.3: Measured volumetric moisture content and the calculated van Genuchten (1980) boundary wetting and drying moisture retention curves for the Fine and Medium sands (A). Calculated van Genuchten (1980) boundary wetting and drying unsaturated hydraulic conductivity curves for the Fine and Medium sands. The pressure head is equivalent to the height of the surface above the water table.

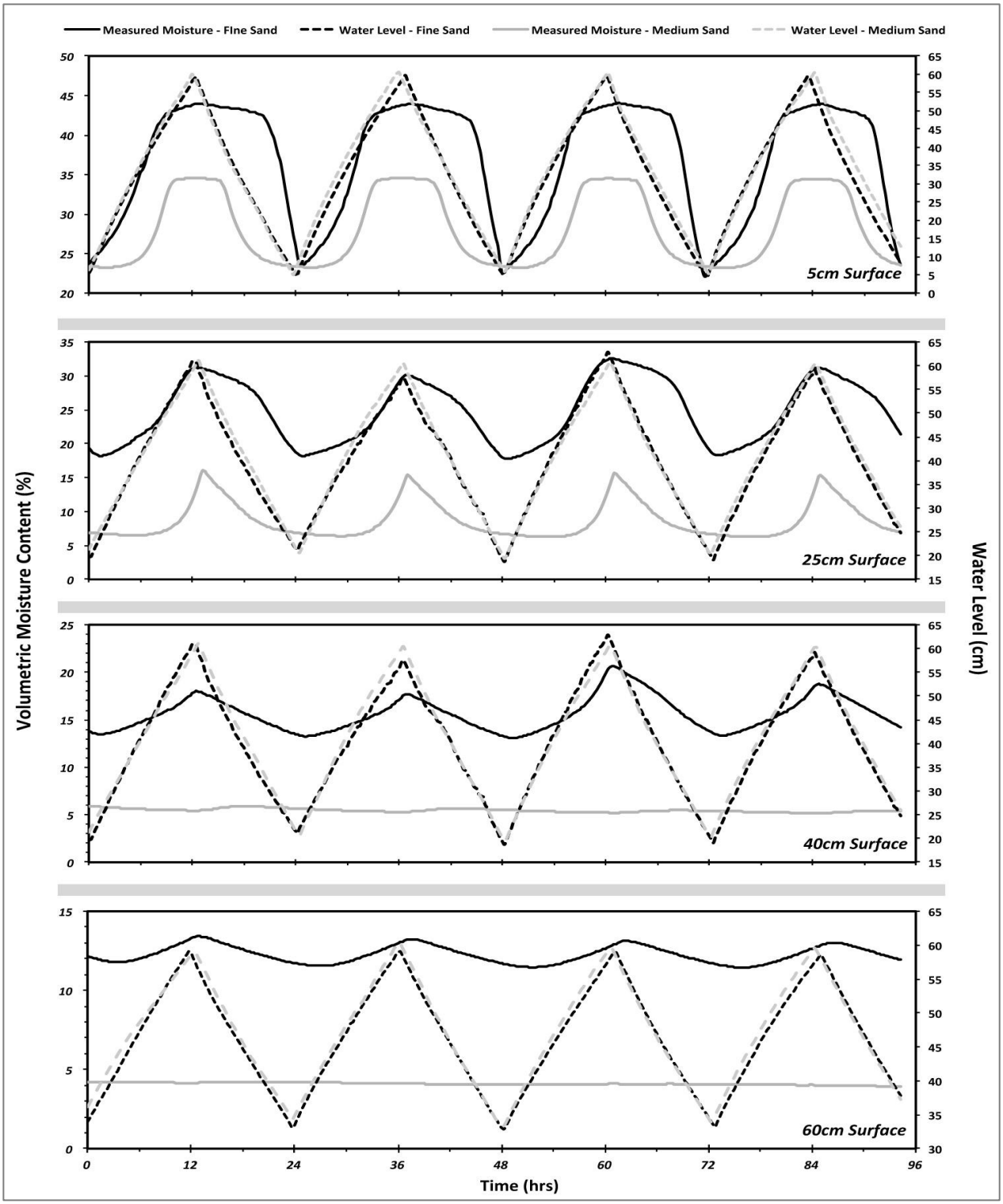

Figure 4.4: Variations in volumetric moisture contents and water level period at each of the four 'proxy' surface elevations for both the medium and fine grain-sizes. The 5 cm surface elevation experienced a 55 cm water level fluctuation, where as the 40 and 25 cm elevations were subjected to a water level fluctuation of 40 cm, and the 60 cm surface elevation was associated with a water level fluctuation of 25 cm.

following the transition from a falling into a rising water level the Haines Jump hysteresis effects are significantly more pronounced in the medium sand (Figure 4.5). Additionally, at the 5 cm surface elevation, the moisture contents for both test sands reached a saturated moisture level during a rising water table prior to the actual high water level occurring. Moreover, at both the 5 cm and 25 cm surface elevations for the medium-grained sand, moisture contents corresponding with a falling water table reached a near dry moisture level prior to actual low water level occurring.

These variations in the temporal symmetry of the moisture contents relative to the groundwater signal between the various grain sizes can be attributed to differences in the arrangement of several moisture retention parameters of the soil profile. These include air-entry value, the pressure head value at which air enters the soil pores as suction is increased during a drying sequence (i.e., value at which soil starts to desaturate); water-entry value, the pressure head value at which water enters the soil pores as suction is decreased during a wetting sequence (i.e., value at which a soil begins to saturate); residual-air value, the pressure head value at which there is no appreciable increase in moisture content as suction is decreased during a wetting sequence; and the residual-water value, pressure head value at which there is no appreciable decrease in moisture content as suction is increased during a drying sequence. A number of researchers have illustrated that each of these values correlate with grain size distribution of the sediment, depicting a decrease in the pressure head values occurring with an increasing in grain size (Yang *et al.*, 2004; Birle *et al.*, 2008; Gallage and Uchimura, 2010; Malaya and Sreedeep, 2012). This finding is a product of the fact that the larger pore volume of the medium sand requires smaller suction gradients (i.e., lower pressure

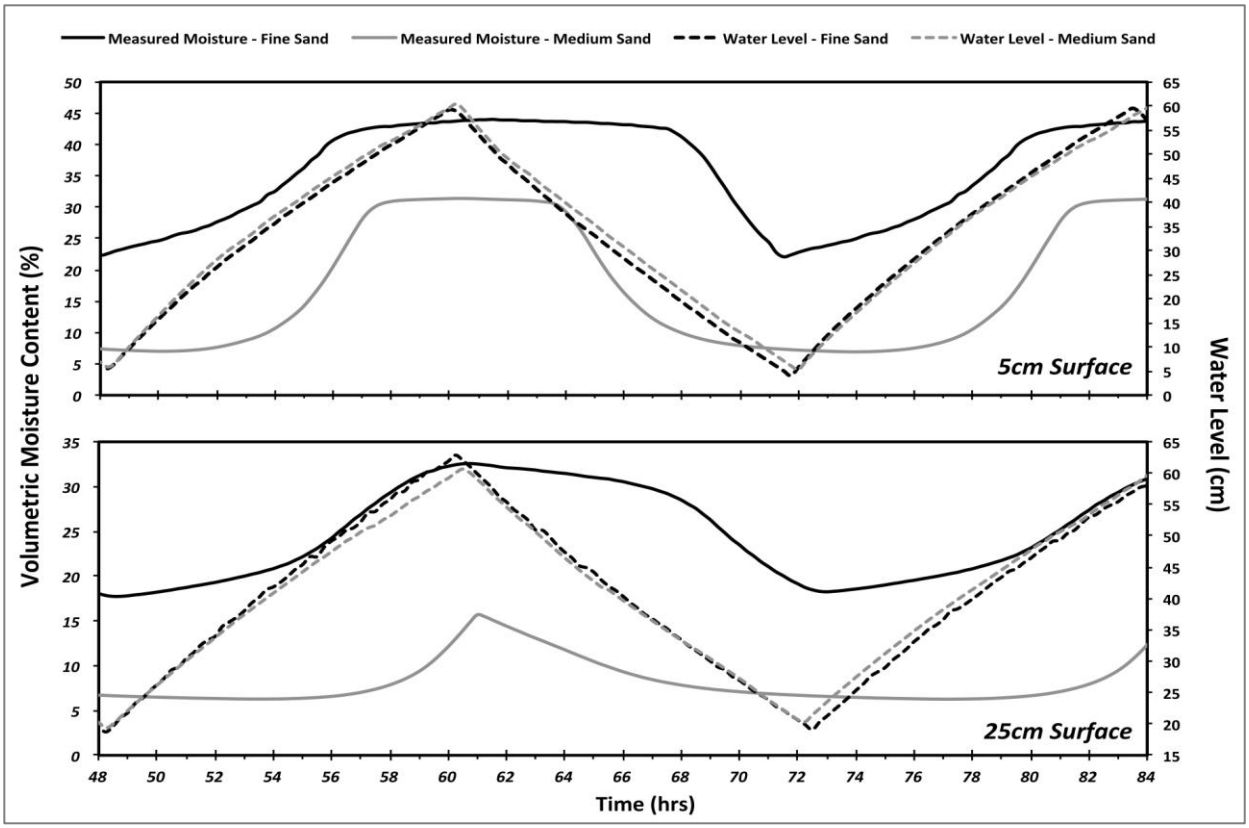

Figure 4.5: A time sequence of measured volumetric moisture contents for both the medium and fine grain-sizes at the 5 cm and 25 cm surface elevation highlighting the temporal variations in moisture content compared to water table fluctuations.

head values) to produce capillary water flows during water table fluctuation (Gallage and Uchimura, 2010). Figure 4.6 confirms this correlation, illustrating that each of the moisture retention parameters have a lower pressure head value for the medium-grained sand. It is this correlation that is the primary driving force controlling the variations in the temporal symmetry of the moisture contents relative to the groundwater signal between the various grain sizes.

The variations in the Haines Jump hysteresis signal between the grain sizes arises due to differences in the air-entry and water-entry values within the sediment profiles of the grain sizes. During a drying sequence the lower pressure head air-entry value of the medium-grained sand results in the soil beginning to drain prior to the fine-grained sand under the same water

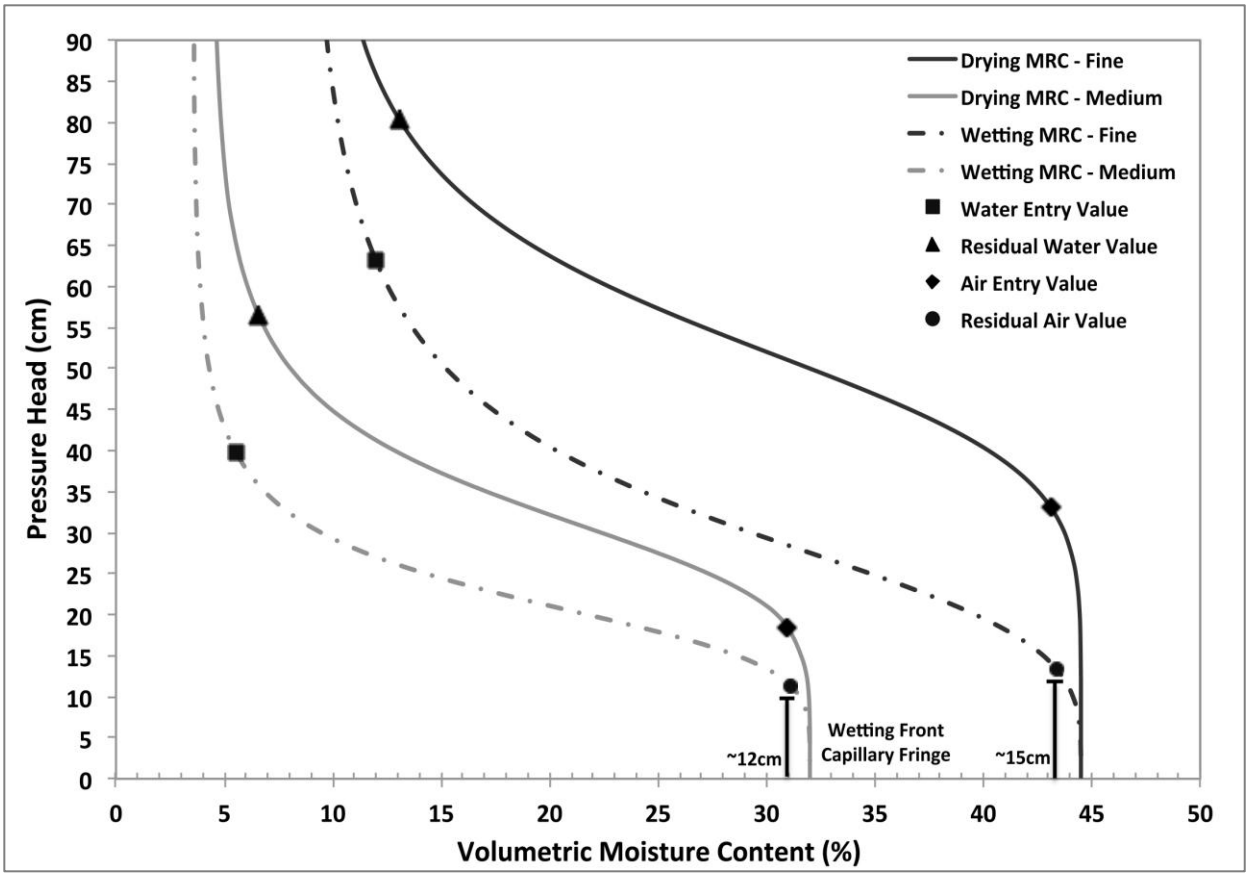

Figure 4.6: Variations in the air-entry, residual-water, water-entry, and residual-air moisture retention parameters between the medium and fine grain-sizes.

table conditions. Furthermore, during a wetting sequence the higher pressure head water-entry value of the fine-grained sands results in the soil beginning to saturate prior to the medium-grained sand under the same water table conditions. With respect to the saturation of the surface level occurring prior to the actual high water level during a rising water table, this phenomenon can be attributed to the development of a saturated layer of sediment extending above the water table, termed capillary fringe, which is product of the residual-air value of the sediment. Yang *et al.* (2004) and Gallage and Uchimura (2010) noted that course-grained soils have a lower residual-air value than fine-grained soils, which in effect asserts that fine-grained sands will reach its relative saturated moisture level at a higher-pressure head value. Figure 4.6

confirms this finding illustrating that the fine-grained sand has a saturated capillary fringe extending approximately 15 cm above the water table where as the medium-grained sand has a capillary fringe of only approximately 12 cm above the water table. Additionally, the occurrence of the medium-grained sand reaching a near dry moisture level prior to actual low water level occurring is associated with the development of the residual-water value of the sediment. The residual-water value for the medium sand occurs at a pressure head value of 57 cm (Figure 4.6), this is a lower pressure head value than the pressure heads of the 5 cm and 25 cm surface layers (60 and 65 cm, respectively), therefore each of these sediment surfaces will experiences low moisture content values prior to actual low water fluctuation. The absence of this phenomenon for the fine-grained sands is due to the fact that the pressure head values at the 5 cm and 25 cm surface layers are smaller than the residual-water pressure head value (80 cm) (Figure 4.6); therefore, the surface layers never fully reach the residual-water moisture content value (~13% moisture by volume).

The final trend evident in the moisture response is that there are significant differences between the test sands in the time lags in moisture content relatively to the water table fluctuations. Table 4.1 illustrates the average time lags between the measured maximum and minimum contents and the associated high and low water table levels. For both sands the duration of the lag increases with elevation above the water table; however, the increase in duration is significantly larger for the medium sand, particularly at the highest surface elevations (40 cm and 60 cm). There is also a larger time lag in reaching minimum moisture content after low water table compared to that for maximum moisture content following high

Table 4.1: Average time lags (minutes) between max/min moisture contents and high/low water table levels for both the medium and fine grain-sizes.

	Fine Sand		Medium Sand	
Surface Elevation	High Water Table	Low Water Table	High Water Table	Low Water Table
5 cm	N/A*	38	N/A*	N/A**
25 cm	42	58	37.5	N/A**
40 cm	61	105	424 (~7hrs)	715 (~12hrs)
60 cm	89	185	787 (~13hrs)	1185 (~20hrs)

* In every case the surface content reached saturation before high water level
** In every case the surface moisture content reached the minimum value before low water level

water table for both grain sizes; and again the time lags are larger for the medium sand, at the highest surface elevations.

The differences in temporal lags between the two sands are a function of the differing hydraulic conductivity in the soil columns. Figure 4.3B illustrates that the medium sand has lower unsaturated hydraulic conductivities than the fine sand at the same pressure head values, particularly at the higher pressure head values; thus the increase in time lag values. This finding corresponds well with the existing literature (Durner, 1994; Kosugi, 1999; Assouline, 2005; Tokunaga, 2009), and illustrates the physical influence of hydraulic conductivity on the capillary flow dynamics of the sediment column with differing grain sizes.

4.4 Discussion

Taking into consideration these findings, the spatial distribution of beach moisture will be expected to vary with differing sediment grain sizes. Figure 4.7 is a schematic representation of the changes in the spatial coverage of the moisture content zones with an increase in grain size from a fine to medium sand. At the 5 cm surface elevation, which is representative of the traditional saturated/near-saturated zone conditions across the fore beach, the decrease in

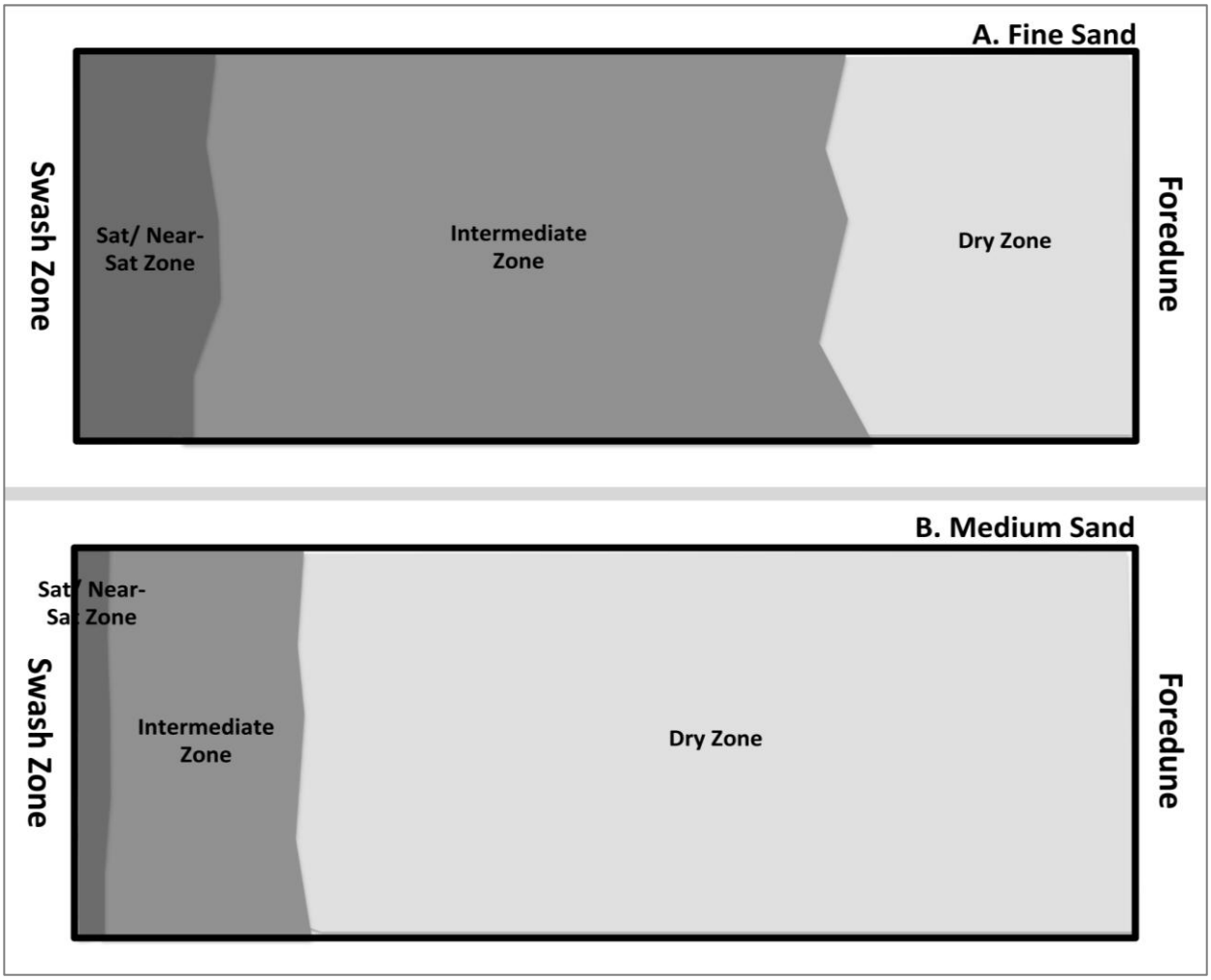

Figure 4.7: Schematic representation of the changes in the spatial coverage of the cross-shore moisture zones with an increase in grain-size from Fine (A) to Medium (B).

moisture contents with the medium-grained sand as well as the greater level of variability between high and low moisture contents at the medium-grained sand compared to the fine-grained will result in the fore beach moving from a saturated/near-saturated moisture zone under fine-grained beach systems to more of an intermediate moisture zone. Secondly, the traditional middle beach associated with the highly variable intermediate moisture zone, represented by moisture conditions at the 25 cm and 40 cm surface elevations, will also experience a dramatic decrease in spatial coverage with increasing grain size as moisture

contents decrease and fluctuate widely between high and low values. This change is particularly evident at the 40 cm surface elevation as the moisture content values for the medium sand exhibit very minimal variability maintaining continuously near-dry moisture levels. Finally, the dry zone will increase in size with the medium grained sand as the spatial coverage of the intermediate moisture zone decreases as the back and middle beach experience drier moisture conditions.

The differences in the development of the capillary fringe and the residual water formation along with the variations in Haines Jump hysteresis effects between the grain sizes at the 5 cm and 25 cm surface elevation lead to notable differences in the non-linear temporal moisture dynamics. During high water table conditions at both the 5 cm and 25 cm surface elevations the fine and medium sands reach a near-saturated moisture level prior to the transition from a rising into a falling water table and remain at this saturated/near-saturated moisture level for a period of time after the transition, however, the fine sand persists for longer time periods at this saturated/near-saturated moisture level. During low water table conditions, at 5 cm and 25 cm surface elevations the medium sand falls to a low moisture content state prior to the transition from a falling to a rising water table and remains at this low moisture state for an extended period of time. By contrast, the fine sand does not reach its peak moisture content until after the transition into a falling water table and moisture content immediately begins to decrease. Consequently, the medium sand exhibits shorter time periods at saturated/near-saturated moisture conditions and longer time periods at low moisture content values. Of note is that at the 5 cm surface elevation the medium-grained sand reaches

it low moisture content state approximately at the same time that the fine-grained sand begins its decrease in moisture content.

Differences in hydraulic conductivity between grain sizes will have a substantial impact on the temporal dynamics of beach surface moisture contents, particularly across the backbeach where the water table is deeper. Independent of grain-size, capillary water flows at a faster rate at higher water contents (low pressure head values) than it does at lower water contents (high pressure head values). Therefore, the moisture content at the surface will lag significantly behind water table oscillations, and do so to a degree that increases both proportionally and non-linearly with the elevation of the beach surface above the water table. The observed time lag values for both of the test sands provide a clear illustration of this concept, showing a marked increase in lag time with depth above the water table; however, the increase is significantly larger for the medium sand than the fine sand (Table 4.1). The slower capillary flows due to the lower hydraulic conductivities for the medium sand results in increased time lags between maximum/minimum water table fluctuation and surface moisture content.

4.5 Conclusion

The goal of this study was to investigate and document the influence of sediment texture on the capillary properties of the sediment column and identify the effects of sediment texture on the spatial and temporal development of beach surface moisture. Under the same hydrological forcing conditions, comparison of surface moisture measurements obtained with the two test sands revealed distinct differences in the capillary properties of the sediment

columns. First, there is a definite decrease in the moisture content of the medium sand at each surface elevation. The larger pores of the medium sediment exhibit less moisture retention at any particular pressure head/surface elevation in comparison to the smaller pore spaces of the finer sediment. This finding is in agreement with the literature and illustrates variation in the capillary moisture retention properties between the sands. Additionally, there are dissimilarities in the symmetry of the moisture content traces between the grain sizes at each surface elevation. These variations in the symmetry of the moisture contents can be attributed to differences in the hysteresis effects on the capillary dynamics of the sediment between the various grain sizes. A distinct Haines Jump signature is present for both grain sizes; however, the dynamics between the grain sizes exhibit very different behaviors. Lastly, for both of the grain sizes the duration of the lag increases consistently with depth above the water table; however, the increase in duration is significantly more drastic for the medium sand than the fine sand, particularly at the highest surface elevations.

These differences in capillary properties were shown to have a direct effect on the spatial and temporal dynamics of surface moisture content. The decrease in the absolute moisture content of the medium-grained sand compared to the fine-grained sand for each surface elevation has a notable influence on the spatial distribution of the moisture content zones across the beach surface. With an increase in grain size from a fine sand to a medium sand, the traditional saturated/near-saturated moisture zone associated the fore beach and the intermediate moisture zone across the middle beach will be compressed toward the swash zone. This results in an increase of the spatial coverage of the dry moisture zone where aeolian processes will be at a maximum.

The capillary properties of hysteresis and hydraulic conductivity of unsaturated soils result in significant departures in the temporal moisture content signals from water table fluctuations. Hysteresis had a more pronounced control on the temporal moisture signal at the shallow surface elevations whereas variations in hydraulic conductivity had a greater effect on the temporal signal at the higher surface elevation for both test sands. However, the results show substantial differences in the temporal dynamics between the grain sizes. At the shallow surface elevations, associated with spatial locations across the fore beach and lower middle beach, both test sands exhibited moisture contents that were sustained for extended periods of time after the fluctuation transitions of the water table; yet, the medium-grained sand maintained those moisture content levels for a shorter time periods during high water table conditions, and over longer time periods at low water table conditions. At the higher surface level elevations, spatially associated with the upper middle beach and back beach, both of the grain sizes experienced moisture contents that temporally lag significantly behind water table fluctuations. However, the medium-grained sand demonstrated momentous increases in time lag values compared to the fine-grained sand.

Chapter 5 -- Evaporation Dynamics at Various Shallow Surface Sediment Depths: Importance of Soil Surface Water Availability

5.1 Introduction

The rate of evaporation from soil surfaces has traditionally been considered to approximate the rate of evaporation from an open water surface, that is, potential evaporation (Penman 1948; Beese *et al.*, 1977; Mahfouf and Noilhan, 1991; van de Griend and Owe, 1994). This approach, however, lends itself to significant inaccuracies as the beach surface is generally in a state of unsaturated moisture conditions varying significantly over both space and time (Atherton *et al*., 2001; Yang and Davidson-Arnott, 2005; Zhu, 2007; Namikas *et al.*, 2010). As a result, traditional methods for calculating evaporation (i.e., potential evaporation) based on saturated surface moisture conditions overestimates actual surface evaporation. This study seeks to address this problem through a set of field experiments designed to evaluate the dynamics of evaporation from the beach surface, under varying moisture conditions.

A number of studies have illustrated that surface moisture and evaporation mutually influence one another (e.g., Morton, 1985; Granger, 1989; Entekhabi *et al.*, 1996; Wilson *et al*., 1997). These studies convey that evaporation of moisture from the sand surface decreases the moisture content, which in turn reduces the rate of actual evaporation from the surface, as water availability is increasingly restricted. Accordingly, the actual rate soil evaporation is recognized to respond to surface moisture conditions in three distinct stages (Holmes, 1961; Ritchie, 1972; Idso *et al*., 1974; Monteith, 1981; Parlange and Katul, 1992; Wilson *et al*., 1997; Aydin *et al.*, 2005).

Figure 5.1 depicts a conceptual model illustrating the stages of soil evaporation over time and with depth.

1) Stage 1:

The process of soil surface evaporation in the first stage may be treated in the same way as water surface evaporation. Thus, actual evaporation proceeds at a high constant-rate approximating the potential evaporation rate as the sediment surface is completely saturated. Accordingly a “wet soil layer” (WSL) extends all the way to the sediment surface and therefore the "evaporative transformation layer” (ETL) has a thickness that is near zero as vaporization of moisture occurs entirely at the soil surface.

2) Stage 2:

The second stage of evaporation is associated with a continual decline in the rate of evaporation as the evaporative system transitions from being controlled by the atmosphere to being limited by the soil moisture conditions of the sediment. Over time, moisture availability within the ETL becomes increasing limited due to evaporative drying, and thus the rate of vaporization will continue to decrease with time, which is the key feature of the falling-rate stage evaporation dynamics.

3) Stage 3:

During the third stage, evaporation at the surface has reached a near-constant low-rate phase, as vapor movement is the dominant mechanism of moisture transport through a “dry soil layer” (DSL) to the surface. Additionally, a number of researchers have demonstrated that the transient vaporization and condensation of moisture at the soil surface becomes an important moisture exchange process within this third stage (e.g., Yamanaka *et al.*, 1997;

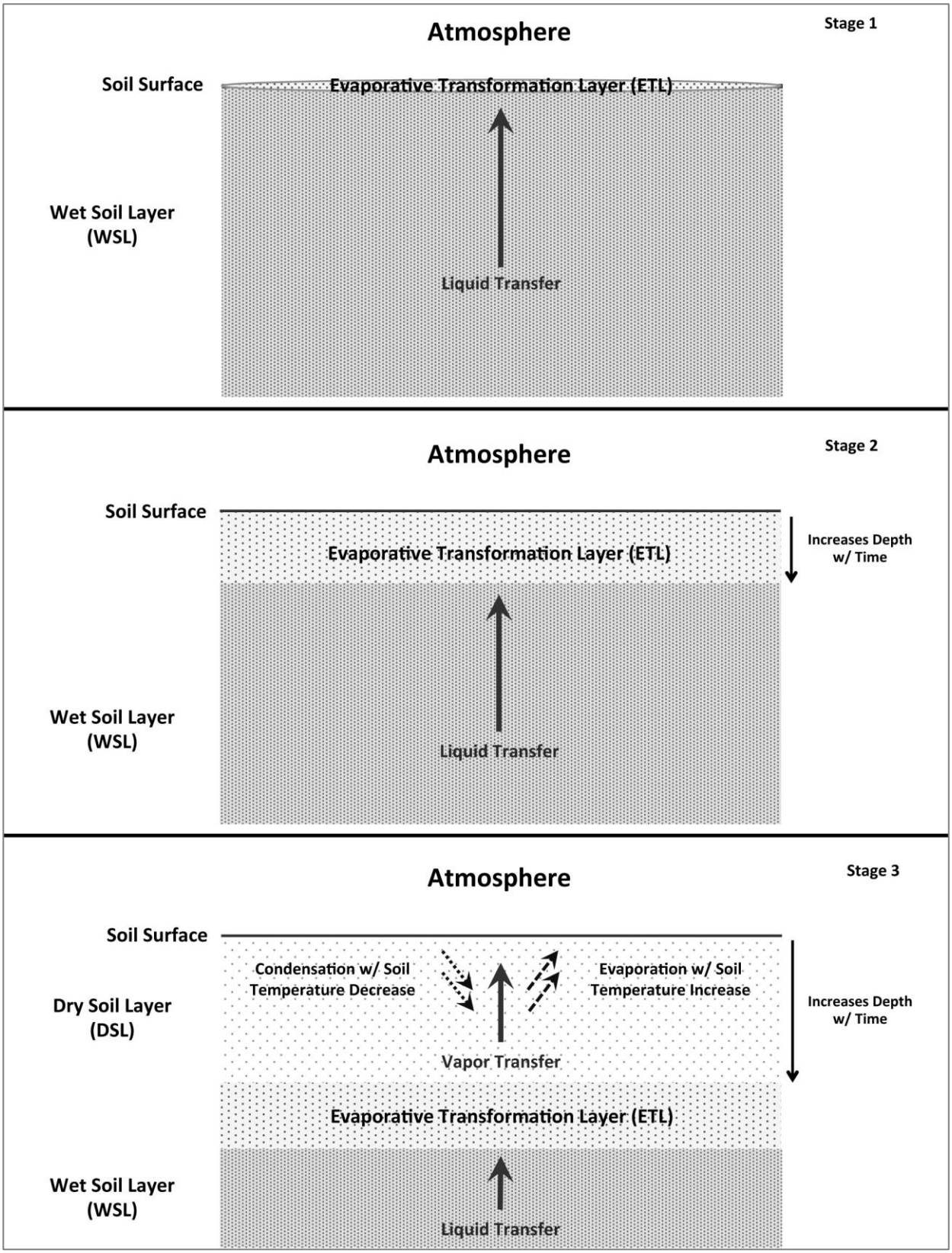

Figure 5.1: Schematic illustration of the conceptual evaporative model

Yamanaka *et al.*, 1998; Yamanaka and Yonetani, 1999), outlining that the DSL acts as evaporation zone (i.e., moisture loss zone) during the day and as condensation zone (i.e., moisture gain zone) in the early evening and overnight hours of the day.

Based on the above model it is evident that evaporative mechanisms will vary with both time and depth and are heavily dependent upon the moisture content of the sand surface. Therefore, more detailed studies on the process of actual surface evaporation are necessary to provide a deeper understanding of evaporation dynamics across the beach surface. The objective of this study is to document the behavior of evaporation dynamics at various sediment depths over time and evaluate these dynamics to the conceptual evaporation model.

5.2 Methods

The field experiment was conducted over the course of 5 days from August 2nd to August 7th, 2012 at Padre Island National Seashore, Texas, on the central Texas shore of the Gulf of Mexico (Figure 5.2). To measure the dynamics of evaporation at the beach surface, native beach sand was collected and put into plastic trays (6.5 cm depth by 25 cm diameter). The plastic trays were utilized to isolate the samples from the influence of groundwater, so that variations in moisture content could be attributed to evaporation and condensation dynamics only.

A total of 8 trays were deployed across-shore from the berm crest to the dune toe in four sets of measurement stations. Each set included a tray of saturated sand from the swash zone and a tray of naturally dry dune sand (Figure 5.3). Moisture contents within each set of sediment trays were recorded using a Delta-T moisture probe with measurement depths of 6

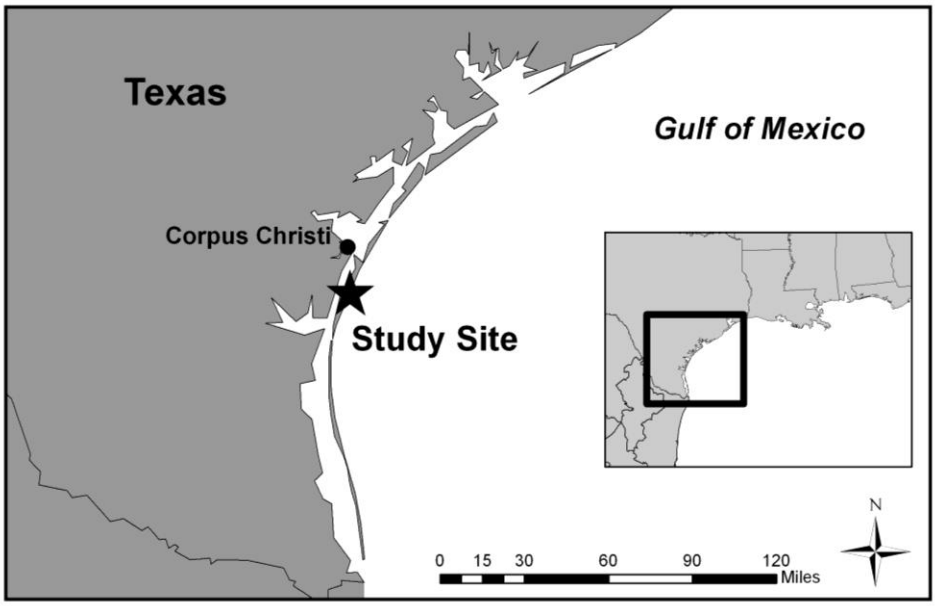

Figure 5.2: Location of Padre Island National Seashore field site


Figure 5.3: Picture of the evaporation trays taken in the field. Dry tray on the left, saturated tray on the right.

cm and 1 cm. Measurement started in the afternoon of August 2nd and ended on the morning of August 7th. Moisture contents of the trays were recorded at dawn, mid-morning, solar noon, mid-afternoon, sunset, and middle night. To monitor potential evaporation during the study period, the evaporation rate from a free water surface was measured using a standard National Weather Service Class A evaporation pan with a Mitutoyo digimatic caliper installed within a stilling well. Measurements of the potential evaporation rate were recorded concurrently with the evaporation tray measurements.

Wind speed was measured with two RM Young model 12102-cup anemometers installed at elevations of 1.5 and 4.5 m above the beach surface. A Qualimetrics model 2020 Micro Response Vane at the top of the weather tower (5 m) was used to monitor wind direction. Air temperature and relative humidity were measured with two Campbell Scientific HMP45C Temperature/Humidity transmitters also at elevations of 1.5 and 4.5 m. Soil temperature was monitored with a pair of Campbell Scientific model 108 temperature sensors buried adjacent to the weather tower at depths of 1 and 50 cm. A continuously recording rain gage was installed to monitor precipitation; however, no rainfall was recorded during the experiment. Finally, radiative energy budgets were monitored using a Hukseflux NR01 four-component net radiometer. All weather instruments were cabled to a Campbell Scientific CR3000 data logger and recorded at 1 hertz for 60-sec blocks spaced at 5-min intervals (Figure 5.4). Topography and instrument locations were surveyed using a Sokkia model 230-R3 total station (Figure 5.5).

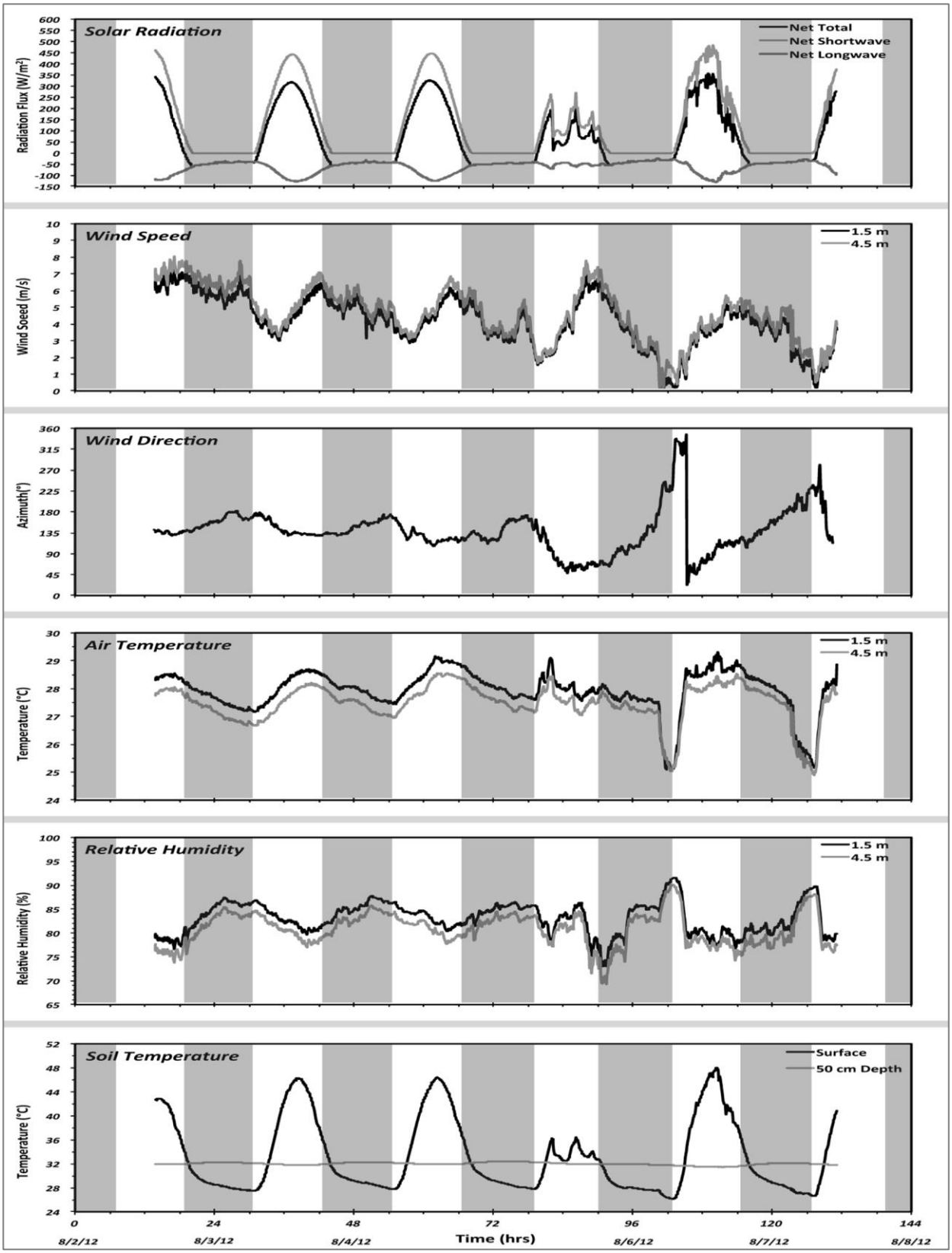

Figure 5.4: Measured meteorological parameters

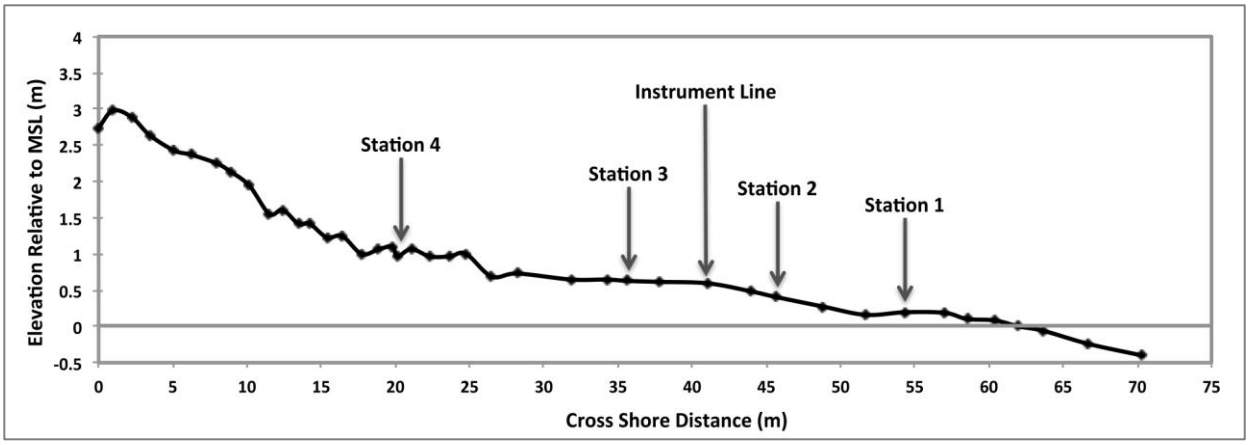

Figure 5.5: Topographic profile of the study site depicting location of meteorological instruments and measurement stations

5.3 Results

5.3.1 Meteorological Parameters

Figure 5.4 shows measured solar radiation, wind speed and direction, air temperature, relative humidity, and soil temperature over the course of the entire study period. All parameters clearly show identifiable diurnal cycles. Solar radiation followed a simple and expected pattern: increasing from sunrise (about 6:45 am local time) to a daily peak value at solar noon (approximately 1:20 pm local time) with a net total of about 300 W/m^2 and then decreasing until sunset (about 8:15 pm). The influence of cloud cover is detectable on the fourth and fifth days of the study period (Aug 5^{th} and 6^{th}). On August 5^{th} the solar radiation signal is significantly decreased throughout the day fluctuating between nearly zero and 200 W/m^2, whereas on August 6^{th} the solar radiation signal reaches its maximum of about 300 W/m^2, however, the signal oscillates quite frequently.

Wind speed variations also exhibited clear cyclic diurnal patterns, increasing in speed throughout the late morning, peaking during the late afternoon and subsequently decreasing

throughout the night and into the early morning hours. The general trend in wind speed is decreasing throughout the study period, with winds speeds consistently around 6.5 m/s on the first day (Aug 2nd) of the study and ending with wind speeds around 2.0 m/s on the morning of the last day (Aug 6th). Wind direction was the only meteorological parameter that did not consistently follow a diurnal cycle. Over the course of the first three days (Aug 2nd – 4th) the wind direction maintained a steady southerly oblique on-shore direction, fluctuating between 110° and 175°. On the fourth and fifth days of the study the winds begin to fluctuate, rotating into a northerly wind throughout the morning then switching into a southerly wind during late afternoon and early evening hours and finally back to a northerly wind during the overnight and early morning hours.

Air temperature increased rapidly each day reaching its daily peak value around 3:00 pm, and then decreased gradually to its daily lows around 4:00 a.m. This trend is particularly evident over the first three days of the study period. However, on the fourth day (Aug 5th) of the study, air temperature maintaining a relatively consistent, albeit lower, temperature during the day and through the night. It is clear that the variations in air temperature are driven by the solar radiation input. Variations in air temperature can also be related to wind direction shifts. This influence is apparent in the sudden drop in air temperatures during the early morning hours on August 6th and 7th as cooler northwesterly air resulted in the sudden decrease in air temperatures. Relative humidity also clearly shows diurnal cycles, which are negatively correlated with variations of air temperature, as expected.

The temperature at the soil surface also showed a very distinct diurnal cycle, as it increased rapidly throughout the early morning reaching its daily peak value around 2:00 in the

afternoon. Around that time it decreased rapidly until just after sunset, when it gradually decreased to its daily lows around sunrise. However, on the fourth day (Aug 5th) of the study, soil surface temperature is significantly decreased in value, fluctuating throughout the day. As with air temperature it is clear that the variations in soil surface temperature are driven by the solar radiation input. At a soil depth of 50 cm the sand maintains a consistent temperature of 32°C.

In general, solar radiation is the major energy source that influences the temperature changes of the air and the soil surface. As the temperature of the soil surface responds to energy input more rapidly than that of the air, the atmospheric pressure subsequently differs to various degrees between them throughout the day. This pressure difference along with wind speed and the relative humidity of the air column controls the rates of moisture transfer between the soil surfaces and the air column, which in turn dictates the evaporation of moisture from a surface.

5.3.2 Potential Evaporation

The potential evaporation rates throughout the study period are shown in Figure 5.6. Rates are plotted at the midpoints of the time period they represent (specifically, a change of 0.1 mm measured from 1:45 am to 7:00 am was calculated as a rate of 0.5 mm/day and plotted at the mid-point of 4:40 am). Since potential evaporation is heavily dictated by the meteorological parameters it is not surprising that there is a distinguished diurnal cycle in the potential evaporation signal. Evaporation rates increased rapidly during the early morning hours reaching a peak in the early afternoon (approximately 3:30 pm) and then subsequently

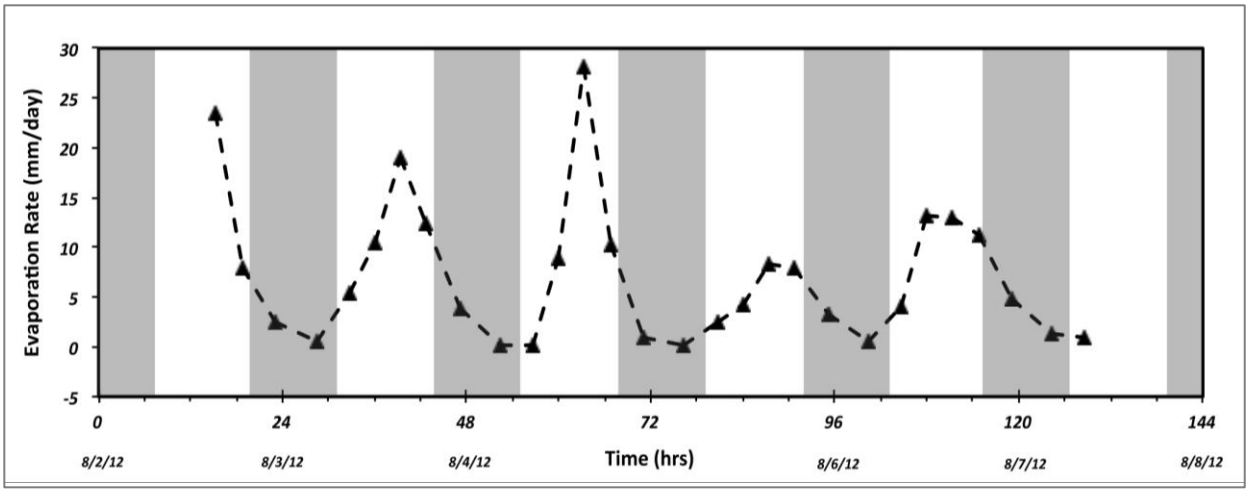

Figure 5.6: Measured potential evaporation rates. Rates are plotted at the mid-point of the time period they encompass.

decreased throughout the late afternoon and early evening hours before reaching a minimum value just before sunrise.

Over the first three days of the study period (Aug 2nd – 4th) peak evaporation rates reached a value of ≥ 20 mm/day, however, peak evaporation rates over the final two days of the study period (Aug 5th -6th) were markedly lower at 8 and 13 mm/day, respectively. These results are expected based on the meteorological parameters, which depict solar radiation, air temperature and soil temperature all having peak values during the mid-day to early afternoon hours over the first three days; yet over the final two days of the study these values were noticeably lower and less consistent throughout the day with frequent fluctuations in values, which ultimately led to lower evaporation rates throughout the day.

5.3.3 Evaporation Dynamics of the Saturated Trays

5.3.3.1 Full (0-6 cm) Sand Layer

Figure 5.7 shows the measured evaporation rates over the entire study period for the saturated trays across the full measurement layer depth (0 to 6 cm), as well as the potential evaporation rates. At the initial time period, the evaporation rate for the full sand layer is 22.7 mm/day, which nearly matches the potential evaporation rate at 23.4 mm/day. This finding equates well with the literature, revealing an actual evaporation response approximating potential evaporation for saturated/near-saturated sediments (Ritchie, 1972; Monteith, 1981; Parlange and Katul, 1992; Aydin *et al.*, 2005). After this initial time period, the evaporation rates for both the full sand layer and the potential evaporation begin to drop, as expected, due to diminishing meteorological conditions to drive the evaporative mechanics. However the evaporation rate for the full sand layer is markedly lower over the next few hours until finally leveling off during the evening and over night periods. Subsequently, the evaporation rates over the course of the next few days do increase, yet at significantly lower values compared to the potential evaporation rate, whereas during the evening and overnight hours the evaporation rates for both systems drop to nearly zero.

The vast disparity between the evaporation rates of the full sand layer and potential evaporation during the daytime hours is very intriguing. This finding suggests that the evaporation dynamics for the full sand layer has transitioned out of the constant-rate stage of Stage 1 and into a falling-rate stage of Stage 2, which implies that the moisture content of the sand layer has dropped below the threshold for which the evaporative system can be controlled by the meteorological parameters and is thus now being limited by the moisture conditions of

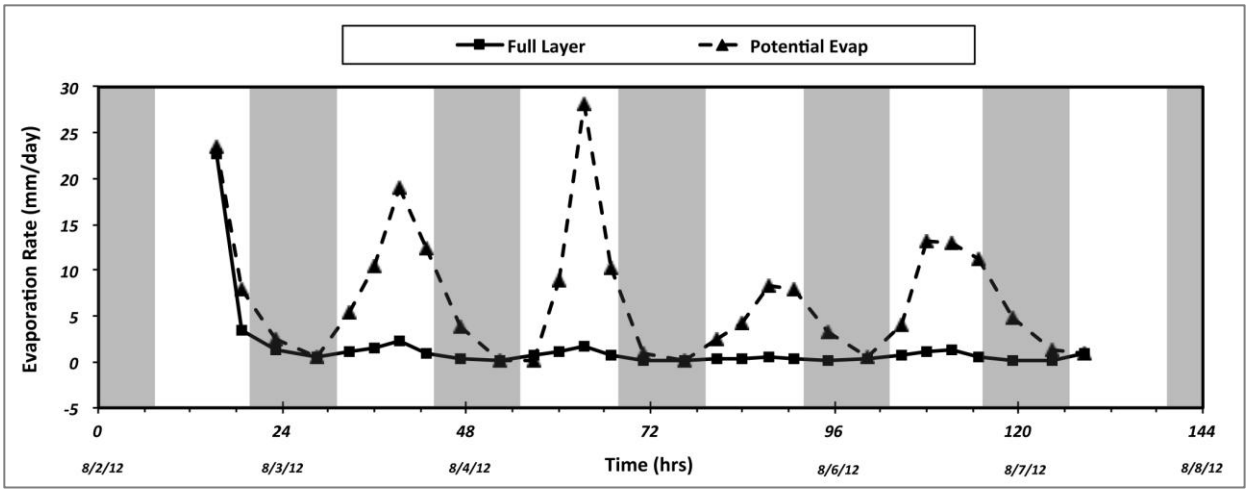

Figure 5.7: Measured evaporation rates of the saturated trays for the full layer depth (0-6 cm) and measured potential evaporation rates. Rates are plotted at the mid-point of the time period they encompass.

the sand layers. This transition along with the continued yet lower evaporation rate of the full sand layer is evidenced in the moisture content signal measured for the full 6 cm sand layer (Figure 5.8). Notice that the moisture content for the full layer begins at a saturation level of ~42% moisture by volume and then subsequently experiences a significant drop in moisture content down to ~36% moisture. This result is fundamentally due to the high evaporation rate over those first few hours. After this initial time period the moisture content continues to decrease throughout the entire study, indicating continued evaporative drying; however, at a markedly slower rate. This finding is indicative of the falling-rate stage evaporation dynamics within Stage 2 of the conceptual evaporation model.

5.3.3.2 Upper (0-1 cm) and Lower (1-6 cm) Sand Layers

Gaining insight into the evaporation dynamics across the top 6 cm of the sand surface is exceedingly beneficial to improving our understanding of the beach evaporation system.

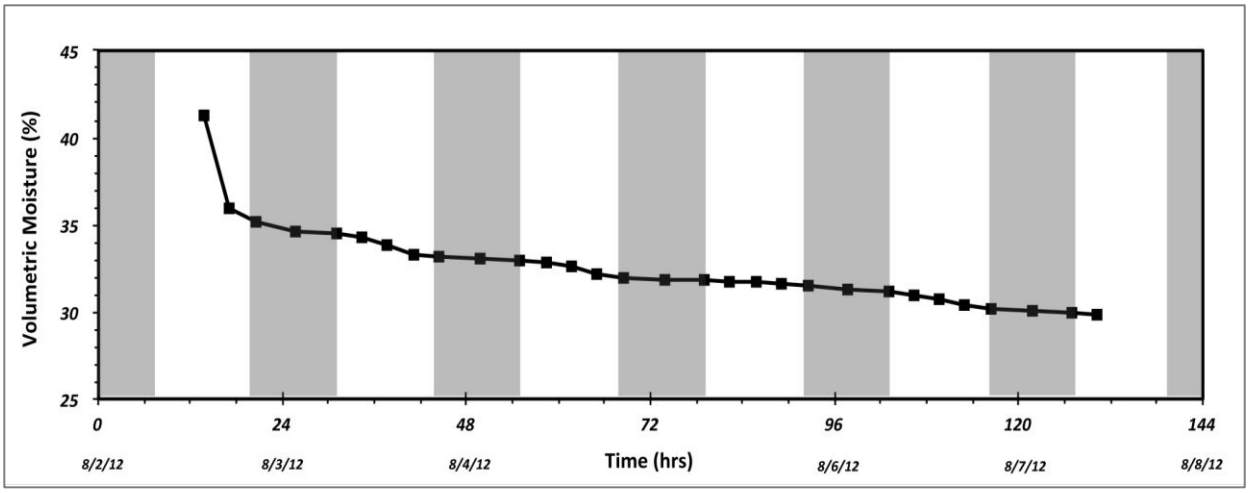

Figure 5.8: Measured moisture content of the saturated trays for the full layer depth (0-6 cm).

However, in the context of aeolian transport systems, insight into the evaporative dynamics directly at the sediment surface (< 1 cm) is ideal. Therefore, to provide a more holistic understanding of the beach evaporative system the full 6 cm layer was divided into an upper (0 to 1 cm depth) and a lower (1 to 6 cm depth) sand layer. Figure 5.9 shows the measured evaporation rates for the saturated trays at the upper and lower layers over the entire study period. The evaporation rate at the upper layer is initially 22.4 mm/day, which equates to 99% of the evaporation rate for the full 6 cm sand layer (22.7 mm/day), whereas the lower layer exhibits a significantly lower evaporation rate at only 0.3 mm/day. This finding illustrates that under saturated soil conditions, evaporation occurs directly at the soil surface with minimal evaporation occurring below the upper surface layer. Accordingly, these findings match well within Stage 1 of the conceptual evaporation model. Due to the saturated moisture conditions of the sand the ETL is located directly at the upper surface layer, and thus the evaporation rate nearly approximates the potential evaporation rate (22.4 mm/day vs. 23.4 mm/day). Conversely, the minimal evaporation rate at the lower layer suggests that this layer is located

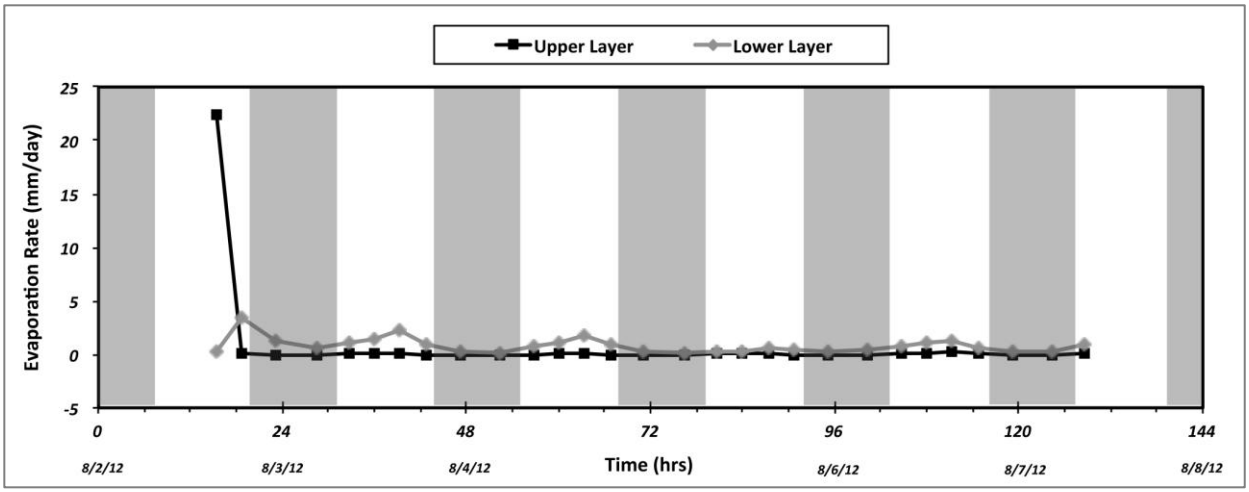

Figure 5.9: Measured evaporation rates of saturated trays for the upper (0-1 cm) and lower (1-6 cm) layers. Negative evaporation rates indicate condensation of moisture. Rates are plotted at the mid-point of the time period they encompass.

below the ETL and is situated largely within the WSL; and therefore mechanically it is primarily transmitting moisture to the upper layer in order to replenish the evaporated moisture.

After these initial few hours the evaporation dynamics completely shift for both the upper and lower sand layers. Figure 5.10 provides a more detailed view of the measured evaporation rates (rates < 4 mm/day) for the upper and lower layers. At the upper layer the evaporation rate drops immediately to a very low rate (0.02 mm/day) and consistently maintains this low rate throughout the entirety of the study period. Additionally, there is a small yet noticeable diurnal evaporation and condensation cycle at the upper sand layer, in which evaporation rates throughout the day are generally greater than zero whereas during the evening and overnight hours the upper sand layer experiences negative rates (i.e., condensation). The evaporation rate for the lower layer, on the other hand, immediate jumps in value to a rate of 3.5 mm/day and then subsequently decreases throughout the first night. Over the course of the next four days the evaporation rate exhibits a small but noticeable

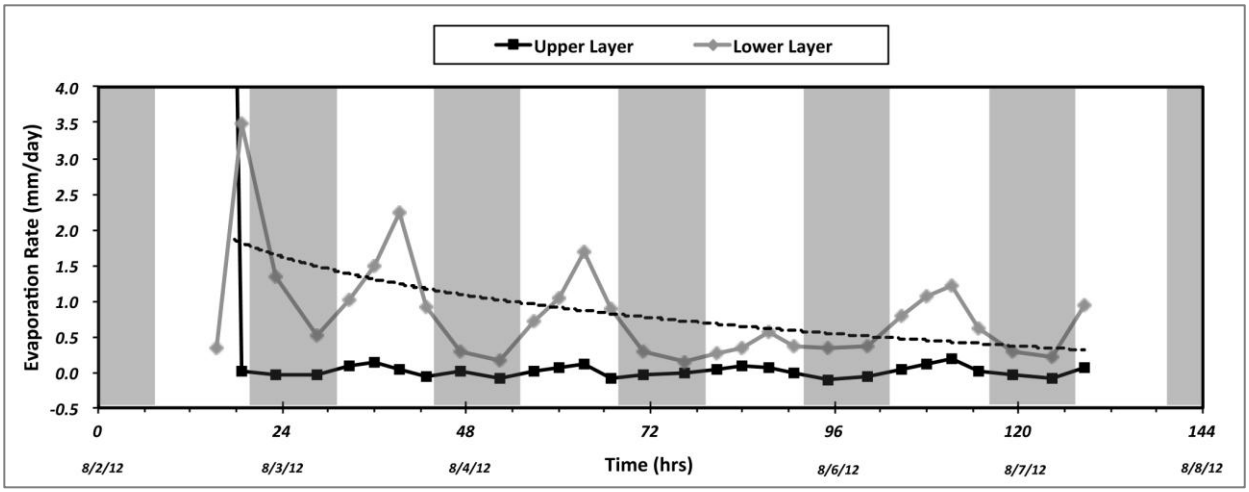

Figure 5.10: Detail view of the measured evaporation rates of saturated trays (< 4 mm/day) for the upper (0-1 cm) and lower (1-6 cm) layers. Negative evaporation rates indicate condensation of moisture. Rates are plotted at the mid-point of the time period they encompass.

diurnal patterns with rates rising during the early morning and peaking in the early afternoon before decreasing to nearly zero overnight. Although the evaporation dynamics at the lower layer exhibits a diurnal pattern there is largely a decreasing trend in the rate of evaporation throughout the study period (note the trendline in Figure 5.10).

These results imply that both sand layers have transitioned out of Stage 1 and immediately into Stage 3 of the evaporation model. The persistent very low rate of evaporation as well as the diurnal cycle of evaporation and condensation at the upper layer implies that a DSL has developed. By contrast, the immediate jump in evaporation rate after the initial time period for the lower sand layer, along with the immediate decrease in evaporate for the upper sand layer, suggests that the ETL has fallen below the surface and is located fully within the lower sand layer. Furthermore, the decreasing rate of evaporation over the course of the study period indicates that the drying front (i.e., lower boundary) of the DSL is slowly increasing in

depth through the lower layer with time and thus the rate of evaporation of moisture is slowing as the lower layer continues to dry.

Furthermore, these dynamics are also evidenced in the measured moisture content signals for the upper and lower sand layers (Figure 5.11). At the upper layer the initial high rate of evaporation produces a significant drop in moisture content, from a saturation level of ~42% moisture by volume down to ~10% moisture by volume. After this initial drop the upper sand layer exhibits virtually no change in moisture content over the course of the rest of the study period. This relatively persistent moisture level is a product of the very low and consistent rate of evaporation throughout the study period. Alternatively at the upper layer, the positive rate of evaporation, yet drastically lower than the potential evaporation rates, produces a slow and steady decrease in moisture content throughout the study period.

5.3.4 Evaporation Dynamics of the Dry Trays

Both the upper (0-1 cm) and lower (1-6 cm) layers exhibit a small but identifiable cycle of evaporation and condensation (Figure 5.12). Throughout the day the sediment generally experiences declining moisture levels, particularly in the early morning hours, and rising moisture levels during the evening and overnight hours. The fluctuations in moisture content are very small (+/- 0.15 - 0.66% by volume per day/night), indicating that the contribution of atmospheric water vapor to the sand is minor. The upper level exhibits larger fluctuations in moisture compared to the lower layer, which implies that it is more heavily influenced by the evaporation and condensation cycle of atmospheric water vapor. However, the lower layer does exhibit a diurnal cycle of evaporation and condensation, indicating that evaporation and

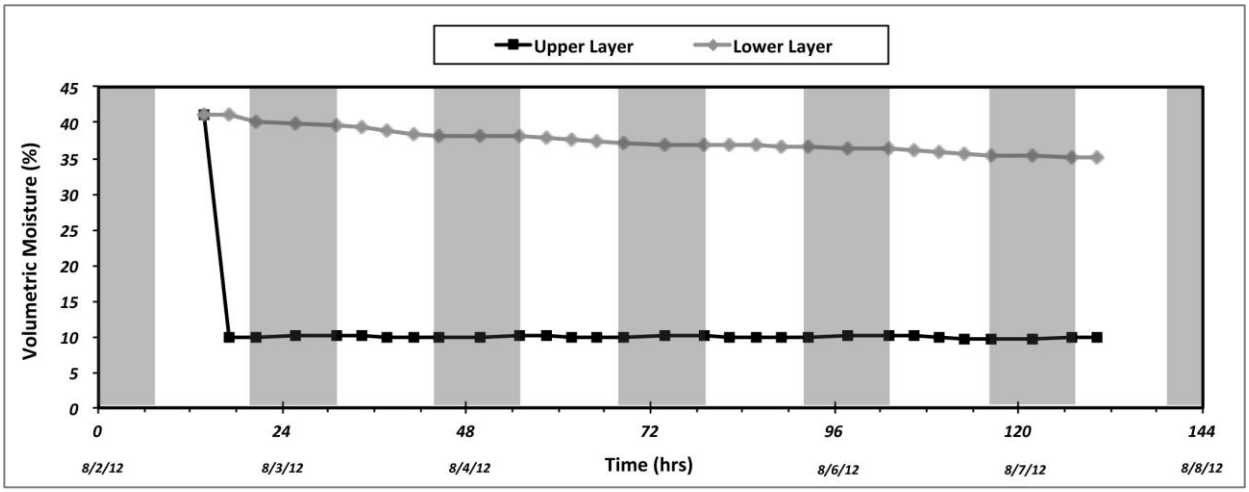

Figure 5.11: Measured moisture contents of saturated trays for the upper (0-1 cm) and lower (1-6cm) layers.

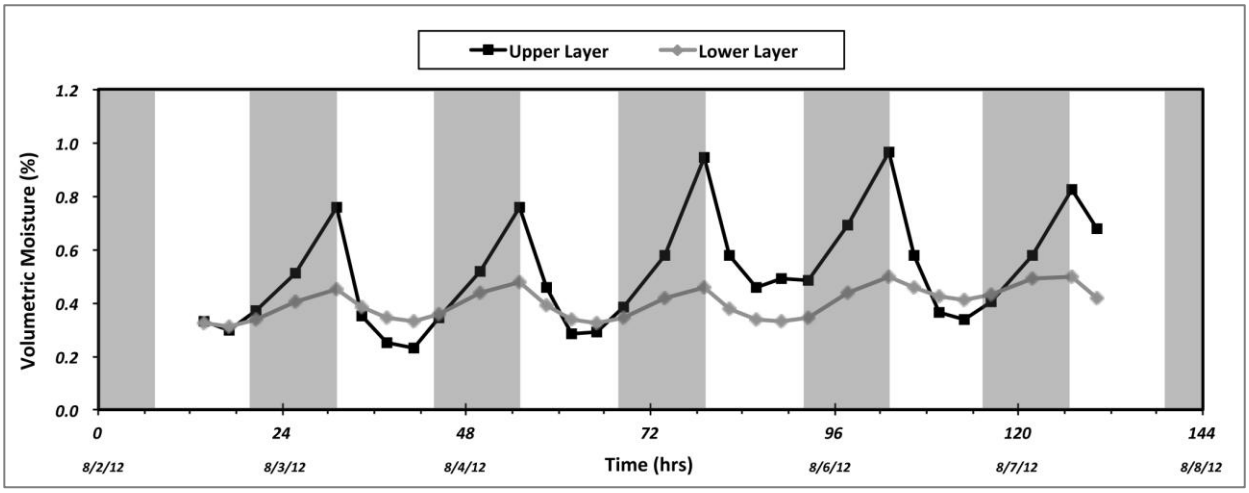

Figure 5.12: Measured moisture contents of the dry trays at the surface (0-1 cm) and below surface (1-6cm) depths.

condensation dynamics can influence the moisture content of a dry sand surface to a depth of at least 6 cm. This suggests that evaporation and condensation dynamics are important at depth.

A number of researchers have associated diurnal fluctuations in moisture content with the cyclic fluctuation in soil surface temperature (Hellwig, 1973; Idso *et al.*, 1974; Hellwig, 1978; He and Kobayashi, 1998), establishing that decreasing moisture content correlates with

increasing soil temperature. Figure 5.13 confirms this association, illustrating that higher soil temperatures correspond with lower moisture contents and vice versa. Regression analysis indicates a weak but significant relationship between soil temperature and moisture content. R^2 values for the upper and lower layers were 0.495 and 0.322, respectively; however, the relationships for both sand layers were determined to be statistically significant at the 99% confidence interval (Table 5.1). These findings correspond well with the dynamics of Stage 3 in the conceptual evaporation model, which hypothesizes that a DSL will act as an evaporation zone during the day as soil temperature values increase and as a condensation zone at night as soil temperature decreases (Yamanaka et al., 1997; Yamanaka et al., 1998; Yamanaka and Yonetani, 1999).

The measured evaporation rates at the upper and lower layers corroborate these findings, generally showing negative evaporation rate values (i.e., condensation rates) occurring during the evening and overnight hours and evaporation rates greater than zero throughout the day (Figure 5.14). Peak rates in condensation average ~0.15 mm/day. However, they occur at different times during the night between the two sand layers. At the upper layer, peak condensation occurred before sunrise (between 1:45 am and 7:00 am local time), whereas peak condensation rates for the lower layer occurred just before midnight local time. Peak evaporation generally occurs during the early morning hours just after sunrise (approximately 7:00 am to 10:20 am local time) at a rate of ~0.27 mm/day on average for both sand layers.

This finding is puzzling considering that the availability of energy to drive the evaporative system occurs during the midday to afternoon hours. However, Hellwig (1973, 1978) attributed these peaks in evaporation during the early morning hours to the “burning off”

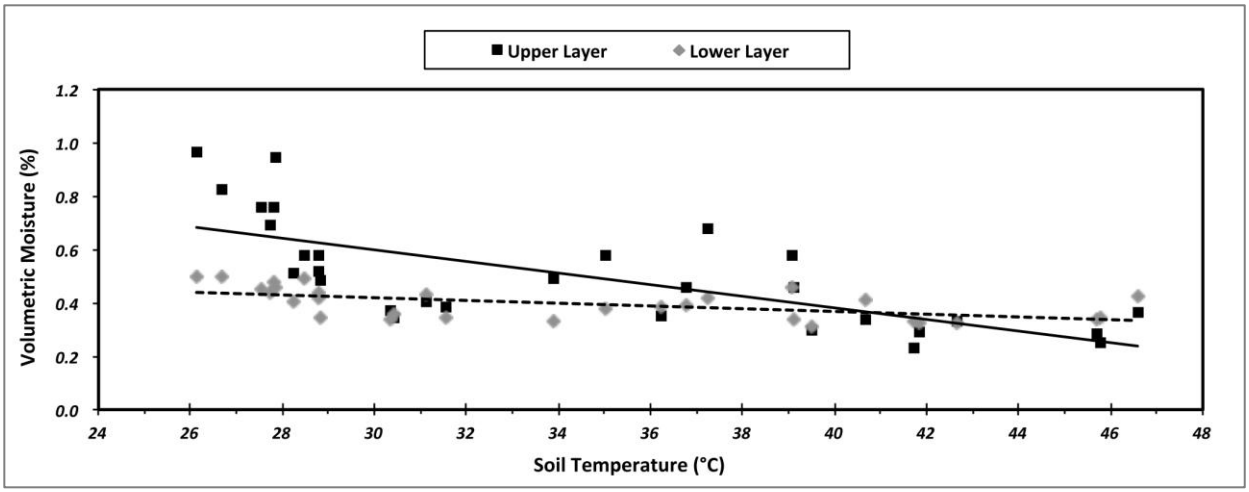

Figure 5.13: Relationship between measured moisture content for the upper (0-1 cm) and lower (1-6cm) layers and soil temperature.

Table 5.1: Coefficients of Determination and Statistical Significance of the Relationship between Soil Temperature and Moisture Content

Sediment Depth	R^2 value	p-value
Upper Layer	0.495	0.0028
Lower Layer	0.322	0.0081

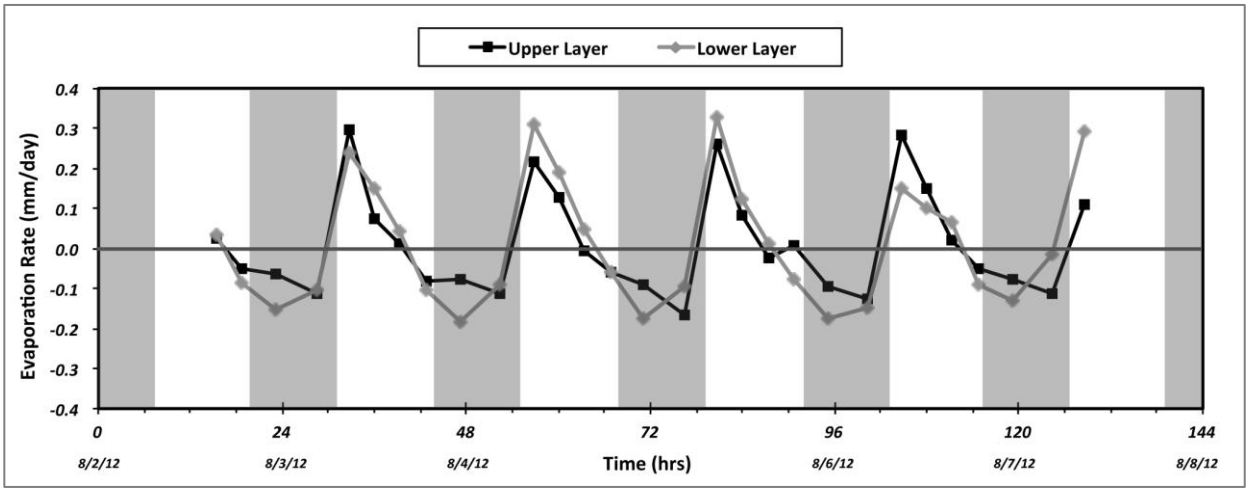

Figure 5.14: Measured evaporation rates of the dry trays at the surface (0-1 cm) and below surface (1-6cm) depths. Negative evaporation rates indicate condensation of moisture. Rates are plotted at the midpoint of the time period they encompass.

of condensation moisture. The author found a strong correlation between evaporation rates and the changes in the soil temperature minus air temperature value for successive measures. In essence, after sunrise both the soil temperature and air temperature begin to increase due to increases in the supply of solar energy; however, soil temperature increases at a much faster rate than the air temperature and a temperature gradient between the soil and air temperatures develops. This temperature gradient increases rapidly during the early morning hours reaching its maximum around solar noon, upon which time the temperature gradient begins to decrease throughout the afternoon hours as soil temperature drops yet air temperature is still rising. Hellwig (1973, 1978) suggests that it is the rapidly increasing temperature gradient between the soil and air temperatures during the early morning hours that results in the high evaporation rates. Figure 5.15 confirms this correlation, illustrating that large increases in the soil minus air temperature gradient over time (> 4 C°) correspond with evaporation rates greater than 0.1 mm/day, which coincidently all occur during the early morning hours (see Figure 5.14 illustrating the time of day for the evaporation rates).

Although the upper layer exhibited larger fluctuations in moisture content (see Figure 5.12), the evaporation rate signals between the upper and lower sand layers are nearly identical (Figure 5.14). This finding is a product of the fact that the lower layer encompasses a volume of sediment that is five times larger than the upper layer (1 to 6 cm depth vs. 0 to 1 cm depth). The smaller changes in moisture by volume measured at the lower sand layer result in the large changes in measured evaporation rates. Nevertheless, this finding implies that evaporation and condensation dynamics are equally effective at depth.

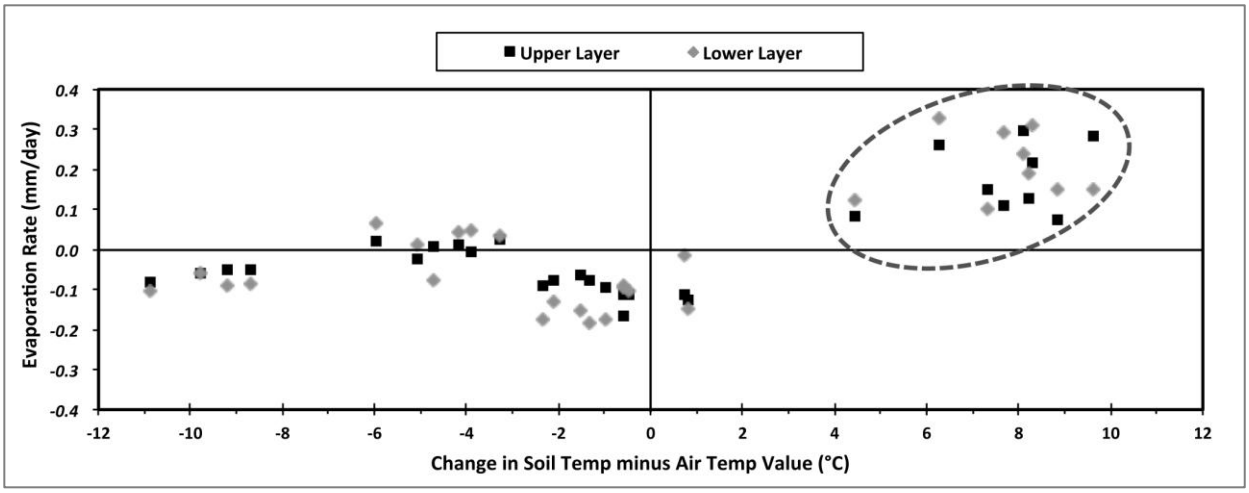

Figure 5.15: Relationship between evaporation rates for the upper (0-1 cm) and lower (1-6cm) layers and the change value of soil minus air temperature for successive measurements.

5.4 Summary and Conclusion

The primary goal of this study was to document and evaluate the behavior of soil surface evaporation under initial saturated and total dry moisture conditions and evaluate these dynamics to the conceptual evaporation model. Several noteworthy findings emerge. For the sediment trays starting with saturated sands, the evaporation dynamics for the full 6 cm sand layer initially exhibits an evaporation rate that approximates the potential evaporation rate (22.7 mm/day for the full layer vs. 23.4 mm/day potential evaporation rate); yet the sand layer is only able to maintain this rate of evaporation for a few hours. After these initial few hours the moisture content of the sand layer drops below saturated/near-saturated conditions, upon which time the evaporation of the layer decreases to a rate significantly below that of the potential rate. These findings fundamentally illustrate that actual sand surface evaporation dynamics do not perpetually approximate the potential evaporation. In reality as the sand layer dries the evaporation dynamics transitions from being controlled by the meteorological conditions to the moisture conditions of the sand.

This finding is extremely beneficial to improving our understanding of beach surface evaporation dynamics; however, it does not provide us with an accurate assessment of evaporation directly at the sand surface. Separating the full 6 cm sand layer is into an upper surface (0 to 1 cm) layer and a lower (1 to 6 cm) illustrates that over the course of the first few hours nearly all the evaporation occurring within the sediment trays occurs at the upper sand layer (22.4 mm/ day at the upper layer vs. 0.3 mm/day at the lower layer). After these first few hours, however, the evaporation rate at the upper layer drops immediately to a very low and persistent rate of evaporation throughout the rest of the study period. By contrast, the evaporation rate at the lower layer actually increases over the next few hours then proceeds to slow and steady decline throughout the study period.

For the sediment trays starting under naturally dry moisture conditions, both the upper and lower sand layers exhibit a small yet visible diurnal evaporation and condensation behavior. Throughout the day the sand generally experiences declining moisture levels, due to evaporation rates greater than zero, and rising moisture content levels during the overnight hours associated with the negative evaporation rate values (i.e., condensation rates). It was determined that the diurnal fluctuations in moisture content values correlated well with the cyclic wave of soil surface temperatures, illustrating that moisture content values decrease with increasing soil temperature. Additionally, peak evaporation generally occurs during the early morning hours just after sunrise for both sand layers. Within the literature it had been suggested that the rapidly increasing temperature gradient between the soil and air temperatures during the early morning hours results in the high evaporation rates over this time period. Analysis of the data confirms this correlation, illustrating that large increases in the

soil minus air temperature gradient over time parallel with the higher evaporation rates found throughout the early morning hours.

Chapter 6 -- Variations in Surface Moisture Contents over Space and Time for a Fine-grained Beach

6.1 Introduction

Beach environments theoretically represent an ideal locale to study the spatial distribution and temporal variations of surface moisture content because they are a relatively simple system. First, native sand on coastal beaches is often well-sorted, which means spatially homogeneous texture, porosity, and hydraulic conductivity (relative to the complex textures of natural soils often which tend to exhibit large spatial variability). Second, beaches usually have sparse vegetation due to high salinity levels and frequent inundation. Finally, the beach surface is topographically relatively uniform with low gradients.

A relatively small number of field studies have provided limited data regarding surface moisture content at various beaches (e.g. Jackson and Nordstrom, 1997; Atherton *et al.*, 2001; Wiggs *et al.*, 2004b; Yang and Davidson-Arnott, 2005; Davidson-Arnott *et al.*, 2005; McKenna Neuman and Langston, 2006; Zhu, 2007; Davidson-Arnott *et al.*, 2008; Bauer *et al.*, 2009; Namikas *et al*., 2010). However, from these reports it is clear that beach surface moisture content dynamics are far from simple, as surface moisture tends to be highly variable in both time and space.

In general, the spatial and temporal patterns of beach surface moisture are controlled by a number of factors including topography, groundwater depth, water table fluctuation timing and magnitude, moisture retention and capillary flow properties of the sediment column, evaporation-condensation cycles, tidal elevation and period, swash effects, and precipitation. However, only a few of the available studies have attempted to link variations in

surface moisture content directly with the processes responsible for those variations (e.g., Atherton *et al.*, 2001; Zhu, 2007). Consequently the currently available database is not sufficient to allow a characterization of beach moisture content that is sufficient for modeling purposes. This study begins to address these gaps by documenting spatial and temporal variabilities in the surface moisture content of a fine-grained beach.

The major purpose of this chapter is to 1) measure, document, and analyze the spatial and temporal patterns of beach surface; and 2) identify the relative importance of the various factors in controlling surface moisture variability. Variations in field-measured moisture content were examined with regard to cross-shore and alongshore variability over time. Key processes regulating this variability were identified, and the relationships among these processes were further clarified.

6.2 Methods

6.2.1 Study Site

The experiment was conducted over the course of 12 days from January 18 - 29, 2012 at Padre Island National Seashore, Texas, on the central Texas coast of the Gulf of Mexico (Figure 6.1). The native sediment is predominately very well sorted fine to very fine quartz, with a mean grain size of approximately 0.13 mm (2.94 phi). The beach environment was approximately 65 m wide with small coppice dunes extending into the backbeach roughly 10 m from an established 2 m high foredune. The central Texas coast experiences a micro tidal range (typically 0.3-0.8 m), with mixed but predominately diurnal tidal cycles (Weise and White, 1991).

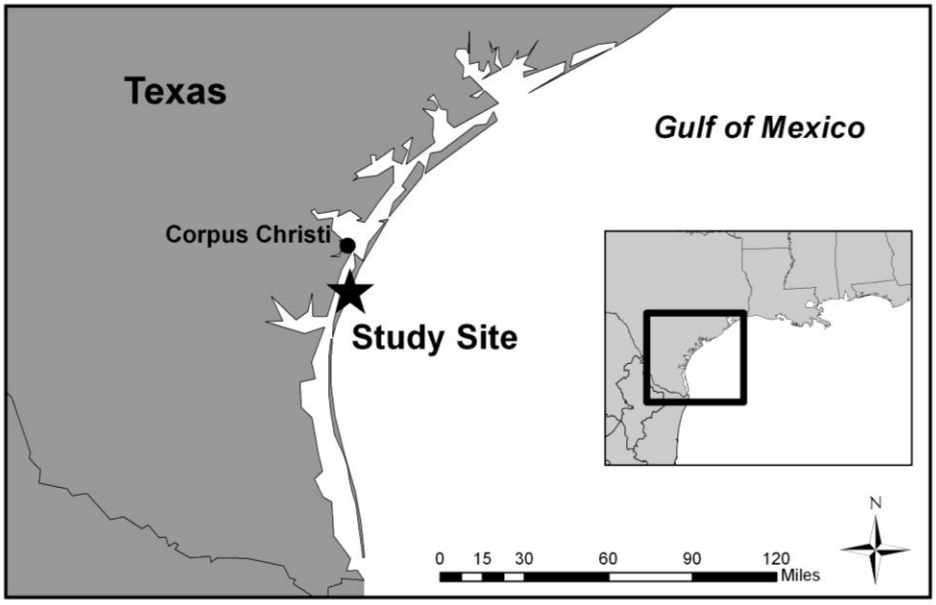

Figure 6.1: Location of Padre Island National Seashore field site.

6.2.2 Field Experiment

To document the spatial and temporal variability in beach surface moisture, a grid of measurement lines was established across the beach surface extending from the dune toe to the fore beach (Figure 6.2). The grid was comprised of 12 along-shore lines spaced at various intervals (from 2.5 m to 5 m) in the cross-shore direction. Each along-shore line included five measurement locations spaced at 5 m intervals. The lines are designated as L1 to L12, with L1 located adjacent to the dune toe in association with groundwater well W1 and L12 located 15 m seaward of well W4. Surface moisture contents were recorded using a Delta-T Theta soil moisture probe modified to collect surface moisture contents to a depth of 1.0 cm (Schmutz and Namikas, 2011). Moisture contents were recorded at dawn, mid-morning, solar noon, mid-afternoon, sunset, and middle night. During high tide, the most seaward lines of the grid were often submersed by swash. It was presumed that the sediment was saturated and measurements were not collected. The infrequent measurement schedule of surface moisture

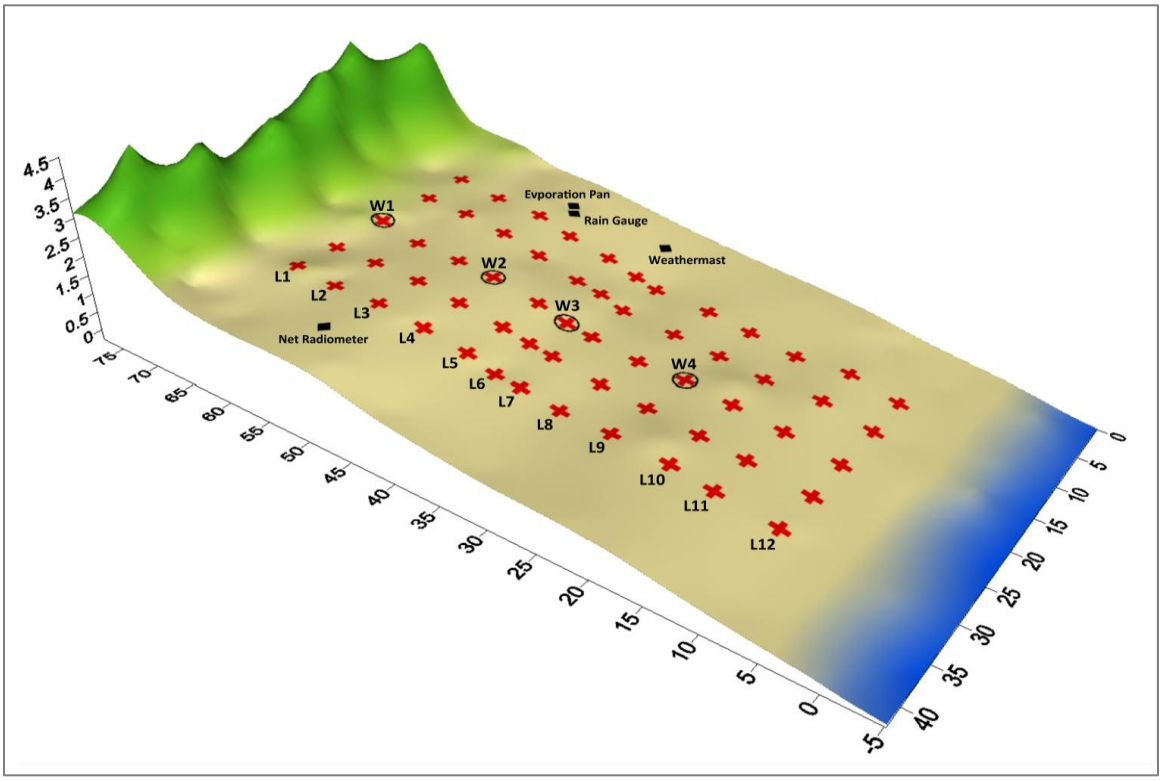

Figure 6.2: Three-dimensional overview of study area showing the surface moisture measurement lines (L1-L12), groundwater wells (W1-W4) and sensor locations. Cross-shore distance is relative to mean sea level (MSL = 0).

contents reflects in part the expected rates of change in surface moisture content, but is also partly intended to minimize the small but cumulative surface disruption that results from probe insertion.

Water table depth and fluctuations were monitored using four groundwater wells installed along a shore-perpendicular transect extending from the berm crest across the middle beach area to the backbeach. The wells were located at distances of 60, 45, 37.5, and 25 m landward of mean sea level, and were designated as wells W1 to W4 (Figure 6.2). The wells consisted of perforated 10 cm diameter circular PVC pipe to allow free water flow. They were screened with fine nylon mesh to prevent the entrance of sand. Pressure transducers (PTs) (Global Water WL400 series and KPSI 730 series) were installed at the bottom of each well to

monitor water level fluctuations (Figure 6.3). Tidal oscillation were monitored initially using a Global Water WL400 series pressure transducer attached to an iron stake that was inserted deep into sand within the surf zone about 50 m seaward of the berm crest. However, the PT failed on the second day of measurement and tidal fluctuations were obtained from a National Oceanic and Atmospheric Association (NOAA) tide gauge at Bob Hall Pier (Figure 6.4), located approximately 10 km north of the study site. Previous work at Padre Island National Seashore has found that the tidal data collected at this station correlates almost perfectly with local measurements.

Potential evaporation above a free water surface was measured using a standard National Weather Service Class A evaporation pan with a Mitutoyo digimatic caliper installed within a stilling well to measure the elevation of the water surface. Measurements of the reference evaporation pan were recorded concurrent to the surface moisture measurement readings (Figure 6.5).

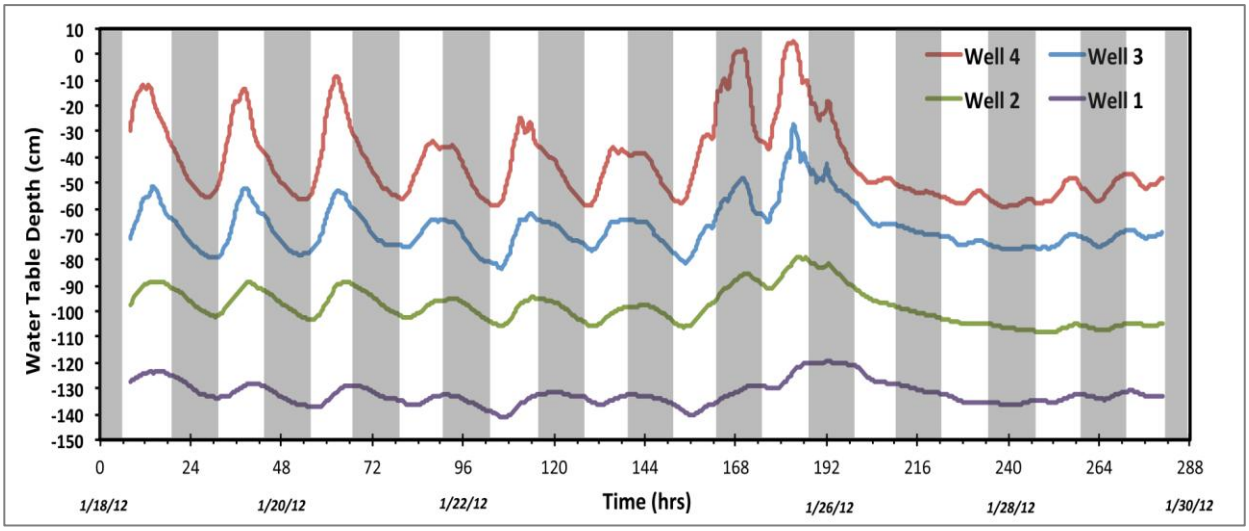

Figure 6.3: Water table depth and fluctuation for each of the four groundwater wells.

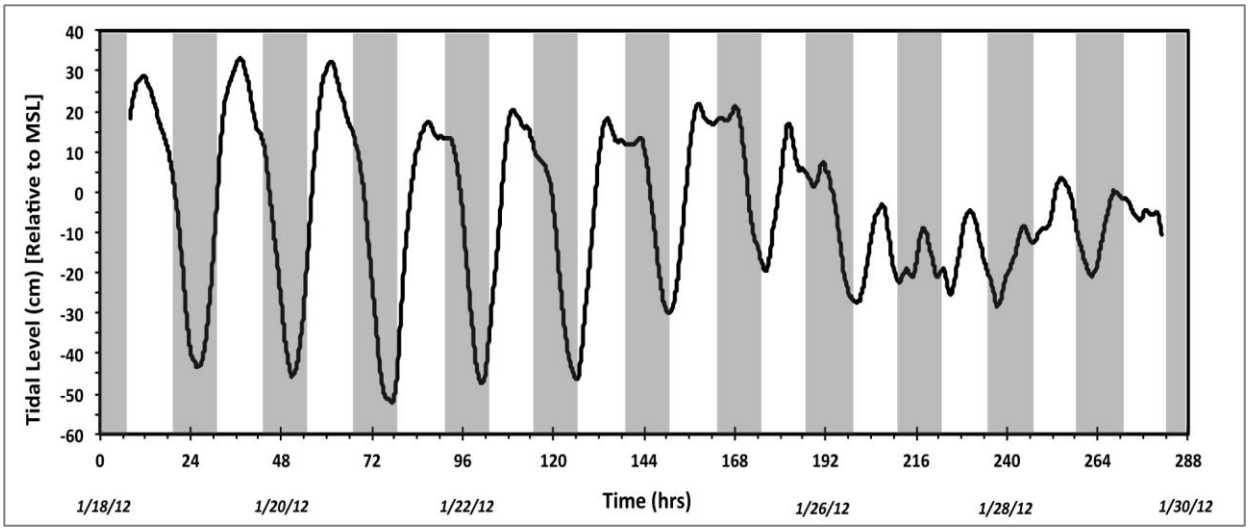

Figure 6.4: Tidal level and fluctuation magnitude

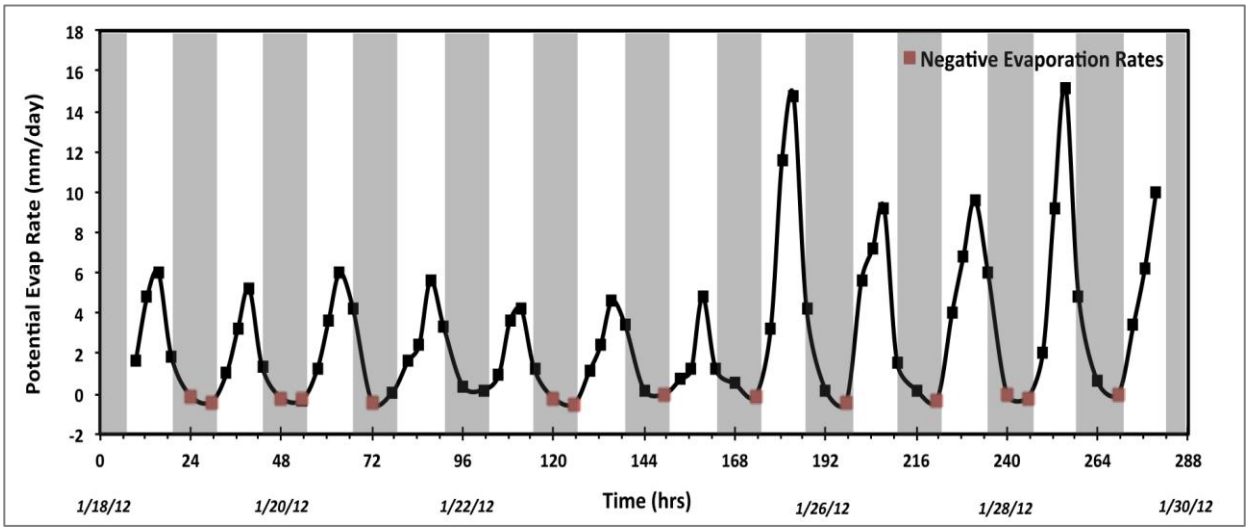

Figure 6.5: Measured potential evaporation rates. Rates are plotted at the midpoint of the time period they encompass. Negative rates are distinguished with a red square.

Wind speed was measured with three RM Young model 12102-cup anemometers installed at elevations of 1, 2.11 and 4.45 m above the beach surface. A Qualimetrics model 2020 Micro Response Vane at the top of the weather tower (5 m) was used to monitor wind direction. Air temperature and relative humidity were measured using two Campbell Scientific HMP45C temperature/humidity transmitters installed at elevations of 1 and 4.45 m above the

beach surface. To measure soil temperature a pair of Campbell Scientific model 108 temperature sensors was buried adjacent to the weather tower at depths of 1 and 20 cm below the surface. Additionally, a continuously recording rain gauge was installed to monitor precipitation; however, no rainfall was recorded during the experiment. Finally, shortwave and longwave radiation were monitored using a Hukseflux NR01 four-component net radiometer. All instruments were cabled to a Campbell Scientific CR3000 data logger and recorded at 1 hertz for 60-sec blocks spaced at 5-min intervals (Figure 6.6).

6.2.3 Moisture Retention Curves and Hydraulic Conductivity

The moisture retention and unsaturated hydraulic conductivity curves are given by the analytical form of the soil hydraulic functions proposed by van Genuchten (1980):

$$\theta\ h\ = \theta_r + \frac{\theta_s - \theta_r}{1+\ \alpha h^{\ n\ m}}$$
$$K\ h\ = \mathrm{K_s}\Theta^{\lambda}\ 1 -\ \ 1 - \Theta^{1/\ m\ \ \ m\ 2} \qquad [1]$$

in which, θ_r and θ_s denote the residual and saturated water contents, respectively, α and n are empirical parameters, m = 1-(1/n), K_s is the saturated hydraulic conductivity, Θ is the effective degree of saturation, and λ is a pore connectivity parameter derived by Mualem (1976) to equal 0.5. To designate the main drying and wetting main boundary moisture retention and unsaturated hydraulic conductivity curves, the function parameters θ_r, θ_s, α, n, m, and K_s are denoted with superscripts *d* and *w* to indicate either a drying or wetting curve, respectively.

Based on moisture content measurements collected at the measurement lines corresponding with the four groundwater wells, the main drying and wetting moisture retention and unsaturated hydraulic conductivity curves were constructed (Figure 6.7).

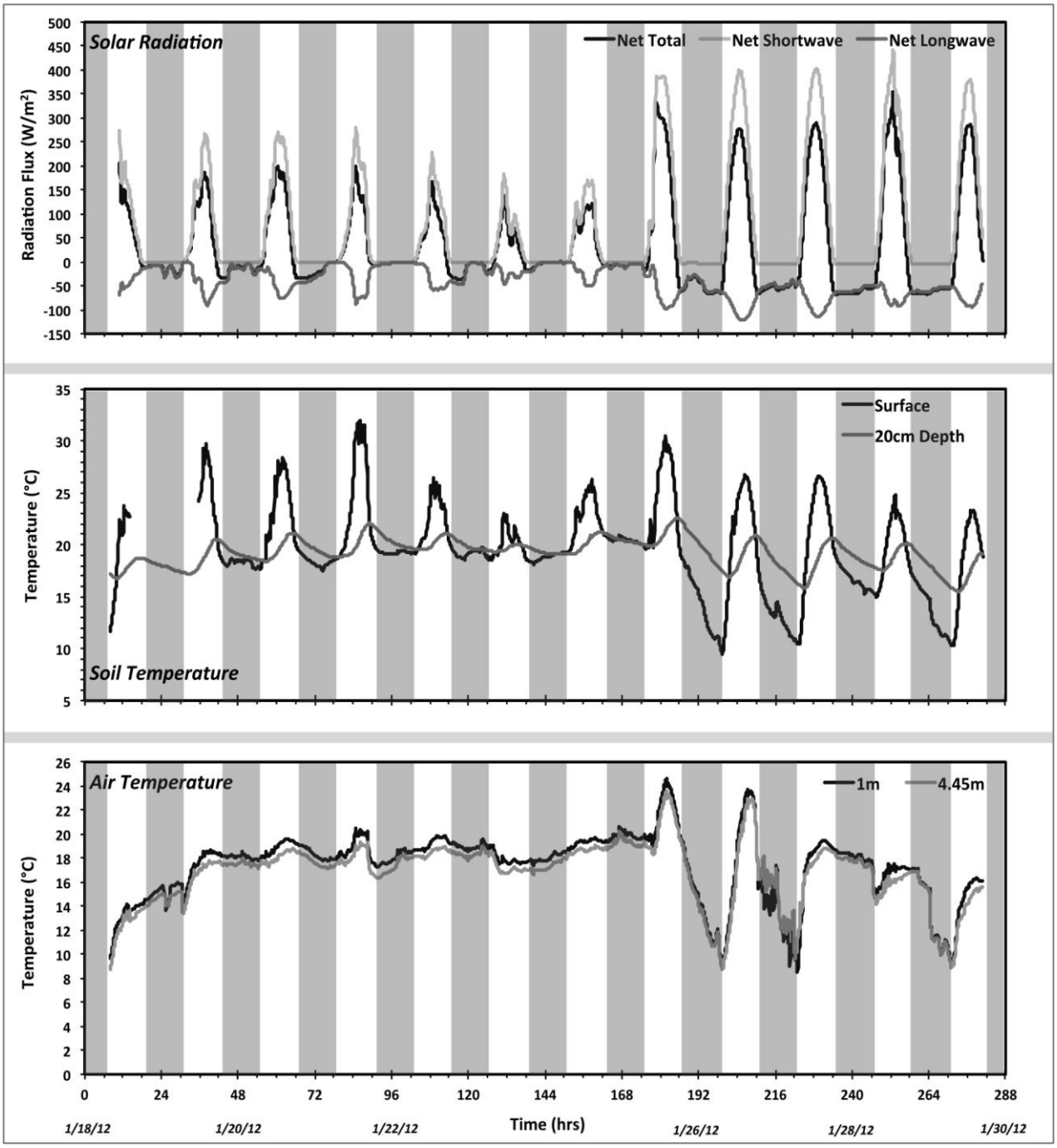

Figure 6.6: Measured meteorological parameters.

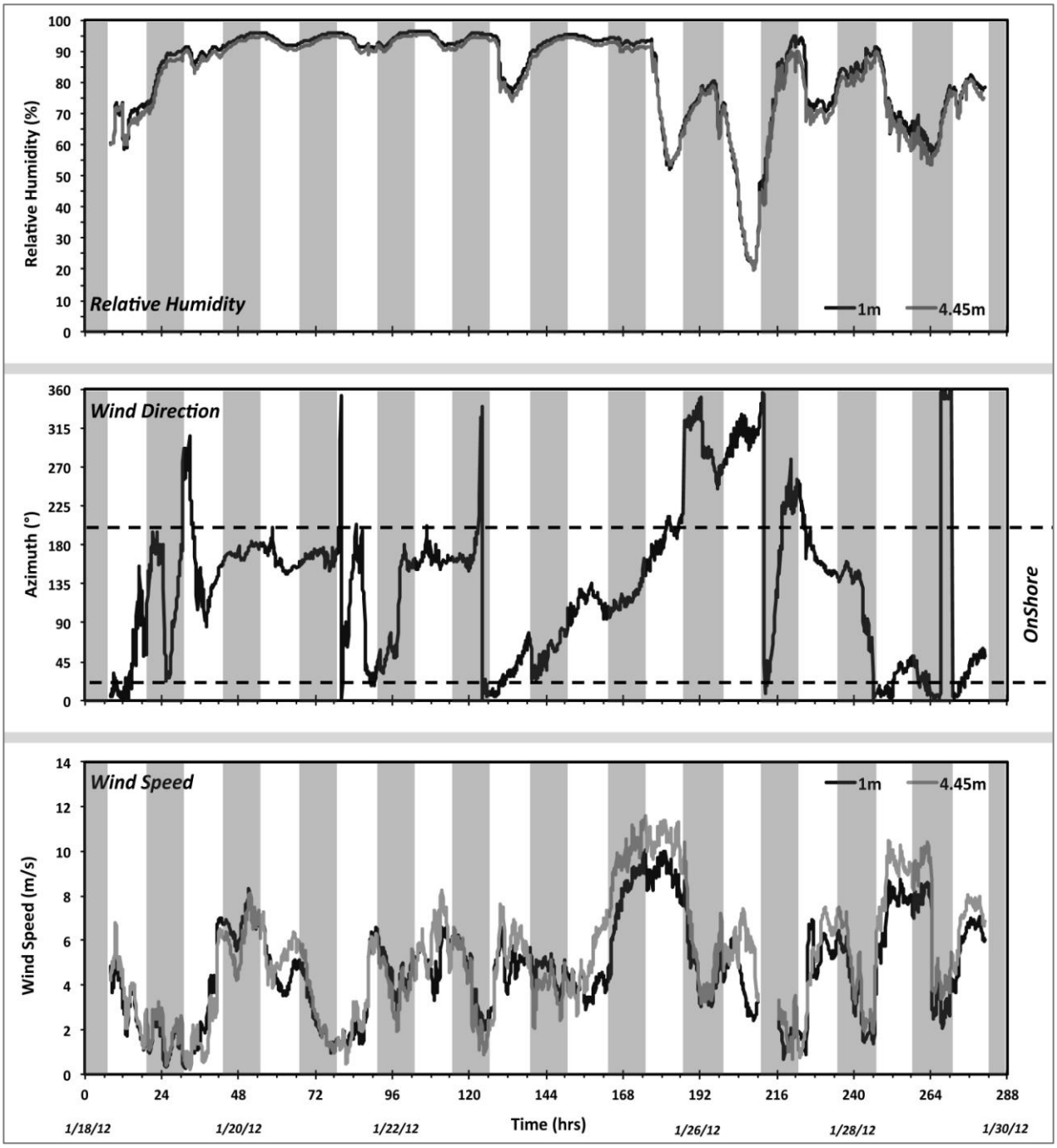

Figure 6.6 cont.: Measured meteorological parameters.

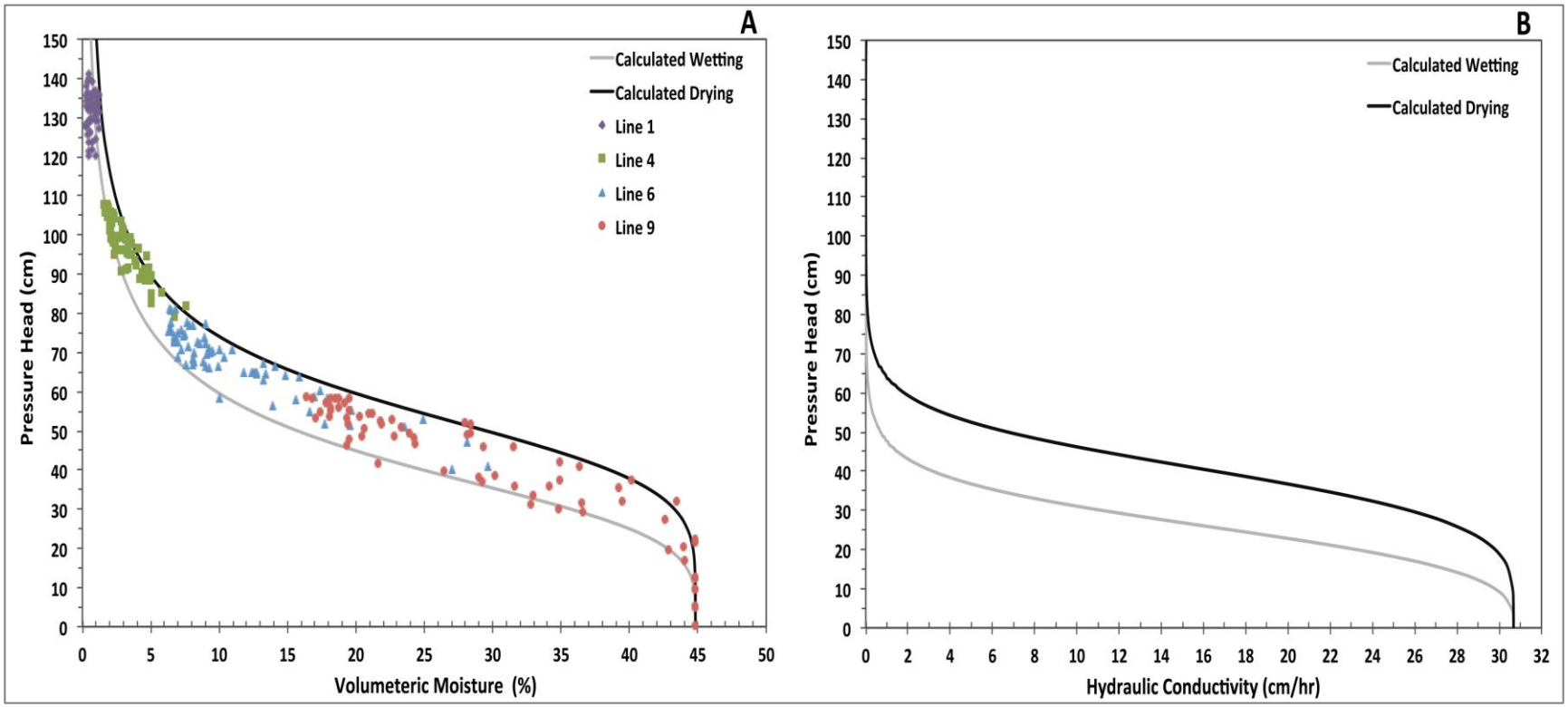

Figure 6.7: Measured volumetric moisture content and the calculated van Genuchten (1980) boundary wetting and drying moisture retention curves (A) as well as the calculated van Genuchten (1980) boundary wetting and drying unsaturated hydraulic conductivity curves (B). The pressure head is equivalent to the height of the surface above the water table.

6.3 Results and Discussion

6.3.1 Potential Evaporation

The potential evaporation rates throughout the study period are shown in Figure 6.5. Rates are plotted at the midpoints of the time period they represent (i.e., a change of 0.1 mm measured from 3:00 am to 7:00 am was calculated as a rate of 0.5 mm/day and plotted at the midpoint of 5:30 am). The data show a distinguished diurnal cycle in the potential evaporation signal with rates increasing rapidly during the early morning hours, reaching a peak in the early afternoon (approximately 3:30 pm) and the subsequently decreasing throughout the late afternoon into the evening hours occasionally exhibiting negative rates overnight.

Over the first seven days of the study period (Jan 18 – 24), the evaporation rate cycle remained fairly consistent with peak rates around 5-6 mm/day. There was however, a slight decrease in peak rates over the last 3 days of this period (Jan 22 – 24). On January 25th, the peak evaporation rate increased markedly and continued at these higher vales (>10 mm/day) throughout the rest of the study period.

These results correlate well the observed meteorological parameters (Figure 6.6). Net radiation values were slightly higher during the first four days compared to the next three days, which subsequently facilitated the slightly lower potential evaporation values on January 22nd, 23rd and 24th. The increased potential evaporation rates from the 25th through the 29th can be attributed to the substantial increase in net radiation values compared to the previous seven days. The radiation values do not, however, account for the notable spikes in evaporation rate on the 25th and 28th. Yet, the higher wind speeds during these two days, consistently exceeding 10 m/s, would have greatly aided in evaporating moisture from the evaporation pan. The

strongest wind speed at any other time during the study period was ~8 m/s during the early morning hours of January 20th.

Although negative evaporation rates did not occur every night, condensation could have occurred if the surface temperature had dropped below the dew point temperature. Figure 6.6 shows that overnight surface temperatures are near (~1° above) or drop below air temperature values and with relatively consistent relative humidity values at 90% to 95%, condensation would have occurred.

6.3.2 Spatial Variations in Surface Moisture

Figure 6.8 plots the minimum, maximum, median, lower quartile, and upper quartile values for all records of volumetric moisture contents in each of the alongshore measurement lines. The whiskers bounding each box indicate the minimum and maximum recorded values, the box is bounded by the lower and upper quartiles of all records, and the line in the box indicates the median of all measurements. The heights of the boxes provide a good indication of the characteristic variability in moisture content observed at each line. It shows that lines L1-L3 and L10-L12 have very low variability (<2%), whereas lines L4-L7 have a slightly higher variability (4-7%) and lines L8 and L9 have the highest variability at 14% and 18%, respectively. This finding occurs because line L8 and L9 are located seaward of L4-L7 and therefore experience larger groundwater fluctuation amplitudes (W4 is collocated with L9, whereas W2 and W3 are collocated with L4 and L6), thus resulting in the larger variations in moisture content. The data also reveals that lines L1-L9 have median values (≤25%), which are substantially smaller than lines L10-L12 (>40%). This finding is a consequence of the location

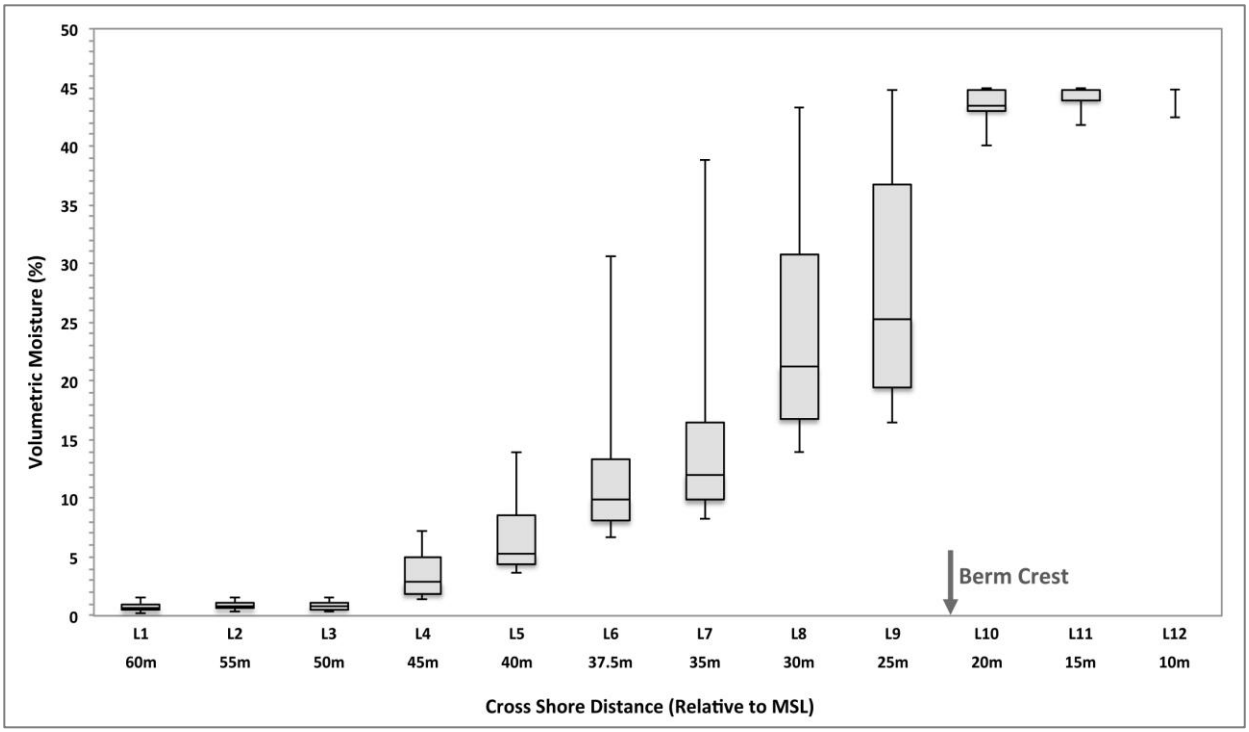

Figure 6.8: Box-Whisker plot of surface moisture content for each measurement lines. The whiskers bounding each box indicate the minimum and maximum recorded values, the box is defined by the lower and upper quartiles of all records, and the line in the box indicates the median of all measurements.

of the berm crest relative to the measurement lines. The berm crest is located at 22 m from the mean sea level shoreline, falling between lines L9 (25 m) and L10 (20 m). Consequently, measurement lines L10-L12 were consistently subjected to swash effects, resulting in the higher surface moisture contents.

Based on the variability shown within the lines, the beach can be characterized spatially in terms of three distinct cross-shore moisture zones (Figure 6.9). The first zone is a low variability saturated/near saturated zone across the fore beach (L10-L12; 0-20 m). Here the beach surface is often submerged during high tide conditions due to swash effects, obviously leading to saturated moisture levels. However, during low tide conditions the beach surface will remain at saturated/near saturated moisture levels due to the presence of the capillary fringe,

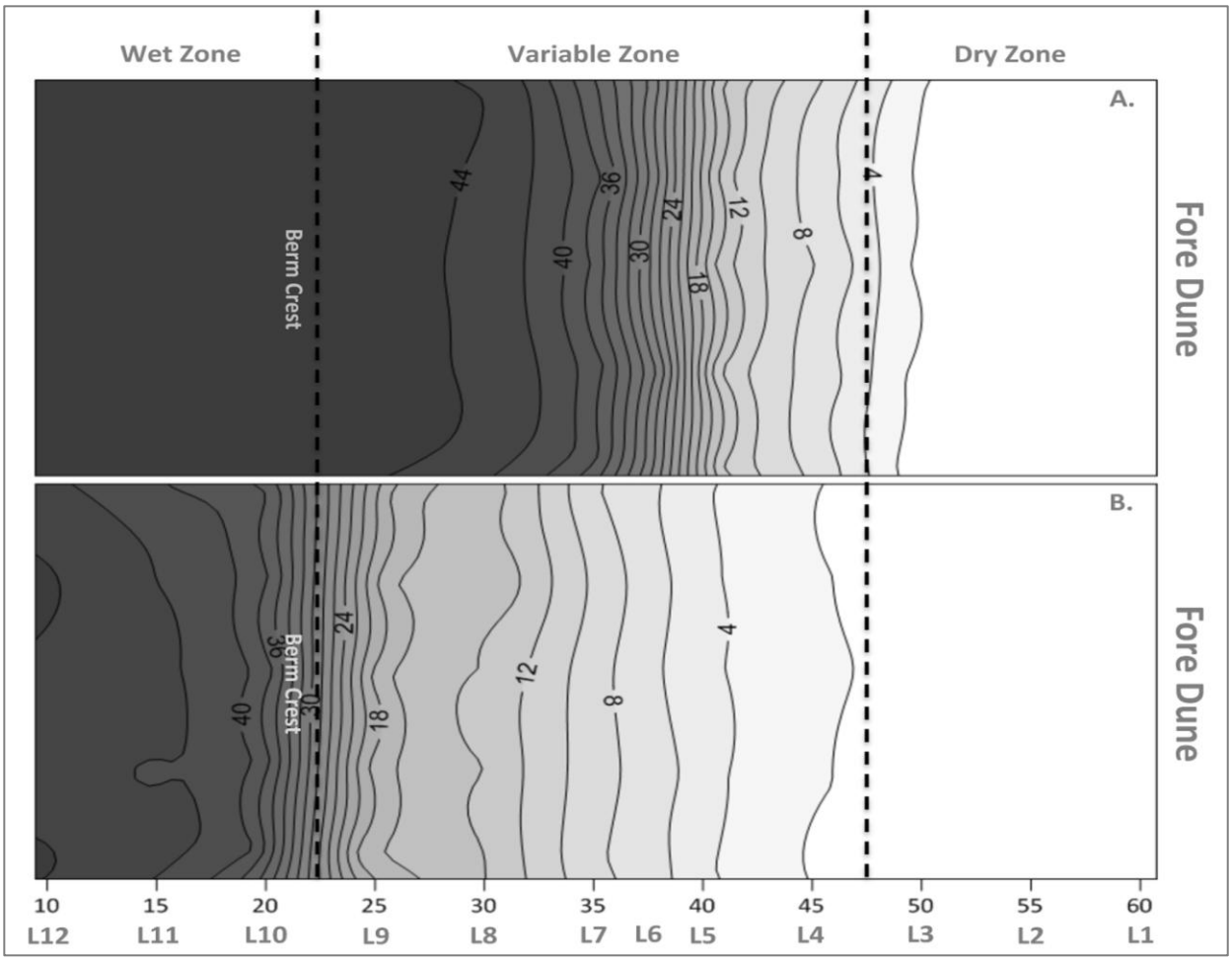

Figure 6.9: Moisture content variability during the maximum (A) and minimum (B) water table elevations. Dashed lines represent the delineation between the wet, variable, and dry moisture zones. Contour lines are spaced at intervals of 2% moisture by volume.

a saturated sediment layer above the water table (Horn, 2002). At this study site the height of the capillary fringe above the water table is approximately 30 cm (Figure 6.7A, see the VG-Drying Curve). As a result, surface moisture contents across the fore beach remain high (>40%) with very little change.

Second, a highly variable moisture zone exists across the middle beach (L4-L9; 25-45 m), where moisture contents ranged from a low of 3% up to saturation at 45%. The groundwater table across the middle beach ranges from a depth of less than 5 cm to 80 cm below the beach

surface (Figure 6.3, see Well 2, Well 3 and Well 4). Accordingly, the beach surface will exhibit pressure head values, which were located in the 'flatter' middle part of the moisture retention profile (Figure 6.7A, see L4, L6, L9). As a result, the moisture gradient is sharp and decreases landward, as any change in the position of the water table leads to large changes in surface moisture content. Accordingly, the middle beach exhibits the largest variations in surface moisture contents.

Lastly, a continuously dry zone exists across the back beach (L1-L3; 50-60 m) adjacent to the foredune, where moisture levels are very low at <2%. At the back beach, the water table is relatively far below the surface and fluctuations of the water table are of small amplitudes (see Figure 6.3, Well 1). As a result, surface moisture contents are very stable with minimal change in moisture content as the beach surface is located in the upper steep ends of the moisture retention profile (See Figure 6.7A, L1).

Aeolian transport is restricted primarily to areas across the beach surface where moisture contents are less than 4% (Azizov, 1977; McKenna Neuman and Langston, 2003; Wiggs *et al.*, 2004a; Davidson-Arnott *et al.*, 2008). Thus, an understanding of the spatial dynamics of the beach surface is vital to determining the available source areas and fetch widths for sediment transport. Results suggest that aeolian transport would occur predominantly across the dry back beach zone as well as in the landward portions of middle beach zone when moisture contents are low, extending spatially ~20 m seaward from the fore dune.

6.3.3 Temporal Variations in Surface Moisture

Figure 6.10 shows a time-series of moisture contents for measurement lines L1 through L12. Several trends in the temporal signal of beach surface moisture content are clearly over both long-term (multi-day) and short-term (daily) temporal variants. Across the long-term there are distinct deviations in the ranges of moisture contents throughout the study period over multi-day intervals. At daily time scales, moisture contents at all measurement lines display well-defined diurnal cycles throughout the entire field experiment.

6.3.3.1 Long-term (Multi-day) Temporal Scale

There are distinct deviations in the ranges of moisture contents throughout the study period over multi-day intervals. Surface moisture contents throughout the first 72 hours experienced the largest fluctuation range. Over the next 78 hours (hour 80-158) there was a noticeable decrease in the fluctuation range, which was followed by a spike, drop, and subsequent spike in moisture contents (hour 158-182) before steadily declining for the next 27 hours (hour 182-209). Finally, over the last 72 hours, of the experiment surface moisture content exhibited the smallest fluctuating range (Figure 6.10).

These variations in surface moisture content are associated with the lunar spring/neap tidal cycle, which heavily regulated the amplitude signal of the beach groundwater. Figure 6.11 illustrates that each of the four groundwater wells has distinct multi-day patterns in their fluctuation signals over the durations of the field experiment, which coincide with the lunar tidal cycle. Subsequently, there are four distinct patterns in the groundwater signal: 1) a large fluctuation range associated with a spring tidal cycle (hours 8-80); 2) a diminishing/falling water

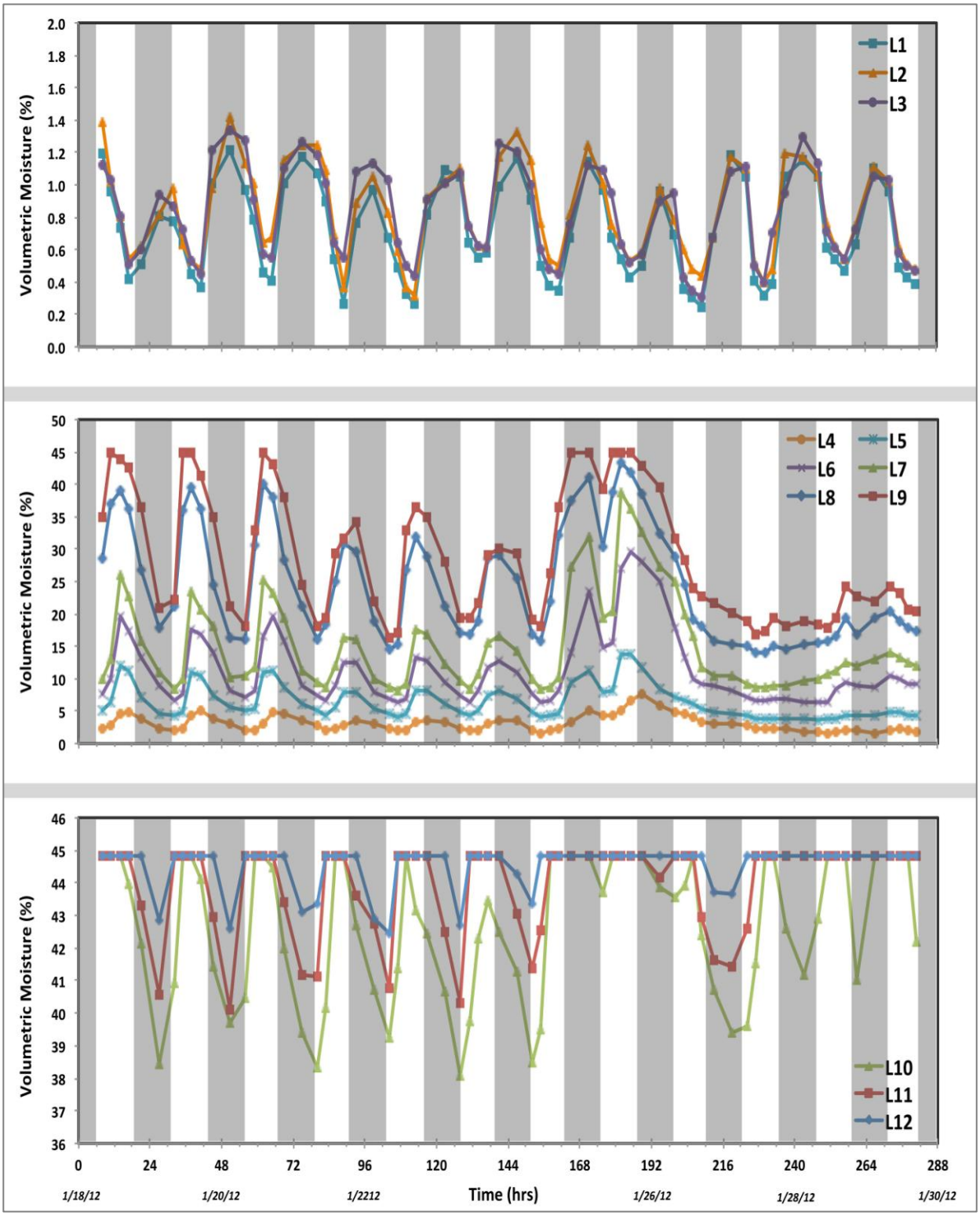

Figure 6.10: Time-series of measured surface moisture contents for each measurement line L1-L12.

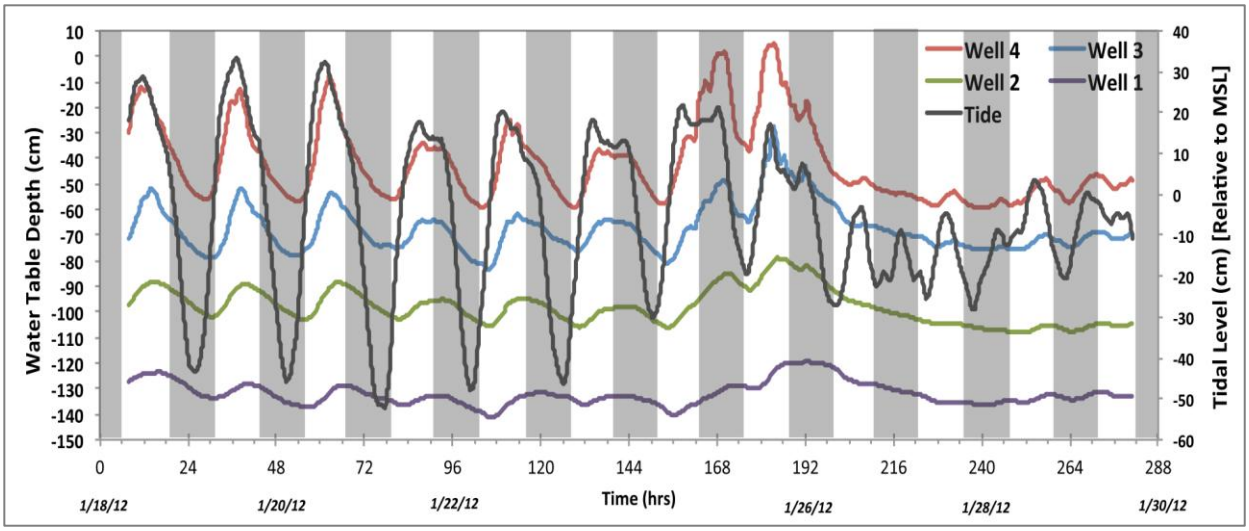

Figure 6.11: Water table depth and fluctuation magnitude for each of the four groundwater wells, and tidal level and fluctuation magnitude.

table range as the system transitions out of the full spring tide (hours 80-158); 3) a noted increase in the water table (hours 158-209), which can be attributed a swash/wave set-up period produced by strong onshore winds (see Figure 6.6, hours 160-190); and finally 4) a very small fluctuation range under a neap tidal cycle (hours 209-281).

Figure 6.12 plots the minimum, maximum, median, lower quartile, and upper quartile values for each of the alongshore moisture content measurement lines categorized by the key influence on groundwater signals (i.e., spring tide, falling tide, wave set-up, and neap tide) for each of the three moisture zones (dry, variable, wet). The data illustrate that the different moisture zones exhibit quite different ranges of moisture content with relation to the larger tidal/groundwater fluctuation stages. The wet zone (L10-L12) and dry zone (L1-L3) remained relatively stable independent of the various groundwater controls, with very little change in moisture content. As expected, differences in surface moisture variability associated with the different groundwater controls are most evident in the variable zone (L4-L9). This zone is

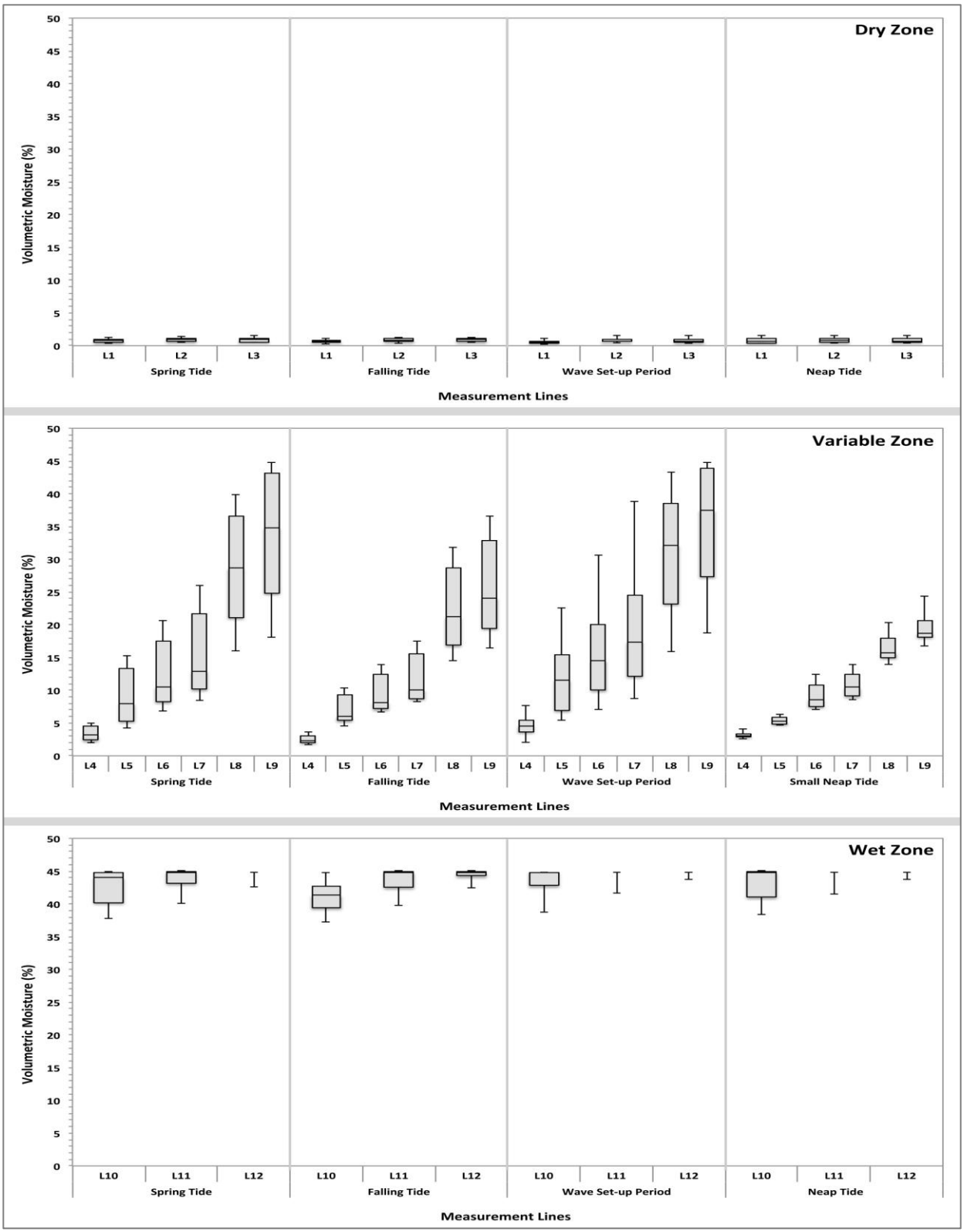

Figure 6.12: Box-Whisker plot of surface moisture content for each measurement lines categorized by the key groundwater signals (i.e., spring tide, falling tide, wave set-up, and neap tide) for each of the three moisture zones (dry, variable, wet).

located in the 'flatter' section of the moisture retention profile, and therefore variations in groundwater fluctuations associated with the different controlling groundwater factors results in marked deviations in the moisture content variability at the surface. At L4 (45 m) moisture content exhibited markedly less variability during the various tide stages compared to the other measurement lines. This finding is not surprising as the line borders the dry zone. Furthermore, there is a noticeable decrease in the moisture contents (max/min, mean, and inter-quartile range) associated with the decrease in groundwater fluctuation from the spring to neap tide, at all measurement lines. This transition is interrupted by the wave set-up period, where moisture contents (max/min, mean, and inter-quartile range) approximate the spring tide conditions.

6.3.3.2 Short-term (Daily) Temporal Scale

Moisture contents at all measurement lines display well-defined diurnal cycles throughout the entire field experiment (Figure 6.10). Maximum and minimum moisture contents at measurement lines L1-L3 consistently occurred during the overnight and late afternoon, respectively. Lines L4-L12, on the other hand, generally exhibited peak moisture contents in the late afternoon to early evening with low moisture content values occurring during the morning. Fundamentally, the variance in the diurnal signal between the measurement lines may imply different controlling processes.

For this study site, groundwater fluctuations have a period of ~25.25 hours, very close to the 24-hour diurnal evaporation-condensation cycle. However, comparison of the groundwater fluctuations with the observed potential evaporation rates reveals that the processes primarily acted in opposition throughout the study period (Figure 6.13). Higher potential evaporation

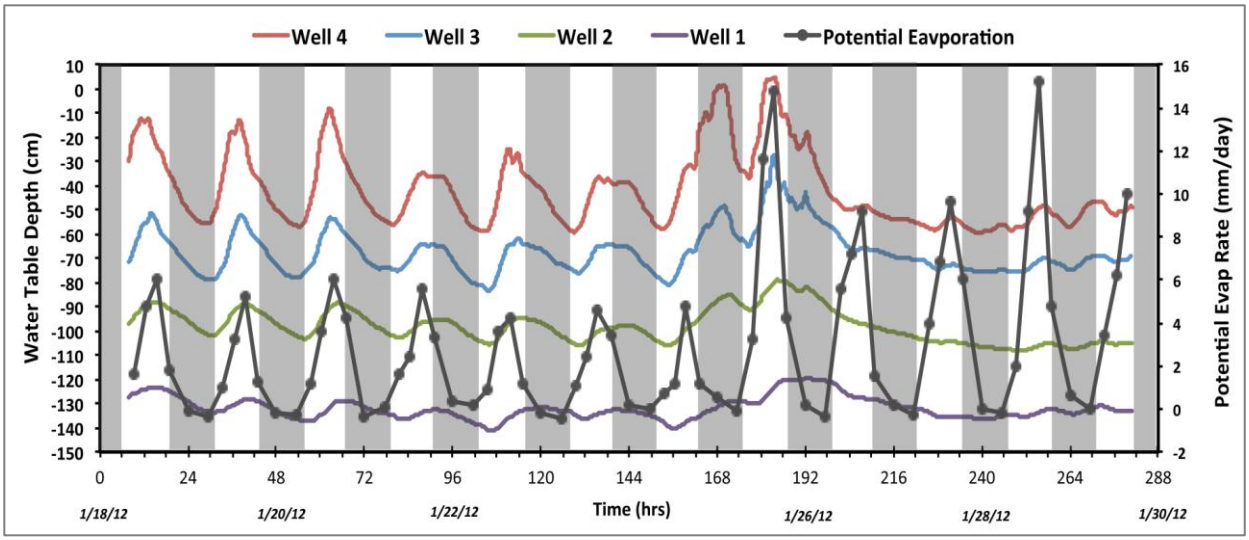

Figure 6.13: Time-series comparison of groundwater fluctuation and potential evaporation rate.

rates tend to approximately coincide with higher groundwater levels whereas low or negative evaporation rates generally correspond with lower groundwater levels. Accordingly, this finding implies that an assessment of the correlation of each process with surface moisture content would demonstrate their relative strength of influence.

Figure 6.14 shows a time-series of moisture contents for measurement lines L1, L4, L6, and L9 superimposed with the water table fluctuations from each of the corresponding groundwater wells W1-W4 to those measurement lines. Results depict a noticeable disparity between surface moisture content and the groundwater cycle at L1/W1. Moisture content fluctuations exhibited a distinct diurnal periodicity, with maximum values consistently occurring during the early morning hours and minimum values during the late afternoon. In comparison, groundwater fluctuations showed no such regularity, with maximum and minimum values shifting each day. Furthermore, it is worth reiterating that the moisture content at this line did not exhibit any variability corresponding with the four groundwater control periods. These

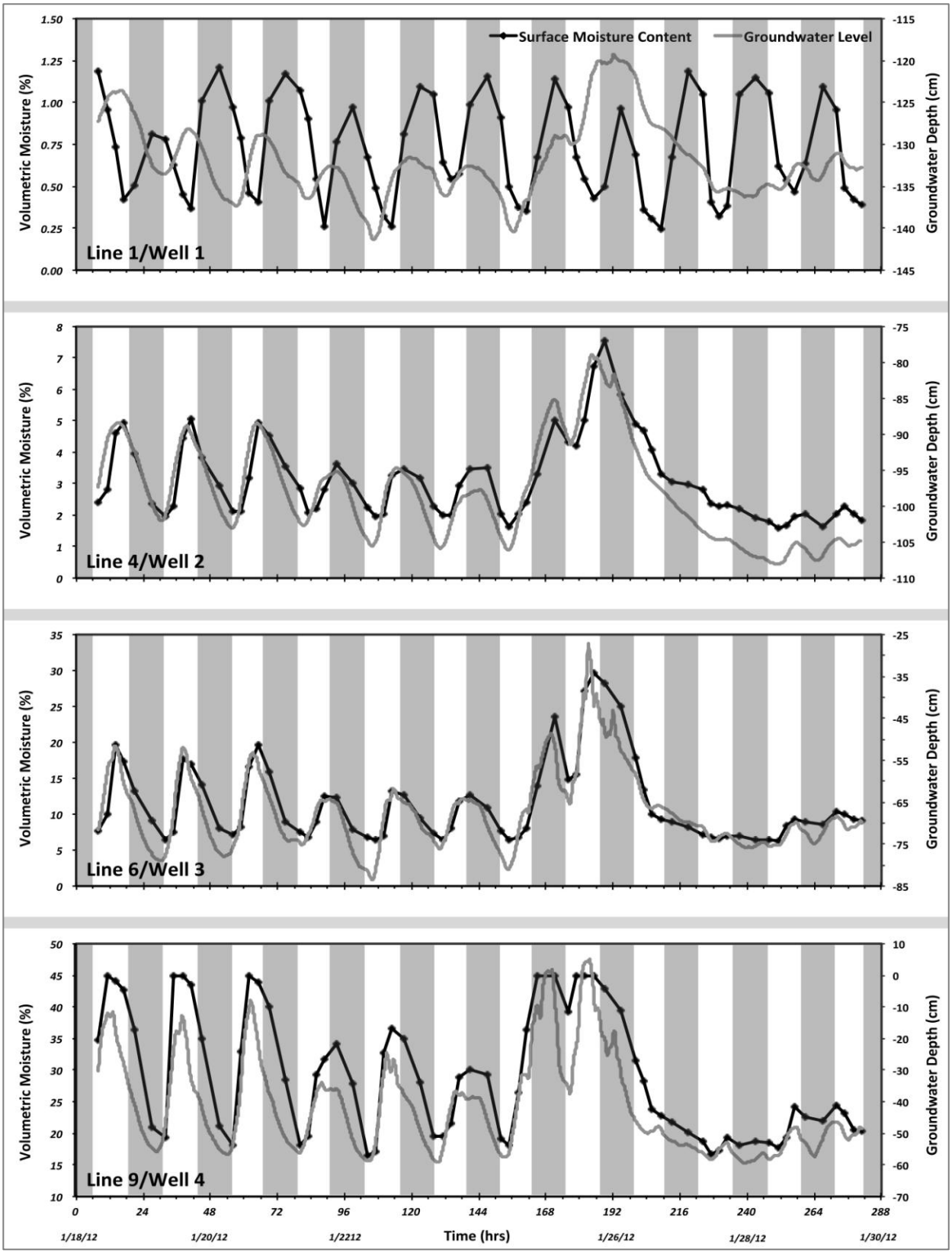

Figure 6.14: Time-series of measured surface moisture content at L1, L4, L6, and L9, and the groundwater elevations at W1, W2, W3, and W4.

findings imply that at L1 the groundwater table has no significant influence on controlling moisture content variations.

Surface moisture content at L1, however, corresponds much more closely with the observed potential evaporation rates measured from the evaporation pan. Figure 6.15 shows a clear decrease in moisture content associated with increases in potential evaporation rates. Note that the evaporation rates in Figure 6.15 are plotted in descending order to emphasize the agreement. Throughout the day the beach surface exhibited a drop in moisture content values as potential evaporation rates increase whereas during the overnight hours the sand surface experienced an increase in moisture as potential evaporation rates fell to near or below zero values. This finding corresponds well with the evaporation-condensation dynamics outlined for a dry soil layer (DSL) in Stage 3 of the conceptual evaporation model, delineated in Chapter 1. The model dictates that under dry soil conditions, the surface layer primarily acts as an evaporation zone during the day, leading to a decrease in moisture content associated with high potential evaporation rates, and as a condensation zone during the overnight hours, facilitating an increase in moisture due to very low and/or negative potential evaporation rates (Yamanaka *et al.*, 1997; Yamanaka *et al.*, 1998; Yamanaka and Yonetani, 1999).

An evaluation of the relationship between surface moisture content, groundwater level, and potential evaporation rate at L4, L6, and L9 reveals that beach surface moisture contents have a much stronger correlation to fluctuations in groundwater level compared to potential evaporation. Surface moisture content at L4, L6, and L9 approximate the groundwater fluctuations (Figure 6.14). However, they are markedly out of phase with the observed potential evaporation rates measured from the evaporation pan (Figure 6.15). Again note that

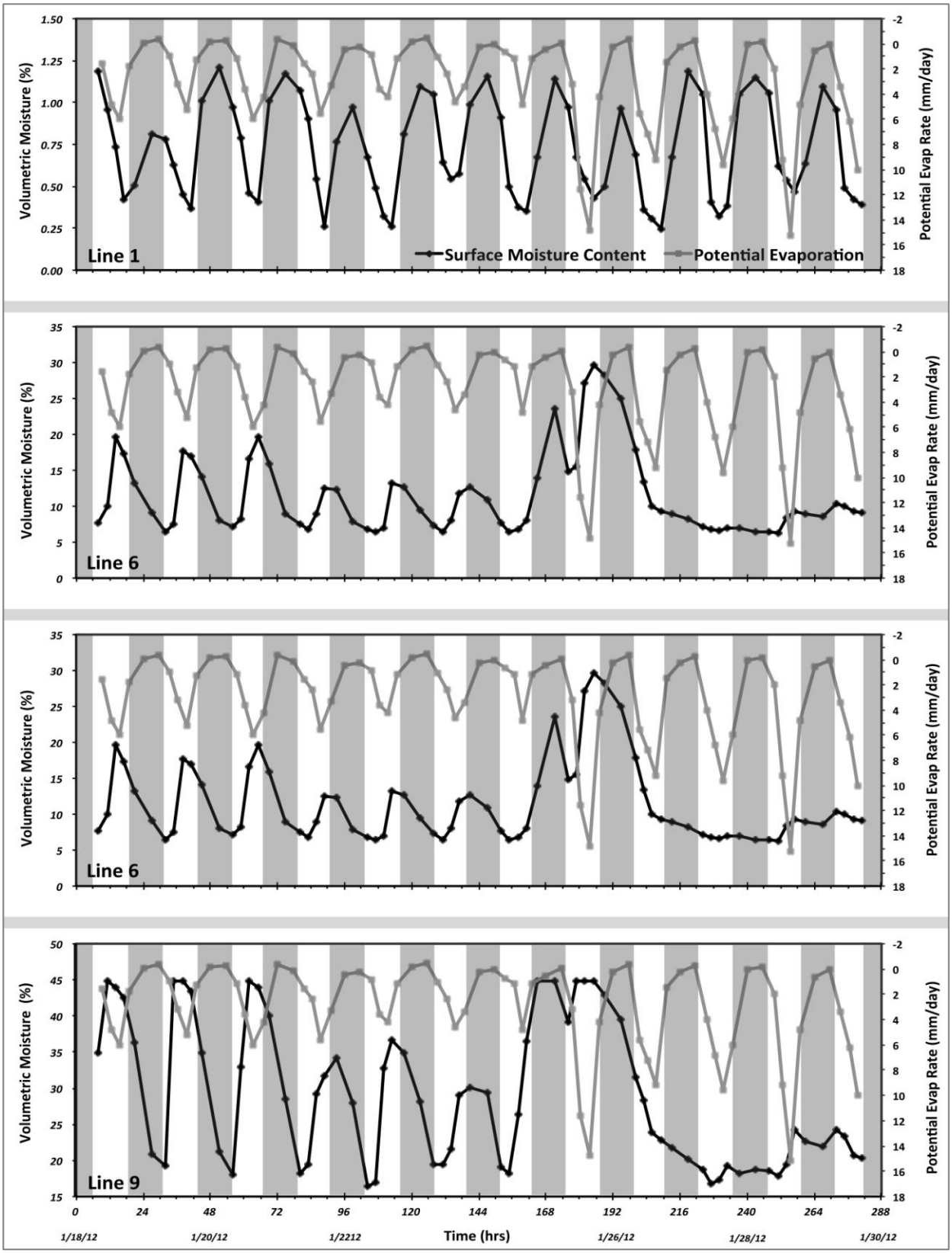

Figure 6.15: Time-series comparison of measured surface moisture content at L1, L4, L6, and L9, and potential evaporation rates.

the evaporation rates in Figure 6.15 are plotted in descending order to emphasize agreement, or in this instance the lack of agreement.

Linear regression of measured moisture content against groundwater level and evaporation rates further demonstrates that surface moisture content at L1 has no significant relationship to groundwater depth, whereas moisture contents lines L4, L6, and L9 strongly correlate to the groundwater depth (Figure 6.16). Additionally, there is no significant relationship between surface moisture content and potential evaporation rates at L4, L6, and L9; however, measurement line L1 demonstrates a clear connection showing moisture content values decreasing with increasing potential evaporation rates (Figure 6.17). Although the R^2 value is relatively low at 0.39, the relationship was determined to be statistically significant at the 99% confidence interval.

6.3.4 Hysteresis and Time Lags in Capillary Transport

The date clearly demonstrates that groundwater dynamics strongly control surface moisture content at L9, L6, and L4. However, the moisture content signals do not exactly sync with water table rise and fall. Although it is difficult to visualize from the time-series charts (Figure 6.14), due to the intermittent nature of the surface measurements, the moisture content signals are skewed relative to the rate of groundwater recharge and depletion, exhibiting moisture contents that remain steady for an extended period of time following the transitions of both high and low water table conditions. These variations can be attributed to the hysteretic nature of capillary flow processes during the wetting and drying sequences.

During the study period, the beach system experienced a number of drying and wetting

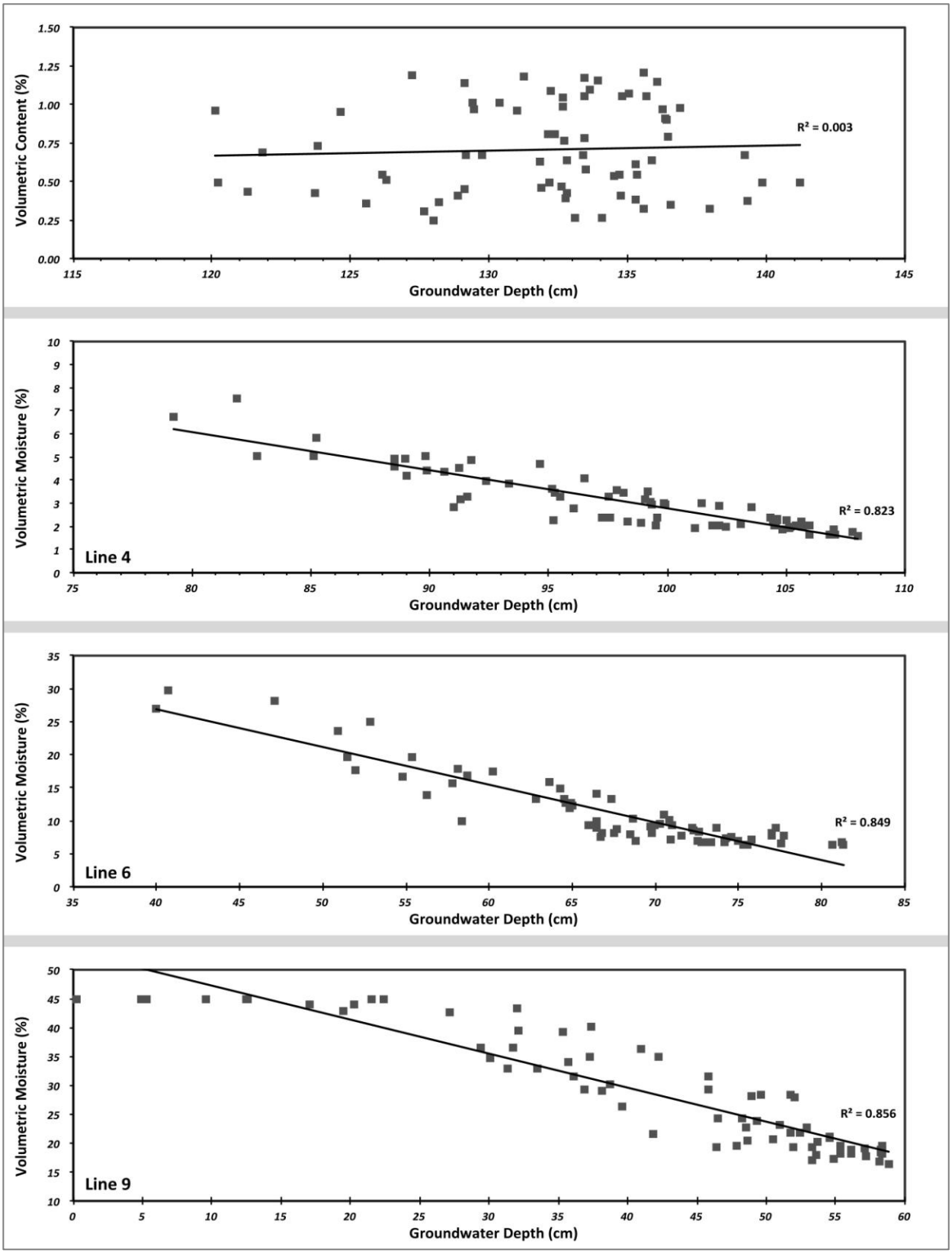

Figure 6.16: Relationship between measured surface moisture content at L1, L4, L6, and L9, and the groundwater depth at W1, W2, W3, and W4.

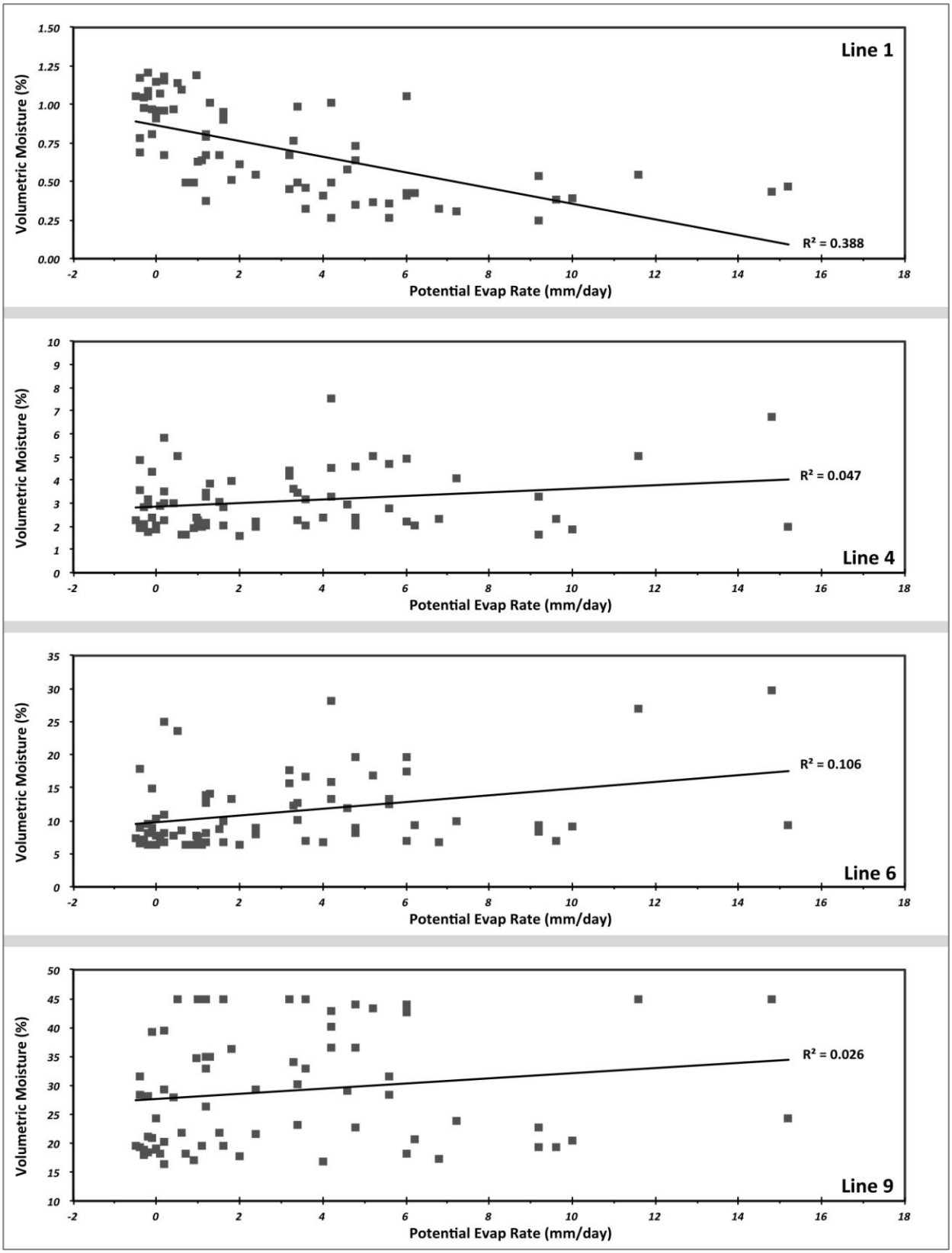

Figure 6.17: Relationship between measured surface moisture content at L1, L4, L6, and L9, and potential evaporation rates.

capillary water flow cycles associated with fluctuations in the water table. Chapter 2 illustrated that a simple and efficient way to assess the hysteretic influence of these drying and wetting cycles on surface moisture is through evaluation of a sequence of water flow scanning loops. When a wetted soil begins to drain, or when a dry soil column is rewetted, the relation between the pressure head and the soil moisture content follows some intermediate moisture retention curve as it moves through the wetting or drying processes. Such intermediate retention curves are called scanning curves and a sequence of these wetting and drying scanning curves form a scanning loop (Childs and Poulovassilis, 1962; Poulovassilis, 1962). The scanning loops illustrate hysteresis effects by depicting higher moisture contents occurring during the drying sequence than during the wetting sequence. Therefore, the strength of the hysteretic signal is relative to the range in moisture content values at any given pressure head. The larger the moisture content range, the stronger the influence of hysteresis on surface moisture dynamics.

Figure 6.18 shows the sequence of scanning loops for L4, L6, and L9 separated into the three tidal stages (spring, falling, and neap). The data demonstrate two basic principles of hysteresis in capillary transport. The first is that hysteresis decreases with increasing pressure head. This is clearly evident in comparing the decrease in the range of moisture content at a given pressure head from L4 to L6 to L9. Secondly, hysteresis is positively correlated with the magnitude of water table fluctuation decrease. It is readily apparent that at each of the measurement lines the hysteretic signal decreases moving from the spring to the neap situation.

These findings indicate that the effect of hysteresis on surface moisture will vary substantially over both space and time. At L9, for example, surface moisture during spring tide

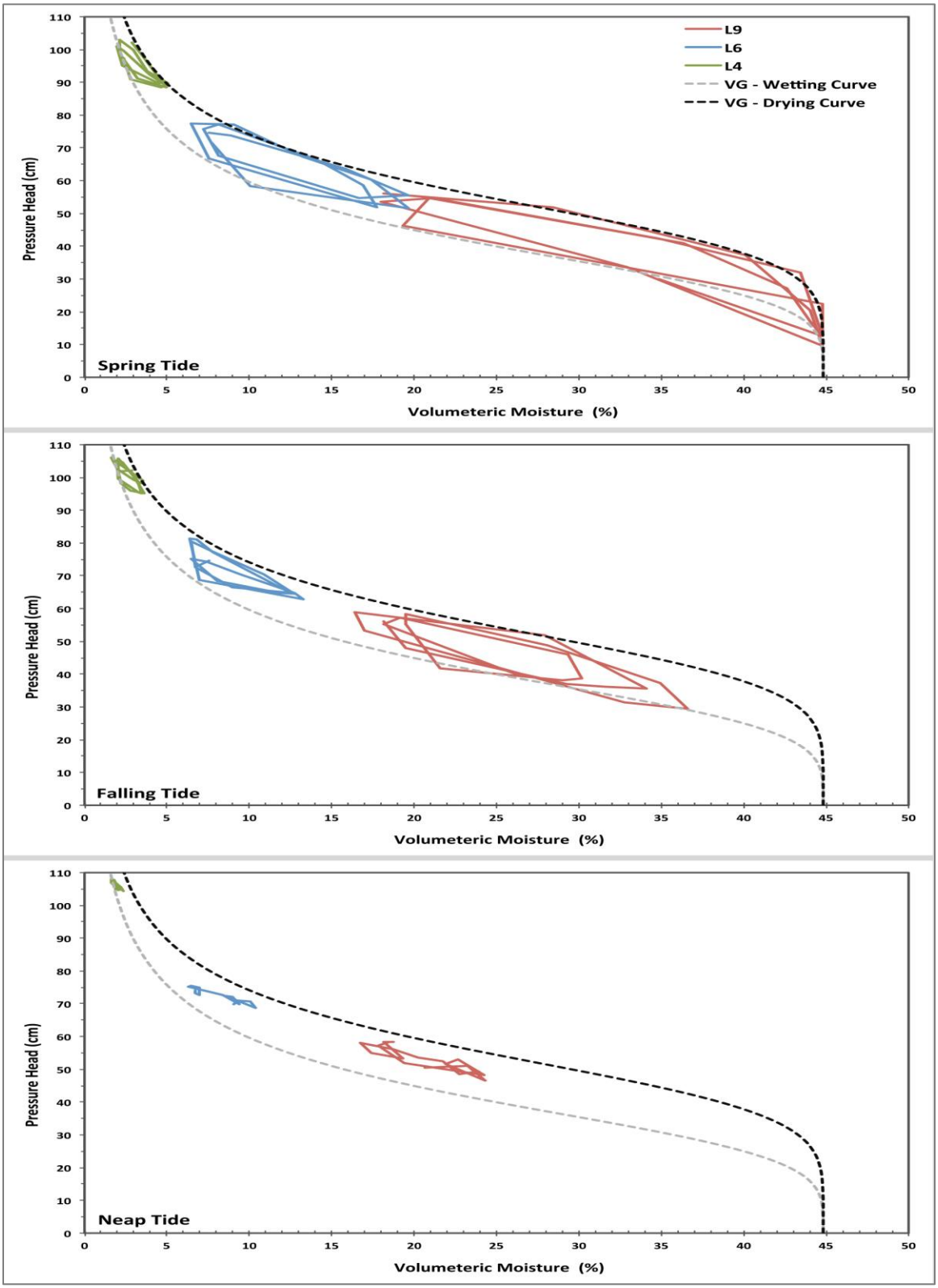

Figure 6.18: Illustration depicting the water flow-scanning loops for measurement lines L4, L6, and L9 separated by the key groundwater signals (i.e., spring tide, falling tide, wave set-up, and neap tide). Also shown are the calculated wetting and drying boundary curves.

can differ by as much as 20% between the wetting and drying stages. With the smaller water fluctuations associated with neap tide, the difference in moisture content is reduced to about 5%. Moving landward, the moisture content difference between the wetting and drying phases decreases considerably, being reduced by 50-60% at L6 and 90-95% at L4 from the spring to neap situations.

In addition to hysteresis effects, there is also a temporal lag in maximum and minimum moisture contents compared to the maximum and minimum water table elevation cycles. Table 6.1 illustrates the average time lags between the measured maximum and minimum moisture contents and the associated high and low water table levels for the spring and falling stages. The neap stage was omitted as clear time lag values could not be identified due to the small groundwater fluctuation range. It should be noted that due to the intermittent nature of the surface moisture measurements the true time of maximum and minimum surface moisture are not known precisely. Nevertheless, three patterns are apparent in regard to the time lag behavior. First, the duration of the lag increased with distance from the shoreline. This is clearly evident in comparing the increase in lag from L9 to L6 to L4. Second, the time lags at low water table are larger than at high water table; and finally, the duration of the lag increased with decreasing tidal range.

These findings are a function of the hydraulic conductivity of the soil profile (Raats, 1992; Durner, 1994; Kosugi, 1999; Assouline 2005, Tokunaga, 2009). Figure 6.7B illustrates that hydraulic conductivity decreases with increasing pressure head as well as shows that lower conductivity values occur during the wetting compared to the drying stage at the same pressure head. Accordingly, slower capillary transport will occur after the transitions from a low water

Table 6.1: Average time lags (hours) between max/min moisture contents and high/low water table levels for each of the spring and falling groundwater signals.

Measurement Lines	Groundwater Signals			
	Spring		Falling	
	High WT	Low WT	High WT	Low WT
L4	1.5	2.75	2	3.25
L6	0.75	2	1.5	2.25
L9	N/A*	1.25	1	1.5

* In every case the surface content reached saturation before high water and remained saturated for some time afterwards.

table (i.e., wetting conditions) and at greater water table depths. These findings, will thus result in larger temporal lags in surface moisture content occurring during low water conditions across the middle and back beach areas, due to their greater groundwater depths at L4, and under smaller tidal fluctuation conditions.

Furthermore, during the spring stage at line L9, moisture contents reached peak levels prior to maximum groundwater level occurring. This observation can be attributed to the development of a saturated capillary fringe extending approximately 12-15 cm above the water table during the wetting sequence (Figure 6.7A). In effect, as the water table rises within the sediment column, the development of the capillary fringe saturates the surface layer prior to the maximum water level occurring.

6.4 Summary and Conclusions

The purpose of this chapter was to measure, document, and analyze the spatial and temporal patterns of beach surface moisture and to identify the relative importance of the various factors controlling surface moisture variability. Results from this chapter indicate that the spatio-temporal distribution of beach surface moisture is primarily a function of the relative

strength between the beach groundwater dynamics (i.e., depth and fluctuation magnitude) and evaporation-condensation processes, over space and time. Spatially, the relative strength of the groundwater system weakens moving landward into the back beach, as both the depth of water table increases and the amplitude of water table fluctuations decreases. The basic patterns that emerges from this is that of a cross-shore gradient with moisture levels typically at or near saturation adjacent to the swash zone and decreasing in the landward direction to become nearly or fully dry approaching the base of the foredune.

Temporally, the data revealed several trends in the beach surface moisture content signal over long-term (multi-day) and short-term (daily) variants. Over the long-term there are distinct deviations in the ranges of moisture contents throughout the study period, which are associated with the lunar tidal cycle: spring, falling, wave set-up, and neap. Results categorizing the influence of the various tidal/groundwater stages (i.e., spring tide, falling tide, wave set-up, and neap tide) for each of the three spatial moisture zones (dry, variable, wet) illustrate that the different moisture zones exhibit quite different ranges of moisture content in relation to the larger tidal/groundwater fluctuation stages.

At short-term (daily) time scales, moisture contents at all measurement lines display well-defined diurnal cycles throughout the entire field experiment. However, there are two distinct temporal trends in the cyclical diurnal signals, which implies different controlling processes. Results indicated that across the fore beach and middle beach areas the influence of the groundwater table is the primary control on beach surface moisture content. However, the relative strength of the groundwater system weakens moving landward into the back beach.

Consequently, the role of evaporation-condensation processes increases, becoming the primarily influence controlling surface moisture content across the back beach.

The basic distribution pattern in beach surface moisture content that develops from these relationships reveals a continuously wet zone across the fore beach with saturated/near-saturated moisture levels, a dry zone across the back beach where surface moisture content were persistently below 2%, and a highly variable zone throughout the middle beach where moisture content varied significantly ranging from saturation to near dry levels at <5%. These findings correspond well with the literature regarding the spatial and temporal dynamics of beach surface moisture (e.g., Atherton *et al.*, 2001; Wiggs *et al.*, 2004b; Yang and Davidson-Arnott, 2005; Zhu, 2007; Bauer *et al.*, 2009; Namikas *et al.*, 2010).

Chapter 7 -- Modeling Surface Moisture Content over Space and Time for a Fine-grained Beach

7.1 Introduction

A key uncertainty in modeling beach-dune interaction and dune development lies in the representation of spatial and temporal variations in beach surface moisture content (Jackson and Nordstrom, 1997; Wiggs *et al*., 2004b; Yang and Davidson-Arnott, 2005; McKenna Neuman and Langston, 2006; Zhu, 2007, Namikas *et al*., 2010). A number of recent studies have investigated variability in beach surface moisture content (e.g., Jackson and Nordstrom, 1998; Sherman *et al.*, 1998; Atherton *et al*., 2001; Yang and Davidson-Arnott, 2005; Zhu, 2007; Bauer *et al*., 2009; Namikas *et al.*, 2010). However, a practical method to model or simulate the considerable spatial and temporal variability in surface moisture revealed by these studies remains to be developed. This is due in part to the fact that surface moisture dynamics of the beach system are controlled by complex coupled interactions between multiple input and output processes, which can exhibit large variability over short temporal scales (minutes to hours) and small spatial scales (meters).

Although the importance of this coupled interaction on beach surface moisture dynamics has been noted and discussed by several researchers (e.g. Jackson and Nordstrom, 1998; Zhu, 2007; Namikas *et al.*, 2010), only Zhu (2007) attempted to examine and model the complex spatial and temporal variability that characterizes the surface moisture content of real beaches. And that study excluded a number of key hydrological factors, such as hysteresis and steady-state capillary flow; which contributed to significant overestimation of predicted surface moisture contents. This inability to model beach surface moisture in a realistic manner is one of

the most significant limitations hindering the development of aeolian sediment transport models. In light of this, the objectives of the present study are to 1) investigate the interrelationships between evaporation, groundwater fluctuations, and soil moisture contents; and 2) assess the viability and accuracy of hysteresis based capillary flow and evaporation models to simulate spatial and temporal variations in surface moisture.

7.2 Hysteretic Surface Moisture Content Model

Surface moisture contents were modeled using hysteretic capillary water flow simulations via the HYDRUS-1D software program developed by Šimůnek *et al.* (1998). HYDRUS calculates hysteretic water flow in the sediment profile by numerically solving the empirically derived hysteretic function developed by Scott *et al.* (1984) and modified by Vogel *et al. (*1996) to incorporate hysteresis in the hydraulic conductivity function.

The procedure requires that both the main drying and wetting boundary moisture retention curves ($\theta^d(h)$ and $\theta^w(h)$) and the unsaturated hydraulic conductivity curves ($K^d(h)$ and $K^w(h)$) are known. Once the soil hydraulic functions have been ascertained the model implements a scaling procedure designed to simplify variability in unsaturated soil hydraulic properties in the direction of flow. The model represents the variability in the hydraulic properties of a given soil profile through a set of scaling transformations, which relate the soil hydraulic characteristics ($\theta(h)$ and $K(h)$) to reference characteristics ($\theta^*(h)$ and $K^*(h)$). The moisture retention and unsaturated hydraulic conductivity curves are thus described as follows:

$$\theta^d\ h\ = \theta_s + \alpha_\theta\ \theta^{d*}\ h\ + \theta_r$$
$$\theta^w\ h\ = \theta_r + \alpha_\theta\ \theta^{w*}\ h\ + \theta_s \qquad [7.1]$$

and

$$K^d\ h\ = \alpha_K K^{d*}(h)$$
$$K^w\ h\ = K_r + \alpha_K K^{w*}(h) \qquad [7.2]$$

in which, α_θ and α_K are mutually independent scaling factors for the water content and the hydraulic conductivity, respectively. The technique is based on the 'similar media concept' introduced by Miller and Miller (1956) for porous media.

Evaporation dynamics are incorporated into the model within HYDRUS via a system-dependent condition at the upper boundary, which is obtained by limiting the absolute value of the flux by the following condition:

$$-K\frac{\partial h}{\partial x} - K\ \leq E \qquad [7.3]$$

where *E* is the evaporation rate at the upper boundary. For a more detailed description of the hysteretic capillary water flow model and the implementation of evaporation into the model see Šimůnek *et al.* (1998).

7.3 Data Analysis

7.3.1 Moisture Retention Curves and Hydraulic Conductivity

Although a number of soil hydraulic models are available within HYDRUS (e.g., Brooks and Corey, 1964; van Genuchten, 1980; Vogel and Císlerová, 1988; Durner, 1994; Kosugi, 1996), the analytical form of the soil hydraulic functions by van Genuchten (1980) was shown to work well with the beach sand from Padre Island National Seashore (Schmutz and Namikas, 2013). The expressions of van Genuchten (1980) are given by:

$$\theta\ h\ = \theta_r + \frac{\theta_s - \theta_r}{1 + \alpha h\ ^{n\ m}}$$

$$K\ h\ = \mathrm{K_s}\Theta^{\lambda}\ \ 1 - \ \ 1 - \Theta^{1/\ m\ \ \ m\ 2} \qquad [7.4]$$

in which, θ_r and θ_s denote the residual and saturated water contents, respectively, α is an empirical parameter denoting the inverse of the air-entry value, n is an empirical parameter representing the pore-size distribution index of the soil profile, m = 1-(1/n), K_s is the saturated hydraulic conductivity, Θ is the effective degree of saturation [= (θ - θ_r)/(θ_r - θ_s)], and λ is a pore connectivity parameter derived by Mualem (1976) to equal 0.5. To designate the main drying and wetting main boundary moisture retention and unsaturated hydraulic conductivity curves, the function parameters θ_r, θ_s, α, n, m, and K_s are denoted with superscripts d and w to indicate either a drying or wetting curve, respectively. Additionally, the following restrictions are expected to hold in most practical soil profile applications: $\theta_r^{\,d} = \theta_r^{w}$, $\alpha^d \le \alpha^w$, $n^d = n^w$, and $K_s^{\,d} = K_s^{\,w}$.

Based on the measured surface moisture contents and groundwater pressure head data collected at the collocated measurement lines and groundwater wells, the main drying, $\theta^d(h)$, and wetting, $\theta^w(h)$ moisture retention and main drying, $K^d(h)$, and wetting, $K^w(h)$ unsaturated hydraulic conductivity curves were constructed. Figure 7.1 shows the calculated curves for the Padre Island beach sand, where θ_r = 0.001 cm^3/cm^3, θ_s = 0.4482 cm^3/cm^3, α^d = 0.0189, α^w = 0.0256, n = 4.781, m = 0.7908 and K_s = 30.68 cm/hr.

7.3.2 Evaporation at the Soil Surface

Chapter 5 illustrated that actual sand surface evaporation dynamics do not consistently approximate the potential evaporation rate. However, direct measurement of actual soil

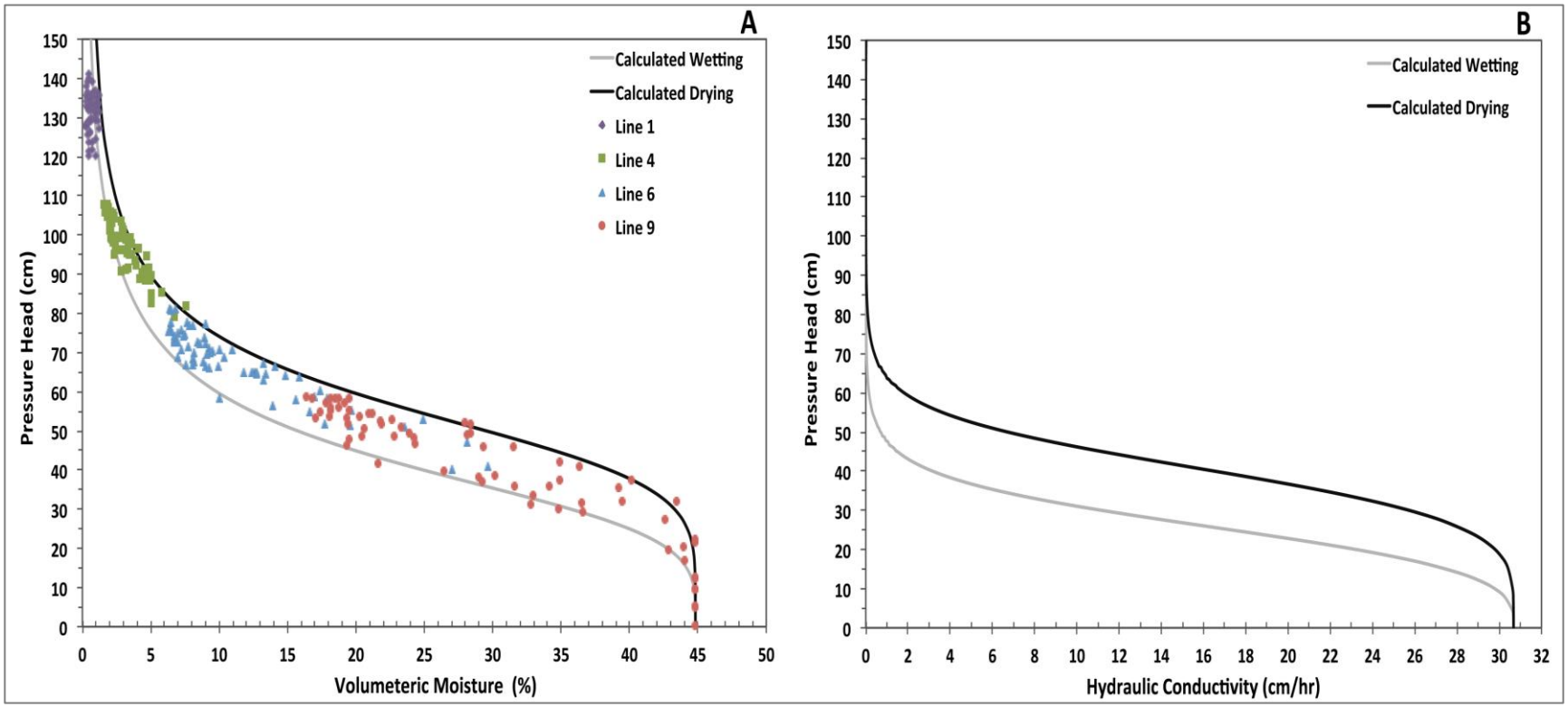

Figure 7.1: Measured volumetric surface moisture contents and the calculated van Genuchten (1980) boundary wetting and drying moisture retention curves (A). The calculated van Genuchten (1980) boundary wetting and drying unsaturated hydraulic conductivity curves (B). The pressure head is equivalent to the height of the surface above the water table.

surface evaporation is extremely difficult, and not possible without substantially impacting other components of the system that are of critical interest to this study (i.e., a lysimeter would require interference with capillary inputs). Nevertheless, previous work has established that actual soil evaporation is a function of potential evaporation and soil surface moisture content (Mahfouf and Noilhan, 1991; van de Griend and Owe, 1994; Gavin and Agnew, 2000; Zhu and Mohanty, 2002; Aluwihare and Watanabe 2003; Aydin *et al.*, 2005). According to Mahfouf and Noilhan (1991) evaporation from a bare soil (E_b) can be calculated as a function of potential evaporation with adjustments for surface moisture content:

$$E_b = \ 1 - \sigma_v \ \beta E_p \qquad [7.5]$$

where σ_v is the fraction of vegetation cover (equal to 0 for a bare soil such as beach sand), E_p is the potential evaporation, and β the moisture availability, given as:

$$\beta = \begin{matrix} \frac{\theta - \theta_r}{\theta_{fc} - \theta_r}, \theta < \theta_{fc} \\ 1 \qquad , \theta \geq \ \theta_{fc} \end{matrix} \qquad [7.6]$$

where θ_r is the residual water content, θ_s is the saturation water content, θ_{fc} is the field capacity water content, and θ is the measured water content. This approach will be adapted here in to determine the evaporation rate of the soil surface.

7.3.3 Interpolation of Groundwater Elevation

Since groundwater elevation was not measured at lines L12, L11, L10, L8, L7, L5, L3, and L2, water table depth at these locations was interpolated from the measured tidal and available groundwater well data. The interpolation processes involved plotting the tidal and groundwater elevations at hourly intervals and fitting a polynomial curves to the data. Water table depths at

each of the other lines were determined from the best-fit equations. Figure 7.2 provides an example of the interpolation process for hours 8, 99, and 251.

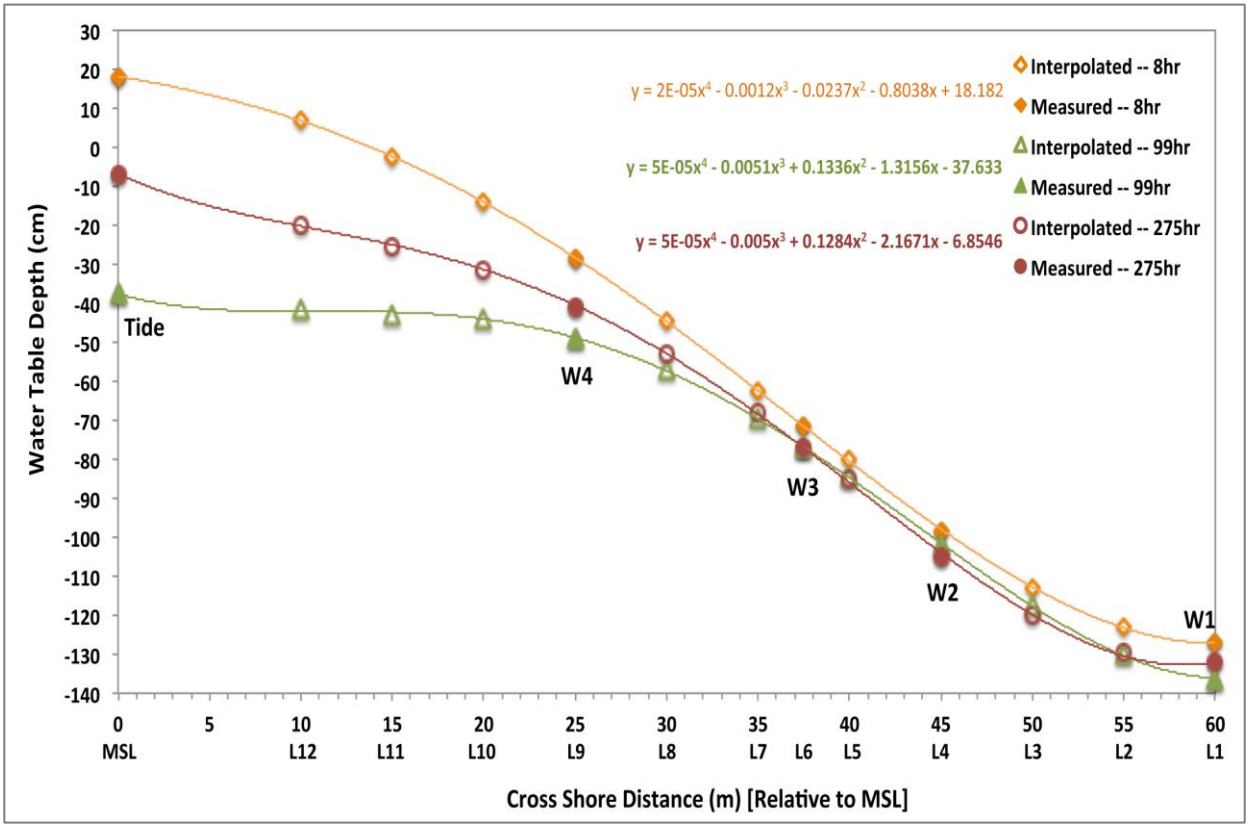

Figure 7.2: Graphic illustrating the interpolation processes for calculating water table depth for the lines L12, L11, L10, L8, L7, L5, L3, and L2.

7.4 Results

7.4.1 Comparison of Measured and Simulated Surface Moisture Contents

To assess the ability of the hysteretic model to reproduce measured surface moisture, a time series of the simulated surface moisture content (with and without the evaporation signal) was plotted against surface moisture contents measured at Lines 1-12 (Figure 7.3). It is clear that the inclusion of evaporation only influences the results for lines L1-L4. The greatest level of influence occurred at lines L1-L3. The simulations not employing evaporation depart radically from the measured surface moisture contents. The inclusion of evaporation provides significant

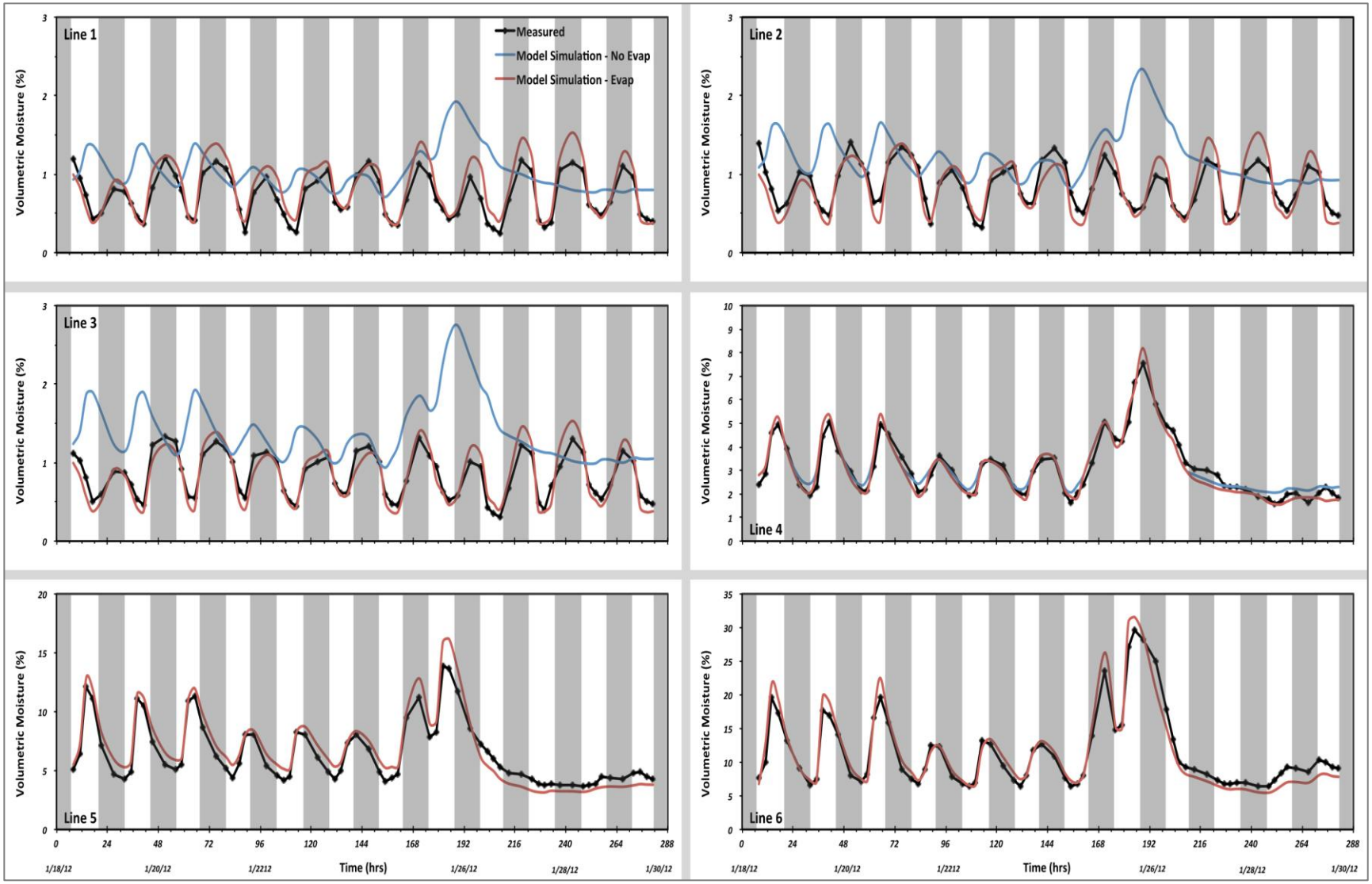

Figure 7.3: Time series of field measured surface moisture contents vs. simulated surface moisture contents both with and without evaporation for line 1 (landward) to line 12 (seaward). For lines 5-12 the two simulations are virtually identical and cannot be distinguished.

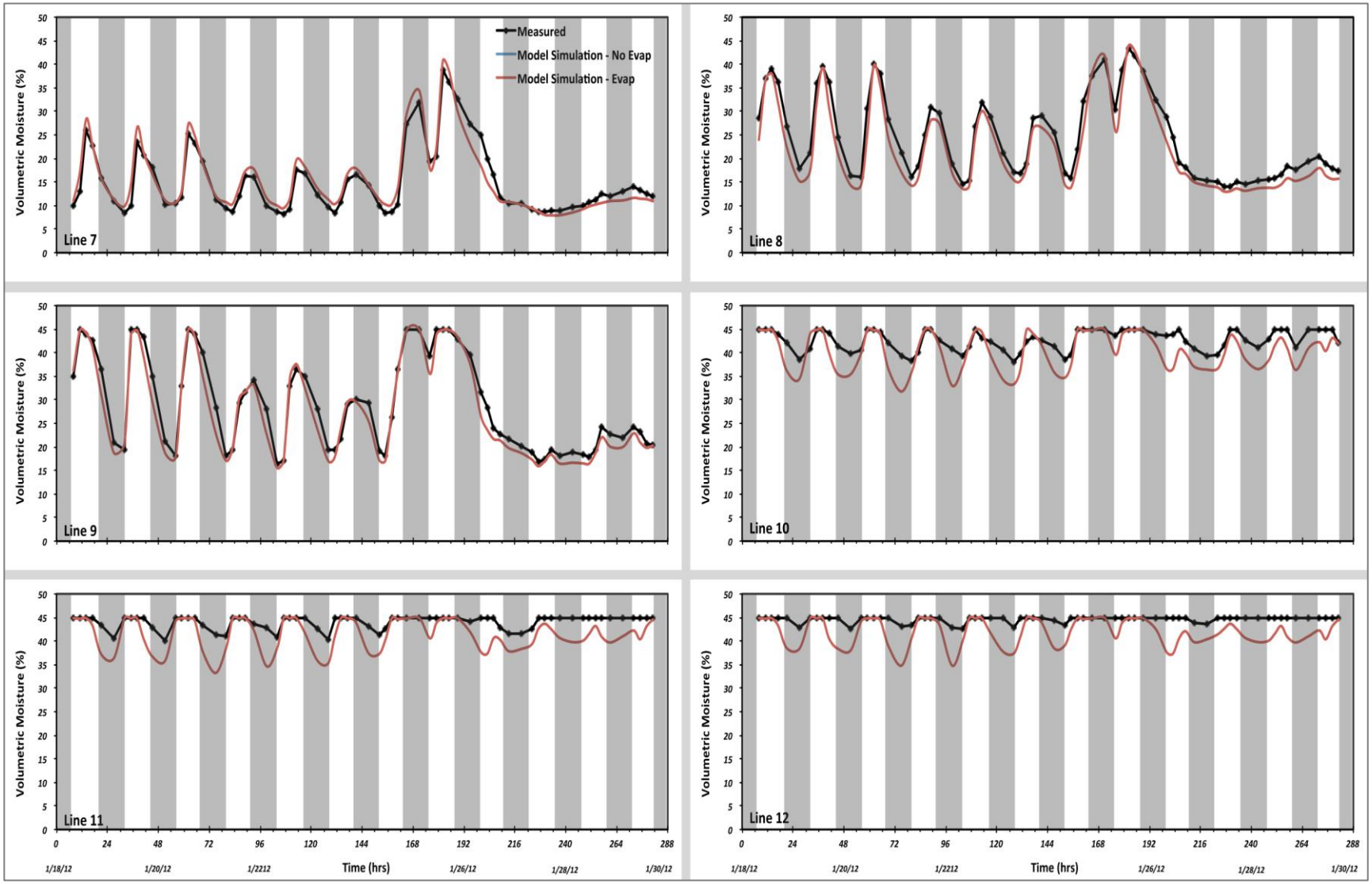

Figure 7.3: Continued.

improvement in predicted surface moisture content, both in the fluctuation range and temporally over the diurnal evaporation and condensation cycle, as simulations are able to accurately predict measured values. This finding confirms the results of Chapter 6, which suggested that surface moisture content at these lines is controlled by evaporation-condensation processes with little influence from the groundwater table. At measurement line L4, the water table is the dominant controlling processes; however, during low water table conditions the simulation employing evaporation shows a better agreement, indicating evaporation processes still exert a minor influence. Furthermore, it is evident that the groundwater table is the dominant control on surface moisture content at the other lines (Figure 7.3). Simulations utilizing evaporation do not substantially modify the predicted surface moisture contents (the simulations with and without evaporation overlap and cannot be distinguished on Figure 7.3).

Spatial variation in the relative influence of evaporation versus groundwater on surface moisture can be further clarified by examining the influence of evaporation on the moisture retention curves (Figure 7.4). It is clear that evaporation process exerts an influence only when pressure head values are large. The critical pressure head values (above which evaporation begins to impose influences) are about 100 cm during a drying sequence and 90 cm during a wetting sequence, which equates to surface moisture content of approximately 3% moisture by volume in both cases. When the pressure head is below these thresholds, the effect evaporation is overwhelmed by that of groundwater. This finding agrees with the results of Zhu (2007), which reported that evaporation processes become significant at a pressure head of approximately 90 cm, equating 4% surface moisture by volume.

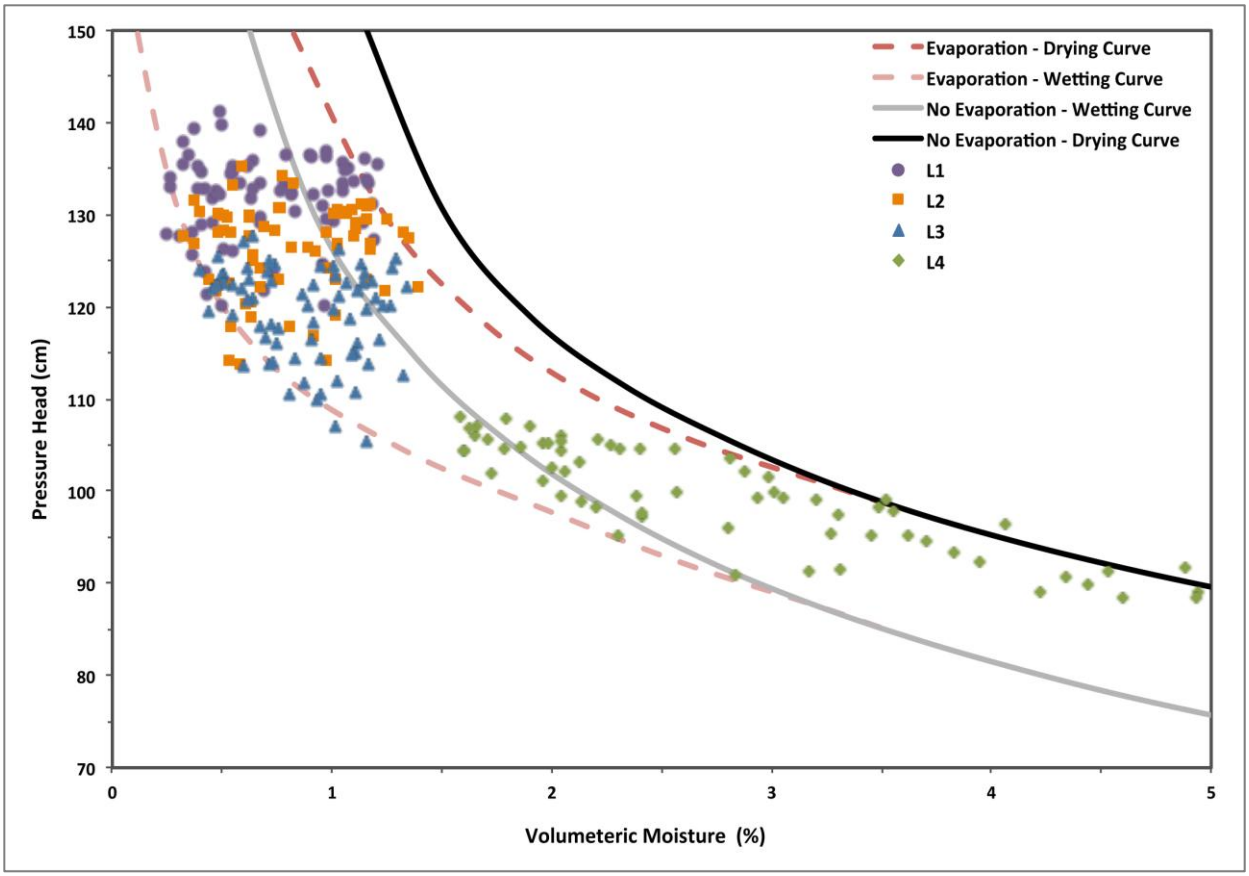

Figure 7.4: Simulated moisture retention curves with and without evaporation.

In the occasion of line L4, simulated surface moisture contents were controlled by groundwater fluctuation, but modified somewhat by evaporation processes. The pressure head values here ranged between 79 cm and 108 cm. Thus shifting back and forth across the threshold so that evaporation played a periodic role. At lines L1-L3, all pressure head values exceeded 105cm and evaporation processes therefore controlled surface moisture contents. Pressure head values at lines L5-L12 ranged between 0 cm and 85 cm, thus evaporation processes had no influence on surface moisture content.

A quantitative assessment of the simulation fit is given in Table 7.1, which provides the absolute standard error in simulated volumetric moisture content for each line as well as an

Table 7.1: Absolute standard error in simulated volumetric moisture content for each line as well as indexed standard error normalized with the median moisture content of each line.

	Measurement Lines											
	L12	L11	L10	L9	L8	L7	L6	L5	L4	L3	L2	L1
Standard Error	3.52	3.44	3.35	2.58	2.67	1.93	1.54	0.95	0.51	0.19	0.15	0.16
Indexed Standard Error	0.08	0.08	0.08	0.10	0.13	0.16	0.15	0.18	0.19	0.21	0.19	0.20

indexed standard error normalized to the median moisture content at that line. The absolute error depicts a substantial decrease in the magnitude of error moving landward from the fore beach (3.52% moisture at L12 to 0.16% moisture at L1). This suggests a significant increase in the accuracy of the model to predict surface moisture content moving landward from the wet fore beach to the drier back beach. However, the indexed error values reveal that the magnitude of error is actually reversed. Across the wet fore beach (L12-L10) the magnitude of error is around 8% (of the median moisture value) and increases to around 20% across the dry back beach (L1-L3). This signifies that the model is more accurate at simulating beach surface moisture under wetter surface conditions. Either approach at assessing the fit of the model is appropriate as they are different ways of considering the same phenomenon. The significance depends on the application/interpretation of interest; the absolute amount of error or the performance of the model under various moisture conditions.

In general, the simulations shown in Figure 7.3 replicate the temporal and spatial variability in surface moisture quite well. However there are some systematic discrepancies worth consideration. At the seaward lines across the fore beach (L12-L10), simulated moisture content matches the measured volume well during high water table conditions, but significantly underpredicts surface moisture contents during lower water table conditions. This outcome is

likely a result from the lack of consideration of swash effects in the modeling approach. Throughout the study period the fore beach was regularly inundated with swash effects even during lower tide conditions. Since the model does not incorporate this additional moisture input, simulated moisture contents were lower than measured surface moisture values.

Across the seaward section of the middle beach (L8 and L9), above the head of the swash, the simulated moisture closely approximates the diurnal fluctuation range associated with each of the four tidal regimes. However, at these lines the model consistently predicts slightly smaller values during the drying sequences. In effect the model is predicting that after a high water level in which the soil layer approaches saturation the soil pores will immediately drain with the transition to a falling water table sequence. A similar situation was encountered in Chapter 2, which reported a similar shortcoming under controlled laboratory conditions. These findings suggest that the HYDRUS hysteresis model is not able to fully capture the Haines Jump hysteresis effects (Haines, 1930) that occur in this zone during the soil drying process.

7.5 Conclusions

Overall, the model simulations successfully captured the dynamics of field-measured surface moisture variations both in the magnitude range and temporally over the diurnal fluctuation cycle. Results illustrate that the inclusion of evaporation processes into the model greatly increases the accuracy of simulated surface moisture contents across the back beach where the water table is relatively deep (>100 cm). Across the middle beach and fore beach where water table depths are less than 100 cm below the surface, evaporation processes did not have any significant influence on the surface moisture content signal. The model

simulations with and without evaporation overlapped and could not be distinguished. This result indicates that water table oscillations controlled the high degree of variability in moisture content across these portions of the beach surface. Additionally, swash effects had a significant influence on surface moisture content across the fore beach. Throughout the study period the fore beach was regularly inundated with swash effects; however, the model does not incorporate this additional moisture input. Accordingly, simulated moisture content significantly underpredicted measured surface moisture contents from lines L12-L10, particularly during low water conditions. These findings correspond well with those from Chapter 6.

Overall, the results of this study indicate that hysteretic modeling of groundwater and evaporation processes provides a reasonably accurate and thorough representation of the evolution of beach surface moisture and thus can be used as a sufficient approach to model the spatial and temporal variability of beach surface moisture content.

Chapter 8 -- Conclusion

8.1 Summary of Study

The goal of this dissertation was to improve understanding of the spatial and temporal dynamics of beach surface moisture content. The study consisted of a suite of laboratory and field experiments that documented and analyzed the role of the key input parameters (groundwater table fluctuations, capillary actions (i.e., moisture retention, hysteresis, and hydraulic conductivity), evaporation-condensation, and sediment size) on beach surface moisture content. These parameters were investigated because they are the critical components of the beach hydrological system, and uncertainty regarding them significantly limits our understanding of beach surface moisture dynamics.

Chapters 2-4 reported on a set of laboratory experiments designed to improve our understanding of capillary processes to governing beach surface moisture. Chapter 2 dealt with identification and modeling of hysteresis and transient time lags in capillary water flow. Previous studies in beach surface moisture dynamics tended to disregard the hysteretic and transient nature of capillary water flow processes; however, the results presented here demonstrated that the spatial and temporal dynamics of beach moisture are heavily influenced by both of these processes. Hysteresis had a more pronounced effect on surface moisture dynamics at shallower water table depths, which is representative of conditions on the fore beach and seaward portions of the middle beach. It was found that surface moisture contents at these water table depths remained steady for a substantial period of time following the transition between a rising and falling water table. However, with greater water table depths (i.e., at the landward portion of the middle beach and back beach areas), moisture dynamics

were profoundly influenced by the transient nature of capillary water flow. The surface moisture contents experienced substantial time lags between water table oscillations and moisture content response, and the time lag was found to increase with increasing elevation of the surface relative to the water table.

Chapter 3 sought to address methodological concerns and validate the utilization of moisture contents at elevations below the true surface as proxy surfaces to represent surface level moisture dynamics closer to the water table. Theoretical analysis suggested that once the moisture retention profile has been established for a given soil, the soil column can be truncated at any pressure head (i.e., height above the water table), and the moisture content values at that elevation would be as indicated by the profile. Results from the laboratory study revealed strong agreement between the proxy and true surface elevations, in terms of both the moisture content range and the symmetry of the moisture content traces. Thus, the findings presented in the chapter demonstrated that the use of proxy surfaces to represent true surface moisture content dynamics at comparable elevations above the water table is reasonable and appropriate.

Chapter 4 focused on documenting the influence of grain size on regulating the capillary processes of a soil column, and how that influence subsequently affected beach surface moisture. Results showed that under the same hydrological forcing conditions, the two grain sizes studied produced marked differences in capillary processes within the sediment column, and these variations led to distinct differences in the spatial and temporal dynamics of surface moisture content. Spatially, an increase in grain size results in a reduction of the extent of the wet and variable moisture zones, as they would shift toward the swash zone. This produces a

corresponding increase in the spatial extent of the dry zone, which would ultimately result in a marked expansion of the region in which aeolian processes are most effective. Temporally, a specific capillary process, depending upon the depth of the water table, significantly dictated the surface moisture content signals. At the shallow depths, hysteresis exerted a more pronounced control on the moisture content signal for both grain sizes. However, the magnitude of hysteresis response varied between the grain sizes depending upon the cyclical location of the water table. For the medium sand the hysteresis effect was more pronounced after low water table conditions compared to after high water table conditions for the fine sand. At the higher water table depths hydraulic conductivity was the dominant factor controlling the moisture content signals for both grain sizes. However, the medium sand demonstrated considerable increases in time lag values compared to the fine-grain sand, which increased with increasing depth.

Chapter 5 examined the role of evaporation and condensation on beach surface moisture content. It primarily focused on improving understanding of evaporation processes with depth over time. Results indicated that the evaporation dynamics of a saturated beach surface differ dramatically from those of a free water surface. Initially, evaporation of moisture from the sand surface occurs almost entirely in the upper most layer (top 1 cm) at a rate that approximates the potential evaporation rate from a free water surface (22.4 mm/day at the upper surface layer vs. 23.4 mm/day for the potential evaporation rate). However, the upper layer is only able to maintain this level of evaporation for a few hours. The initial rapid evaporation rate causes a significant drop in the moisture content of the upper layer, which results in a significant decrease in evaporation rates. After this time period the rate of

evaporation at the upper layer stabilizes and remains approximately constant at a rate of 0.02 mm/day. Below the upper surface layer (depth of 1 to 6 cm) virtually no evaporation of moisture occurs during the initial few hours, as the evaporation rate is 0.3 mm/day. After these initial few hours, however, the lower layer becomes the dominant source of moisture for evaporation, as the evaporation rate jumps to 3.5 mm/day. Capillary forces draw moisture from this layer to replenish the water evaporating in the upper layer, which maintains the constant moisture level there. Evaporation rates fall much more slowly from this point on.

Evaluation of the dry sand trays found that the evaporation rates between the upper and lower sand surface layers to be nearly identical, fluctuating over a range of about 0.32 mm/day. Both the upper and lower sand layers exhibited a small yet measureable diurnal cycle of evaporation and condensation with the peak evaporation rate at 0.27 mm/day on average and a low rate of -0.15 mm/day on average. Analysis determined that these diurnal fluctuations in moisture contents correlated with the cyclic change in soil surface temperature, illustrating that moisture content decreased with increasing soil temperature. Additionally, peak evaporation generally transpired during the early morning hours just after sunrise. This finding agrees with the literature where it has been suggested that the rapidly increasing temperature gradient between the soil and air temperatures during the early morning, results in the high evaporation rates during this time period (Hellwig, 1973, 1978).

Chapters 6 and 7 focused on documenting, analyzing, and modeling the spatial and temporal surface moisture patterns of an actual beach environment. Field measurements of surface moisture content, presented in Chapter 6, show that the beach surface is characterized by three moisture-content zones: a consistently dry (moisture content <2%) back beach

extending about 20 m from the dune toe, a variable content zone (moisture contents ranged from <5% up to saturation at 45%) across the middle beach extending seaward from the dry zone about 20 m to the berm crest, and finally a persistently wet fore beach zone, in which moisture content consistently remained near saturation. Spatially, the position of these zones is controlled by the depth and fluctuation magnitude of the water table. The basic pattern that emerges is a cross-shore gradient with beach surface moisture contents decreasing in the landward direction as the depth of the water table increases and the amplitude of water table fluctuation decreases. Temporally, moisture contents varied over both short-term (daily) and long-term (multi-day) sequences. Over the short-term, surface moisture content dynamics display well-defined diurnal cyclic fluctuations. However, the fundamental parameter controlling these fluctuations varied spatially. Results showed that diurnal fluctuations in the groundwater table played a significant role in influencing surface moisture across the wet and variable-content zones, whereas evaporation and condensation processes were the dominant factors in the dry zone. Over the longer term, variations in the lunar spring/neap tidal range produced distinct changes in the range of moisture contents, as it regulated the amplitude of the beach groundwater table over multi-day time scales.

Finally, Chapter 7 demonstrated that a hysteresis based modeling approach provides a quite accurate and thorough representation of field-measured beach surface moisture dynamics. Simulations of surface moisture contents revealed that the inclusion of evaporation only influences predicted surface moisture contents across the dry back beach. The simulations not employing evaporation depart radically from the measured surface moisture contents, whereas the inclusion of evaporation greatly increases the accuracy of model. Simulations of

surface moisture across the wet fore beach and moisture variable middle beach, on the other hand, are virtually unchanged by the inclusion of evaporation. This finding confirms the results of Chapter 6, which suggested that evaporation and condensation processes are the dominant control across the dry back beach.

The work presented in this dissertation provides significant advances in the study of beach surface moisture. It represents perhaps the most comprehensive attempt that has been made to date to document and explain intermediate-scale variability in surface moisture content in light of the micro-scale processes that drive the system. The study provides a significant advancement in both our theoretical understanding of beach hydrology and our predictive capabilities for spatial and temporal surface moisture modeling.

8.2 Future Work

This study has succeeded in documenting and modeling the dynamics of beach surface moisture and results represent a significant improvement on previous capabilities in this area. However, it is worthwhile to consider the limitations of this study and recognize areas where additional future work could further advance our understanding of beach surface moisture dynamics. The predominant impediments that necessitate future work within this study include additional analysis of collected data as well as new inquiries that require further experiments.

8.2.1 Additional Analysis

1) Further insight into the dynamics of the surface moisture/water table relationship could be derived from an analysis of the full data set collected within the laboratory

experiments. Moisture contents were recorded across the full soil column for each of the water table oscillation ranges; however, only specific data were pulled from this larger dataset in order to focus the analysis on replicating the surface moisture/water table relationships found across northern Gulf of Mexico beaches (Zhu, 2007; Namikas *et al.*, 2010). Re-analyzing the full dataset will provide a more comprehensive analysis of beach surface moisture under a larger variety groundwater fluctuation ranges.

8.2.2 New Inquiries

1) It would be desirable to have moisture profile measurements from the water table to the beach surface to confirm the moisture retention profile. This was attempted unsuccessfully, as a series of moisture probes deployed within the sand column did not work properly. The moisture retention profile of the sand column was determined according to measured surface moisture and pressure head data. Although this method proved more than adequate to conduct the analyses, a more detailed record of the vertical moisture profile of the sand column would have provided full verification of the moisture retention profile, which is a fundamental component of the surface moisture model.

2) Further analysis of evaporation dynamics at more defined depth increments (i.e., 0 to 0.5 cm, 0.5 to 1 cm, 1 to 1.5 cm, etc.) would provide a deeper understanding of evaporation dynamics at depth. Only two depth layers were utilized within this study, 0 to 1 cm and 1 to 6 cm. Consequently, the progression of the 'Evaporative Transformation Layer' (ETL) with depth through the beach surface is not understood fully, as the 1 to 6 cm sand layer encompasses a total of 5 cm. To date, a set of laboratory and field experiments monitoring the evaporation

dynamics of a sand surface at these depth increments has been conducted. However, analysis of these data has yet to be completed and thus was not included within this study.

3) It would be desirable to have smaller time increments between evaporation measurements than the three- to four-hour increments recorded within this study. Increments of half hour (30 min) time scales, particularly over the first 12 hours, would significantly improve our understanding of evaporation dynamics. This would provide a more detailed record of the sediment surface as it transitions through the evaporation stages with time. The same set of laboratory and field experiments mentioned directly above has sought to accomplish this. Again however, analysis of this data has yet to be completed and thus was not included within this study.

4) Further insight into interrelationship between groundwater fluctuation and evaporation-condensation cycle on beach surface moisture is warranted. Depending upon the period difference between the two cycles, the relative strength of each process on surface moisture content could either enhance or isolate their influence. Results from this study revealed that the two processes primarily acted in opposition. Therefore, our understanding of the role of these processes on surface moisture content is incomplete. More field experiments are needed in order to fully evaluate the relationship between groundwater and evaporation-condensation on beach surface moisture. Conducting the field experiment during a time period in which there will be nightly high tides and daily low tides would be ideal.

5) The documentation of surface moisture contents over a broader range of grain size and hydrological conditions would significantly improve our understanding of the spatial and temporal variability in beach surface moisture generated by these processes. Chapter 4 began

the process of accomplishing this goal though a set of laboratory experiments; however, a more extensive analysis of surface moisture dynamics needs to be conducted on natural beaches systems.

References

Aagaard T, Davidson-Arnott RGD, Greenwood B, Nielsen J. 2004: Sediment supply from shoreface to dunes – linking sediment transport measurements and long term morphological evolution. *Geomorphology* 60: 205–24.

Abu-Hamdeh NH. 2003. Thermal properties of soils as affected by density and water content. *Biosystems Engineering* 86: 97-102.

Aitchison GD. 1960. Relationships of moisture stress and effective stress functions in unsaturated soils. *Proceedings from Conference on Pore Pressure and Suction in Soils*: 47–52.

Aluwihare S, Watanabe K. 2003. Measurement of evaporation on bare soil and estimating surface resistance. *Journal of Environmental Engineering* 129: 1157-1168.

Arens SM. 1996. Rates of aeolian transport on a beach in a temperate humid climate. *Geomorphology* 17: 3–18.

Arya, L.M. and J.F. Paris. 1981. A physio-empirical model to predict the soil moisture characteristic from particle-size distribution and bulk density data. *Soil Science Society of America Journal* 45: 1023–1030.

Assouline S. 2005. On the relationships between the pore size distribution index and characteristics of the soil hydraulic functions. *Water Resources Research* 41: W07019.

Atherton RJ, Baird AJ, Wiggs GFS. 2001. Inter-tidal dynamics of surface moisture content on a meso-tidal beach. *Journal of Coastal Research* 17: 482-489.

Aubertin M, Mbonimpa M, Bussière B, Chapuis RP. 2003. A model to predict the water retention curve from basic geotechnical properties. *Canadian Geotechnical Journal* 40: 1104–1122.

Aydin M, Yang SL, Kurt N, Yano T. 2005. Test of a simple model for estimating evaporation from bare soils in different environments. *Ecological Modelling* 182: 91-105.

Azizov A. 1977. Influence of soil moisture in the resistance of soil to wind erosion. *Soviet Soil Science* 1: 105-108.

Barbour SL. 1998. Nineteenth Canadian geotechnical colloquium: The soil-water characteristic curve: A historical perspective. *Canadian Geotechnical Journal* 35: 873–894.

Barrilleaux TC, Grace JB. 2000. Growth and invasive potential of Sapium sebiferum (*Euphorbiaceae*) within the coastal prairie region: The effects of soil and moisture regime. *American Journal of Botany* 87 (8): 1099-1106.

Bauer BO, Davidson-Arnott RGD, Hesp PA, Namikas SL, Ollerhead J, Walker IWJ. 2009. Aeolian sediment transport conditions on a beach: Surface moisture, wind fetch, and mean transport rates. *Geomorphology* 105: 106-116.

Bauer BO, Davidson-Arnott RGD. 2002. A general framework for modeling sediment supply to coastal dunes including wind angle, beach geometry, and fetch effects. *Geomorphology* 49: 89–108.

Bauer BO, Sherman DJ, Nordstrom KF, Gares PA. 1990. Aeolian transport and measurement across a beach and dune at Castroville, California. In: Nordstrom, K.F., Psuty, N.P., Carter, R.W.G. (Eds.), Coastal Dunes: Form and Process. Wiley, New York, pp. 39-55.

Bauer BO, Davidson-Arnott RGD, Hesp PA, Namikas SL, Ollerhead J, Walker IWJ. 2009. Aeolian sediment transport conditions on a beach: Surface moisture, wind fetch, and mean transport rates. *Geomorphology* 105: 106-116.

Beese F, van der Ploeg RR, Ritchie W. 1977. Test of a soil water model under field conditions. *Soil Science Society of America Journal* 41: 979-984.

Birle E, Heyer D, Vogt N. 2008. Influence of the initial water content and dry density on the soil-water retention curve and the shrinkage behavior of a compacted clay. *Acta Geotechnica* 3 (3): 191–200.

Bosilovich MG, Sun WY. 1998. Monthly simulation of surface layer fluxes and soil properties during FIFE. *Journal of the Atmospheric Sciences* 55: 1170-1184

Brooks RH, Corey AT. 1964. Hydraulic properties of porous media. Hydrology Papers No. 3, Colorado State University, Fort Collins, CO.

Campbell GS. 1974. A simple method for determining unsaturated conductivity from moisture retention data. *Soil Science* 117: 311–314.

Campbell GS., 1985. *Soil Physics with Basic: Transport Models for Soil-Plant System*. Elsevier, New York.

Cartwright N, Nielsen P, Perrochet P. 2005. Influence of capillarity on a simple harmonic oscillating water table: Sand column experiments and modeling. *Water Resources Research* 41: W08416.

Cartwright N, Nielsen P, Perrochet P. 2009. Behavior of a shallow water table under periodic flow conditions. *Water Resources Research* 45: W03416.

Chen X, Hu Q. 2004. Groundwater influences on soil moisture and surface evaporation. *Journal of Hydrology* 297: 285-300.

Childs EC, and Collis-George N. 1950. The permeability of porous materials. *Proceedings of the Royal Society London* Series A: 392-405.

Childs EC, Poulovassilis A. 1962. The moving profile above a moving water table. *Journal of Soil Science* 13: 272-285.

Childs EC. 1969. *An introduction to the physical basis of soil water phenomena*. John Willey & Sons Ltd, New York. 493p.

Chuang MH, Yeh HD. 2006. An analytical solution for the head distribution in a tidal leaky confined aquifer extending an infinite distance under the sea. *Advances in Water Resources* 30: 439-445.

Cornelis WM, Ronsyn J, van Merivenne M, Hartmann R. 2001. Evaluation of pedotransfer functions for predicting the soil moisture retention curve. *Soil Science Society of America Journal* 65: 638-648.

Croney D, and Coleman JD. 1954. Soil structure in relation to soil suction (pF). *Journal of Soil Science* 5: 75–84.

Davidson-Arnott RGD, Dawson JD. 2001. Moisture and fetch effects on rates of aeolian sediment transport, Skallingen, Denmark. Proceedings Canadian Coastal Conference, Quebec City, Canadian Coastal Science and Engineering Association, Ottawa, Canada: 309–321.

Davidson-Arnott RGD, MacQuarrie K, Aagaard T. 2005. The effects of wind gusts, moisture content and fetch length on sand transport on a beach. *Geomorphology* 68: 115-129.

Davidson-Arnott RGD, Yang Y, Ollerhead JW, Hesp PA, Walker IWJ. 2008. The effects of surface moisture on aeolian sediment transport threshold and mass flux on a beach. *Earth Surface Processes and Landforms* 33: 55-74.

Durner W. 1994. Hydraulic conductivity estimation for soils with heterogeneous pore structure. *Water Resources Research* 32: 211-223.

Eltahir EAB, 1998: A soil moisture–rainfall feedback mechanism. 1. Theory and observations. *Water Resources Research* 34: 765–776.

Entekhabi D, Rodriguez-Iturbe I, Castelli F. 1996. Mutual interaction of soil moisture state and atmospheric processes. *Journal of Hydrology* 184: 3-17

Fredlund DG, Xing A, Huang S. 1994. Predicting the permeability function for unsaturated soils using the soil-water characteristic curve. *Canadian Geotechnical Journal* 31: 533– 546.

Fredlund DG, Rahardjo H. 1993. Soil mechanics for unsaturated soils. John Wiley & Sons, Inc., New York.

Gallage CPK, and Uchimura T. 2010. Effects of dry density and grain size distribution on soil-water characteristic curves of sandy soils. *Soils and Foundations* 50: 161–172.

Gardner R. McLaren S. 1999. Infiltration and moisture movement in coastal sand dunes, Studland, Dorset, UK: Preliminary results. *Journal of Coastal Research* 15: 936-949.

Gavin H, Agnew CT. 2000. Estimating evaporation and surface resistance from a wet grassland. *Physics and Chemistry of the Earth (B)* 25: 599-603.

Granger RJ. 1989. Evaporation from natural non-saturated surfaces. *Journal of Hydrology* 111: 21-29.

Gupta SC, Larson WE. 1979. Estimating soil water retention characteristic from particle size distribution, organic matter content, and bulk density. *Water Resources Research* 15: 1633–1635.

Haines W. 1930. Studies in the physical properties of soil: V. The hysteresis effect in capillary properties, and the modes of moisture distribution associated therewith. *Journal of Agricultural Science* 20: 97–116.

Hanks RJ. 1992. *Applied Soil Physics: Soil Water and Temperature Applications*. Spinger- Verlag: New York.

Haverkamp R. Parlange JY. 1986. Predicting the water retention curve from particle size distribution: Sandy soil without organic matter. *Soil Science* 142: 325–339.

He W, Kobayashi T. 1998. A rational parameterization of evaporation from dry, bare soil. *Journal of the Meteorological Society of Japan* 76: 955-963.

Hellwig DHR. 1973. Evaporation of water from sand 3: Diurnal variations. *Journal of Hydrology* 18: 109-118.

Hellwig DHR. 1978. Evaporation of water from sand 6: The Influence of the depth of the water table on diurnal variations. *Journal of Hydrology* 39: 129-138.

Hesp PA. 1991. Ecological processes and plant adaptations on coastal dunes. *Journal of Arid Environments* 21: 165-191.

Hillel,D. 1971. *Soil and Water: Physical Principles and Processes*. Academic Press, New York, 288p.

Hillel D. 1980. *Applications of Soil Physics. Academic Press*. New York, 385p.

Hinz C. 1998. Analysis of unsaturated/saturated water flow near a fluctuating water table. *Journal of Contaminant Hydrology* 33: 50-80.

Holmes RM. 1961. Estimation of soil moisture content using evaporation data. Proceedings of Hydrology Symposium, No. 2 Evaporation. Queen's Printer, Ottawa, pp. 184-196.

Horn DP. 2002. Beach groundwater dynamics. *Geomorphology* 48: 121-146.

Houser C. 2009. Synchronization of transport and supply in beach-dune interaction. *Progress in Physical Geography* 33: 733-746.

Hugenholtz CH, Wolfe SA, Walker IWJ, Moorman BJ. 2009. Spatial and temporal patterns of aeolian sediment transport on an inland parabolic dune, Bigstick Sand Hills, Saskatchewan, Canada. *Geomorphology* 105: 158–170.

Idso SB, Reginato RJ, Jackson RD, Kimball BA, Nakayama FS, 1974: The three stages of drying of a field soil. *Soil Science Society of America Proceedings* 38: 831- 837.

Jackson NL, Nordstrom KF. 1997. Effects of time-dependent moisture content of surface sediments on aeolian transport rates across a beach, Wildwood, New Jersey, USA. *Earth Surface Processes and Landforms* 22: 611-622.

Jackson NL, Nordstrom KF. 1998. Aeolian transport of sediment on a beach during and rainfall, Wildwood, NJ, USA. *Geomorphology* 22: 151-157.

Kessler A, Rubin H. 1987. Relationships between water infiltration and oil spill migration in sandy soils. *Journal of Hydrology* 91: 197-204.

Kool JB, Parker JC. 1987. Development and evaluation of closed-form expressions for hysteretic soil hydraulic properties. *Water Resources Research* 23: 105-114.

Kosugi K. 1996. Lognormal distribution model for unsaturated soil hydraulic properties. *Water Resources Research* 32: 2697-2703.

Kosugi K., 1999. General model for unsaturated hydraulic conductivity for soils with lognormal pore-size distribution. *Soil Science Society of America Journal* 63: 270–277.

Lehmann P, Stauffer F, Hinz C, Dury O, Flühler H. 1998. Effect of hysteresis on water flow in a sand column with a fluctuating capillary fringe. *Journal of Contaminant Hydrology* 33: 81–100.

Mahfouf JF, Noilhan J. 1991. Comparative study of various formations from bare soil using in situ data. *Journal of Applied Meteorology* 30: 1354-1365.

Malaya C, Sreedeep S. 2012. Critical review on the parameters influencing soil-water characteristic curve. *Journal of Irrigation and Drainage Engineering* 138: 55-62.

McKenna Neuman C, Langston G. 2006. Measurement of water content as a control of particle entrainment by wind. *Earth Surface Processes and Landforms* 31: 303-317.

McKenna Neuman CL, Langston G. 2003. Spatial analysis of surface moisture content on beaches subject to aeolian transport. *Proceedings of the Canadian Coastal Conference* (Kingston, Ontario, Canada): 1-10.

Miller EE, Miller RD. 1956. Physical theory for capillary flow phenomena. *Journal of Applied Physics* 27: 324.

Monteith JL. 1981. Evaporation and surface temperature. *Quarterly Journal of the Royal Meteorological Society* 107: 1-27.

Morton FI. 1985. The complementary relationship areal evapotranspiration model: How it works. Proceedings of the National Conference on Advances in Evapotranspiration *American Society of Agricultural Engineers*: 377-384.

Mualem Y. 1976. A new model for predicting the hydraulic conductivity of unsaturated porous media. *Water Resources Research* 12: 513–522.

Namikas SL, Edwards BL, Bitton MCA, Booth JL, Zhu Y. 2010. Temporal and spatial variabilities in the surface moisture content of a fine-grained beach. *Geomorphology* 114: 303-310.

Nielsen P, Perrochet P. 2000. Water table dynamics under capillary fringes: experiments and modeling. *Advances in Water Resources* 23: 503-515.

Nimmo JR. 2004. Porosity and pore size distribution. In Hillel, D., ed. *Encyclopedia of Soils in the Environment* 3: 95-303.

Olyphant GA. 2003. Temporal and spatial (down profile) variability of unsaturated soil hydraulic properties determined from a combination of repeated field experiments and inverse modeling. *Journal of Hydrology* 281: 23-35.

Parlange MB, Katul GG. 1992. Estimation of the diurnal variation of potential evaporation from a wet bare soil surface. *Journal of Hydrology* 132: 71-89.

Parlange JY. 1976. Capillary hysteresis and the relationship between drying and wetting curves. *Water Resources Research* 12: 224–228.

Penman HL. 1948. Natural evapotranspiration from open water, bare soil and grass. *Proceedings of the Royal Society of London Series A* 193: 120-145.

Philip JR, de Vries DA. 1957. Moisture movement in porous materials under temperature gradients. *Transactions of the American Geophysical Union* 38, 222–232.

Poulovassilis A. 1962. Hysteresis of pore water, an application of the concept of independent domains. *Soil Science* 93: 405–412.

Psuty NP. 1988. Sediment budget and beach/dune interaction. *Journal of Coastal Research Special Issue* 3: 1-4.

Raats PAC, Gardner WR. 1974. Movement of water in the unsaturated zone near a water table. In van Scholfgaarde J (Ed), *Drainage for Agriculture*, Agronomy Series 17, *American Society of Agronomy*: Madison, WI; 311-357 and 401-405.

Raats PAC. 1992. A superclass of soils. In: Van Genuchten, M.Th., Leij, F.J., Lund, L.J. (Eds.), *Indirect Methods for Estimating the Hydraulic Properties of Unsaturated Soils*. *Proceedings of an International Workshop*: 45–51.

Raubenheimer B, Guza RT, Elgar S. 1999. Tidal water table fluctuations in a sandy ocean beach. *Water Resources Research* 35: 2313-2320.

Ravi S, Zobeck TM, Over TM, Okin GS, D'Odorico P. 2006. On the effect of moisture bonding forces in air-dry soils on threshold friction velocity of wind erosion. *Sedimentology* 53: 597–609.

Richards LA. 1931. Capillary conduction of liquids through porous medium. *Physics* 1: 318-333.

Ritchie JT. 1972. Model for predicting evaporation from a row crop with incomplete cover. *Water Resources Research* 8: 1204-1213.

Ruz MH, Meur-Ferec C. 2004 Influence of high water levels on aeolian sand transport: upper beach/dune evolution on a macrotidal coast, Wissant Bay, northern France. *Geomorphology* 60: 73–87.

Schmutz PP, Namikas SL. 2011. Utility of the Delta-T theta probe for obtaining surface moisture measurements from beaches. *Journal of Coastal Research* 27: 478-484.

Schmutz PP, Namikas SL. 2013. Measurement and modeling of moisture content above an oscillating water table: Implications for beach surface moisture dynamics. *Earth Surface Processes and Landforms* 38: 1317–1325.

Scott PS, Farquhar GJ, Kouwen N. 1984. Hysteresis effects on net infiltration. *American Society of Agricultural Engineering* 48: 1006-1010.

Sherman DJ, Jackson DWT, Namikas SL, Wang J. 1998. Wind-blown sand on beaches: An evaluation of models. *Geomorphology* 22: 113-133.

Sherman DJ, Bauer BO. 1993. Dynamics of beach-dune interaction. *Progress in Physical Geography* 17: 413-447.

Sherman DJ, Lyons W. 1994. Beach-state controls on aeolian sand delivery to coastal dunes. *Physical Geography* 15: 381-395.

Short AD, Hesp PA. 1982. Wave, beach and dune interactions in southeastern Australia. *Marine Geology* 48: 259-284.

Šimůnek J, Sejna M, van Genuchten MT. 1998. The HYDRUS-1D software package for simulating the movement of water, heat, and multiple solutes in variably saturated media. US Salinity Laboratory, ARS, USDA: Riverside, California.

Stankovich JM, Lockington DA. 1995. Brooks-Corey and van Genuchten soil-water-retention models. *Journal of Irrigation and Drainage Engineering* 121: 1-7.

Stauffer F. 1996. Hysteretic unsaturated flow modeling. *Proceedings of the Second International Conference on Hydroinformatics*, Zurich, Switzerland: 589-595.

Stauffer F. Kinzelbach W. 2001. Cyclic hysteretic flow in porous medium column: model, experiment, and simulations. *Journal of Hydrology* 240: 264-275.

Terzaghi K. 1943. *Theoretical Soil Mechanics*. Wiley Publications, New York.

Tokunaga TK, Olson KR, Wan J. 2004. Conditions necessary for capillary hysteresis in porous media: Tests of grain size and surface tension influences. *Water Resources Research* 40: W05111.

Tokunaga TK. 2009. Hydraulic properties of adsorbed water films in unsaturated porous media. *Water Resources Research* 45: W06415.

van de Griend AA, Owe M. 1994. Bare soil surface resistance to evaporation by vapor diffusion under semiarid conditions. *Water Resource Research* 30: 181-188.

van Genuchten MT. 1980. A closed-form equation for predicting the hydraulic conductivity of unsaturated soils. *Soil Science Society of America Journal* 44: 892–898.

van Genuchten MT, Nielsen DR. 1985. On describing and predicting the hydraulic properties of unsaturated soils. *Annals of Geophysics* 3: 615-628.

Vogel T, Císlerová M. 1988. On the reliability of unsaturated hydraulic conductivity calculated from the moisture retention curve. *Transport in Porous Media* 3: 1-15.

Vogel T, Huang K, Zhang R, van Genuchten MT. 1996. The HYDRUS code for simulating one-dimensional water flow, solute transport, and heat movement in variably-saturated media, Version 5.0, Research Report No 140, U.S. Salinity Laboratory, USDA, ARS, Riverside, CA, 1996.

Weise BR, White WA 1991. Padre Island National Seashore: A guide to the geology, natural environments, and history of a Texas barrier island. Texas Bureau of Economic Geology, Guidebook 17.

Werner AD, Lockington DA. 2003. Influence of hysteresis on tidal capillary fringe dynamics in a well-sorted sand. *Advances in Water Resources* 26: 1199-1204.

Wiggs CFS, Atherton RJ, Baird AJ. 2004a. Thresholds of aeolian sand transport: Establishing suitable values. *Sedimentology* 51: 95–108.

Wiggs CFS, Baird AJ, Atherton RJ. 2004b. The dynamic effects of moisture on the entrainment and transport of sand by wind. *Geomorphology* 59: 13-30.

Wilson GW, Fredlund DG, Barbour SL. 1997. The effect of soil suction on evaporative fluxes from soil surfaces. *Canadian Geotechnical Journal* 34: 145-155.

Wythers KR, Lauenroth WK, Paruelo JM. 1999. Bare-soil evaporation under semiarid field conditions. *Soil Science Society of America Journal* 63: 1341-1349.

Yamanaka T, Takeda A, Sugita F. 1997. A modified surface resistance approach for representing bare-soil evaporation: wind-tunnel experiments under various atmospheric conditions. *Water Resources Research* 33: 2117–2128.

Yamanaka T, Takeda, A, Shimada J. 1998. Evaporation beneath the soil surface: Some observational evidences and numerical experiments. *Hydrological Processes* 12, 2193–2203.

Yamanaka T, Yonetani T. 1999. Dynamics of the evaporation zone in dry sandy soils. *Journal of Hydrology* 217(1): 135-148.

Yang H, Rhardjo H, Leong E, Fredlund DG. 2004. Factors affecting drying and wetting soil-water characteristic curves of sandy soils. *Canadian Geotechnical Journal*, 41, 908–920.

Yang Y, Davidson-Arnott RGD. 2005. Rapid measurement of surface moisture content on a beach. *Journal of Coastal Research* 21(3): 447-452.

Zhu J, Mohanty BP. 2002. Upscaling soil hydraulic properties for steady state evaporation and infiltration. *Water Resources Research* 38 (9): 1-13.

Zhu Y. 2007. *Modeling spatial and temporal variations of surface moisture content and groundwater table fluctuations on a fine-grained beach, Padre Island, Texas*. Ph.D. Dissertation, Department of Geography & Anthropology, Louisiana State University: Baton Rouge, Louisiana, US.

Vita

Phillip Schmutz was born in Metairie, Louisiana in 1981. He grew up in Lake Charles, Louisiana until he moved to Tyler, Texas during high school. After graduating in 2000 from Robert E. Lee High School, he went to Baylor University where he earned a Bachelor of Arts in Geography and Environmental Studies. During his time at Baylor he developed a profound interest in the physical processes of the coastal environment, thanks in part to Dr. Jennifer Rahn. Through her guidance and support Phillip found himself embarking on the next chapter of his life at Louisiana State University. He completed his master's degree from LSU in 2007, upon which he continued his education in geography, pursuing a doctoral degree from the same institution. During his tenure at LSU he met and married (August 2008) his wife Dr. Amy Potter, who received her doctorate from LSU in geography in December 2011. They moved to Savannah, Georgia in August 2013 when Amy was offered a tenure-track Assistant Professor of Geography position in the History Department at Armstrong State University.